

On the other hand,  $c_s$  is unstable if any eigenvalue has positive real part:

$$\text{Re}(\lambda_j) > 0 \quad \text{any } j \tag{9.39}$$

These results are eminently reasonable in view of Eq. (9.33). If the largest real part of the system eigenvalues is equal to zero, a *critical case* arises and further analysis is needed to determine local system dynamic characteristics (see, for example, Ref. 10). Fortunately, we need not compute all the eigenvalues to check the inequalities listed above. First, suppose that the determinant in Eq. (9.34) has been expanded to provide an  $m$ th-order algebraic equation.

$$\lambda^m + B_1\lambda^{m-1} + \dots + B_{m-1}\lambda + B_m = 0 \tag{9.40}$$

Now we can apply the Hurwitz criterion,<sup>†</sup> which asserts that all roots of (9.40) have negative real parts if and only if the following conditions are met:

$$\begin{aligned} & B_1 > 0 \\ & \det \begin{bmatrix} B_1 & B_3 \\ 1 & B_2 \end{bmatrix} > 0 \\ & \det \begin{bmatrix} B_1 & B_3 & B_5 \\ 1 & B_2 & B_4 \\ 0 & B_1 & B_3 \end{bmatrix} > 0 \\ & \vdots \\ & \det \begin{bmatrix} B_1 & B_3 & B_5 & \dots & 0 \\ 1 & B_2 & B_4 & \dots & 0 \\ 0 & B_1 & B_3 & \dots & 0 \\ 0 & 1 & B_2 & \dots & 0 \\ \dots & \dots & \dots & \dots & B_m \end{bmatrix} > 0 \end{aligned} \tag{9.41}$$

As an example, we shall investigate the situation where a single substrate limits growth and examine the dynamic version of the Monod chemostat model. Application of the general unsteady-state mass balance (9.27) to both biophase and substrate and use of Monod's expression (7.10) for the specific growth rate yields

$$\frac{dx}{dt} = D(x_0 - x) + \frac{\mu_{max}sx}{s + K_s} \tag{9.42a}$$

and

$$\frac{ds}{dt} = D(s_0 - s) - \frac{1}{Y_{X/S}} \frac{\mu_{max}sx}{s + K_s} \tag{9.42b}$$

For the case of sterile feed ( $x_0 = 0$ ), there are *two* possible steady states, the non-trivial one given earlier in Eqs. (7.14) and (7.15) and the "washout" solution

<sup>†</sup> C. F. Walter, "Kinetic and Biological and Biochemical Control Mechanisms," p. 335 in E. Kun and S. Grisola (eds.), *Biochemical Regulatory Mechanisms in Eucaryotic Cells*, John Wiley & Sons, Inc., New York, 1972.

$x = 0, s = s_0$ . We can determine which of these steady states will be observed in a continuous culture by determining their stability. Local stability can be studied using the linearized form of Eqs. (9.42). The results of such a local-stability study of the Monod chemostat are summarized below.

	$D > \frac{\mu_{max}s_0}{K_s + s_0}$	$D < \frac{\mu_{max}s_0}{K_s + s_0}$
Nontrivial steady-state [Eqs. (7.14, 7.15)]	Unstable	Stable
Washout steady-state	Stable	Unstable

Another prediction of this analysis is that concentrations cannot approach their steady-state values in a damped oscillatory fashion. As such oscillatory phenomena have been observed experimentally, this substrate-and-cell model is insufficient to predict all dynamic features of some reactors.

Other weaknesses in the dynamic model of the Monod chemostat are known. It predicts instantaneous response of the specific growth rate to a change in substrate concentration: experimentally, a lag is present (see Prob. 10.6). Moreover, growth-rate hysteresis and variations in the yield factor have been established. Steady oscillations have been found in several experimental studies (Fig. 9.6). Consequently, while the Monod chemostat model is quite successful for steady-state purposes in many cases, it has numerous drawbacks as a dynamic representation.

By introducing additional variables into the model, i.e., by giving it more "structure," some of the phenomena unexplained by the Monod model can be accounted for. The need for structured models in such cases rests on conceptual

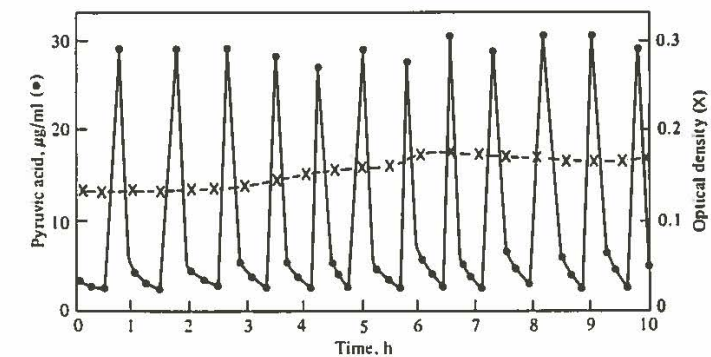


Figure 9.6 These sustained oscillations of pyruvate concentration (●) were observed in continuous culture of *E. coli*. Notice that the cell concentration (crosses) remains approximately constant. (Reprinted from B. Sikyia, "Continuous Cultivation of Microorganisms," *Suom. Kemistil.*, vol. 38, p. 180, 1965.)

points mentioned earlier in Chap. 7 and in this chapter's introduction. In a transient situation, the balanced-growth approximation does not apply if the time scale of the environmental changes are comparable to the time scale for biological response (e.g., by induction or repression of enzyme synthesis). In such situations, the biological kinetics model should be expanded to include more components (or pseudocomponents; Sec. 7.4) of the cell phase.

We have already examined the two-component structured model of Williams in Sec. 7.4.1. Applied to continuous culture dynamics, this model reproduces several experimental features not anticipated by the Monod model. Extending the analogy between the Monod growth-rate equation (7.10) and enzyme kinetics, Jeffreson and Smith [11] include in their dynamic chemostat model an intermediate species which is an analog of the enzyme-substrate complex. Ramkrishna, Fredrickson, and Tsuchiya [12] consider an inhibitor of cell growth in their dynamic model. In a sense, this approach can be viewed as adding more structure to the nutrient phase.

A completely different viewpoint has been taken by Lee, Jackman, and Schroeder [13], who consider the influence of flocculation on the overall growth process. We have already observed that the individual cells in many microbial systems form aggregates called flocs. Metabolic processes within such flocs could presumably be different from those in individual dispersed cells; nutrients, for example, would have to diffuse into the floc to reach cells in its interior. Thus, the biophase is viewed as having two components (flocs and individuals) with different kinetics but also with the possibility of interchange of individual cells between the two different morphological forms of behavior. The resulting model exhibits overall yield-factor fluctuations, growth-rate hysteresis, and slower responses than the Monod model—all more compatible with experimental findings than Monod's model.

Yet another conceptual attack is apparent in the model of Young, Bruley, and Bungay [14]. They propose that because of resistances in the mass transport processes which bring nutrient into the cell, the substrate concentration within the cell is not equal at every instant to the external nutrient concentration, and it is the former quantity which directly influences the cell's growth rate. The model based on this view point exhibits lags in response to environmental changes, as has often been observed experimentally.

In closing our review of chemostat dynamics, we should note another potentially important phenomenon not embodied in the Monod model. In situations where excessive nutrient inhibits growth, the specific growth-rate expression given in Eq. (7.32)

$$\mu = \frac{\mu_{\max} s}{K_s + s + s^2/K_p}$$

should be used. A chemostat with this specific growth rate can behave significantly differently from the classical Monod chemostat: now there can be three steady states for some operating conditions. Dynamic behavior for such a system can be complex, and nonlinear effects not considered in a local stability analysis

can be quite important. It has been suggested that this model with its unusual characteristics may help explain the operating difficulties which are common in anaerobic digestion processes. Some aspects of substrate-inhibition effects in CSTRs will be explored further in Chap. 14.

Mixed culture systems involving multiple cellular species can exhibit complicated dynamic behavior. We shall investigate these types of bioreaction systems in detail in Chap. 13. There, we shall also introduce additional general mathematical methods and results useful for analyzing and describing reactor dynamics.

### 9.3 REACTORS WITH NONIDEAL MIXING

Now we depart from the ideal cases of completely mixed tanks or plug-flow tubular reactors, situations which can be approximated under small-scale laboratory conditions, and consider more realistic conditions encountered in larger scale process reactors. We shall be concerned in this section with methods to characterize mixing and flow patterns in reaction vessels, with application of this knowledge for reactor design, and with examination of some of the interactions which arise between biological or biocatalyzed reactions and the mixing and flow patterns in the vessel. First, we consider mixing times in agitated tanks to introduce important time scales, to show the existence of large-scale circulation patterns in reactor vessels, and to get some feeling for orders of magnitudes of the circulation times encountered in different bioreactor situations.

#### 9.3.1 Mixing Times in Agitated Tanks

The mixing time denotes the time required for the tank composition to achieve a specified level of homogeneity following addition of a tracer pulse at a single point in the vessel. The tracer might be a salt solution, an acid or base, or a heated or cooled pulse of fluid. The circulation characteristics of the vessel and mixing time can be measured by continuously monitoring the tracer concentration at one or several points in the vessel. As shown schematically in Fig. 9.7, different types of reactor internals and agitators give rise to different circulation and mixing time characteristics. In the sketched responses in Fig. 9.7, periodic patterns in the tracer concentration are evident, indicating a characteristic number of bulk circulations of fluid required before achieving composition homogeneity. The circulation time is also important because it indicates approximately the characteristic time interval during which a cell or biocatalyst suspended in the agitated fluid will circulate through different regions of the reactor, possibly encountering different reaction conditions along the way. Then, as mentioned before, one must consider whether or not the fluctuations encountered are of sufficient magnitude and on an appropriate time scale to influence local kinetic behavior significantly. We shall return in the conclusion of this section on mixing to examination of some experimental studies of mixing effects on biocatalyst performance.

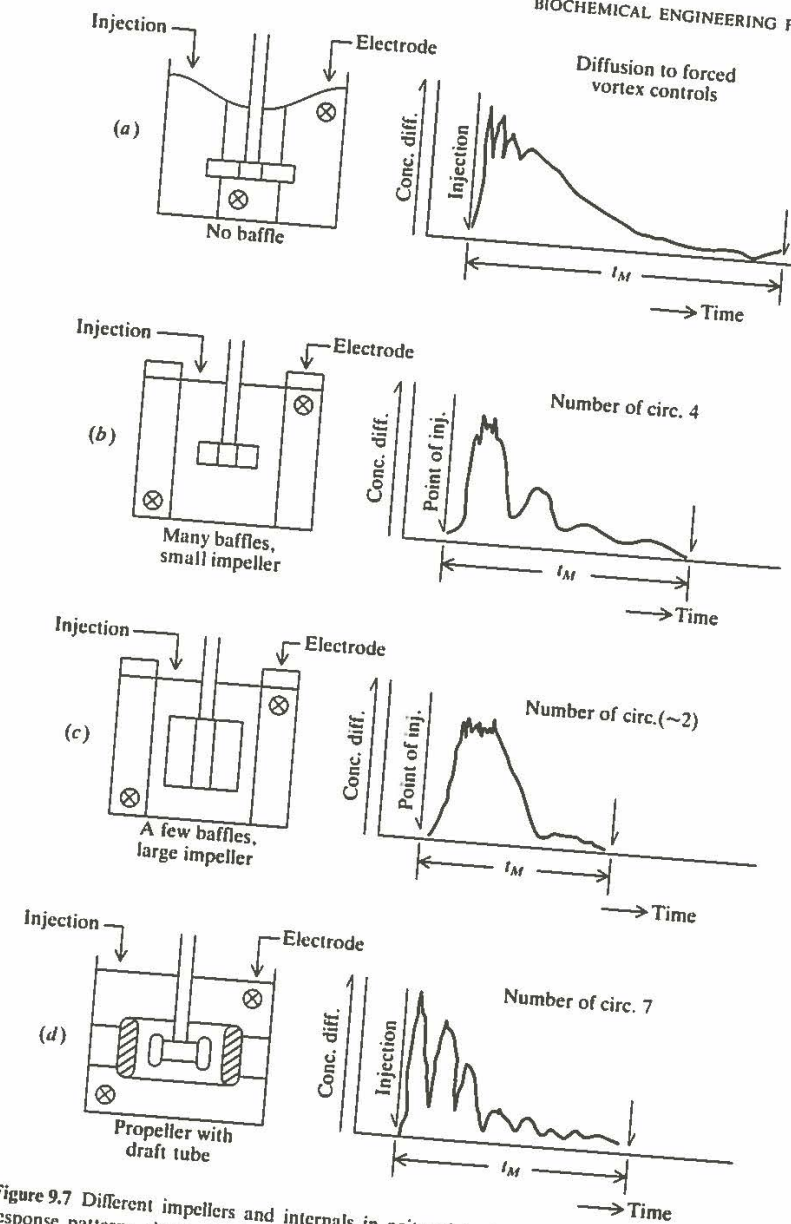


Figure 9.7 Different impellers and internals in agitated tanks and the corresponding characteristic response patterns observed following pulse injection of tracer. The latter are plotted as deviations from the tracer concentration in the final, completely mixed state (After Nagata [15]).

Mixing time correlations developed for Newtonian fluids and mycelial cultures and experimental data on mixing times in microbial polysaccharide solutions may be found in the review of Charles [18]. Mixing times of 29 to 104 s were measured in fermentation tanks of size 2.5 to 160 m<sup>3</sup>. In some cases mixing times of several minutes have been reported. Studies of a 25 m<sup>3</sup> deep jet aeration system revealed a mixing time of 80 s in water. Charles reported mixing times of around 6 min in 1% xanthan solution at 300 rpm with no air flow, decreasing to around one minute at 500 rpm and with 0.25% air flow. On the other hand, mixing times in the range of 2 to 3 s have been mentioned in small reactors. These figures give a sense of the order of magnitude range which might be expected at different reactor scales in different types of bioreactor fluids. Here our concern is with large-scale fluid circulation and possible composition and temperature nonuniformities. Finer scale considerations having to do with turbulence and its interaction with mass transfer and cells is provided in Chap. 8.

Clearly consideration of a single circulation time in, say, an agitated tank is a conceptual approximation. If we monitor the sojourn of various parcels of fluid from the impeller region, different paths through the vessel will be followed by different fluid parcels, giving rise to correspondingly different circulation times. Bryant [19] has described how the *circulation time distribution*  $f_c(t)$  can be experimentally determined by use of a small, neutrally buoyant radio transmitter and a monitoring antenna placed in the vessel. By definition,  $f_c(t) dt$  is the fraction of circulations which have circulation time between  $t$  and  $t + dt$ . Bryant indicates that the circulation time distribution for agitated tanks can usually be well approximated by the functional form of a log-normal distribution

$$f_c(t) = \frac{1}{\sigma_t \sqrt{2\pi}} \exp \left[ -\frac{(\ln t - t_l)^2}{2\sigma_t^2} \right] \quad (9.43)$$

The two parameters in this representation, the log-mean circulation time  $t_l$  and log-mean circulation time standard deviation  $\sigma_t$ , are related to the mean circulation time  $\bar{t}$  and standard deviation  $\sigma$  of  $f_c$  by

$$\bar{t} = e^{(t_l + \sigma_t^2/2)} \quad (9.44a)$$

$$\sigma = \bar{t}^2 (e^{\sigma_t^2} - 1) \quad (9.44b)$$

Experimental measurements give  $\bar{t}$  and  $\sigma$  which can then be used in Eq. (9.44) to determine parameter values for  $f_c$  in Eq. (9.43). Later in this chapter we shall apply the circulation time distribution concept to calculate effects of fluid circulation on overall bioreactor performance.

### 9.3.2 Residence Time Distributions

Let us now try to imagine what happens to a small parcel of fluid after it has entered a continuous-flow bioreactor. Because of mixing in the vessel, this fluid will be broken into smaller parts, which separate and disperse throughout the vessel. Thus, some fraction of this fluid element will rapidly find its way to the

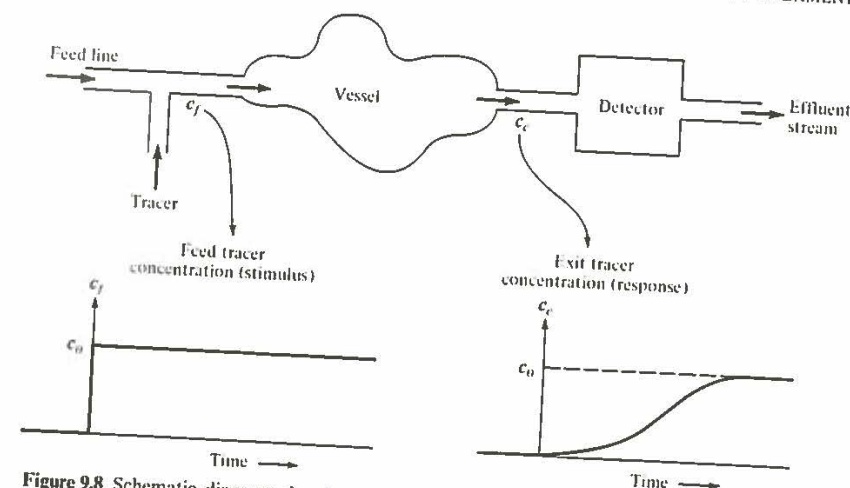


Figure 9.8 Schematic diagram showing experimental measurement of the response ( $\mathcal{F}$  curve) to a step tracer input.

effluent stream, while other portions of it will wander about the vessel for varying times before entering the exit pipe. Viewed differently, this scenario indicates that the effluent stream is a mixture of fluid elements which have resided in the reactor for different lengths of time. Determination of the distribution of these residence times in the exit stream is a valuable indicator of the mixing and flow patterns within the vessel. Methods for determining the residence time distribution are reviewed next.

We shall consider first an arbitrary vessel with one feed and one effluent line, and it will be assumed for the moment that there is no back diffusion of vessel fluid into the feed line or of effluent fluid into the vessel. In order to probe the mixing characteristics of the vessel, we conduct a *stimulus-response* experiment using an inert tracer: at some datum time designated  $t = 0$ , we introduce tracer at concentration  $c^*$  into the feed line and maintain this tracer feed for  $t > 0$ . Then we monitor the system response (in this case the exit tracer concentration) to this specific stimulus. Figure 9.8 shows schematically the general features of this experiment, as well as the shape of a typical exit concentration response  $c(t)$ .

Under these conditions, the response to a unit-step tracer input  $c_0(t) = H(t)$  where

$$H(t) = \begin{cases} 0 & t < 0 \\ 1 & t \geq 0 \end{cases} \quad (9.45)$$

is obtained by dividing the  $c(t)$  function obtained in the above experiment by the tracer feed concentration  $c^*$  used in that experiment. The result, the unit-step response of the mixing vessel, is called the  $\mathcal{F}$  function (Fig. 9.8):

$$\mathcal{F}(t) = \frac{c(t)}{c^*} = \text{response to unit-step input of tracer} \quad (9.46)$$

What is needed in many cases is not the  $\mathcal{F}$  function but the residence-time-distribution (RTD) function<sup>†</sup>  $\mathcal{E}(t)$ , which is defined by

$$\mathcal{E}(t) dt = \text{fraction of fluid in exit stream which has been in vessel for time between } t \text{ and } t + dt \quad (9.47)$$

Thus, for example, the fraction of the exit stream which has resided in the vessel for times smaller than  $t$  is

$$\int_0^t \mathcal{E}(x) dx$$

It follows from definition (9.47) that

$$\int_0^\infty \mathcal{E}(x) dx = 1 \quad (9.48)$$

A simple thought experiment will now serve to clarify the relationship between the  $\mathcal{E}$  and  $\mathcal{F}$  functions. Returning to the stimulus-response experiment of Fig. 9.8, let us imagine the vessel contents to consist of two different types of fluid. Fluid I contains tracer at concentration  $c^*$ , and fluid II is devoid of tracer. Consequently, all elements of fluid I must have entered the vessel at some time greater than zero. Then, any fluid I in the effluent at time  $t$  has been in the system for a time less than  $t$ . On the other hand, fluid II had to be in the vessel at  $t = 0$  since only fluid I has entered since then. All fluid II elements in the effluent at time  $t$  consequently have residence times greater than  $t$ . Assuming that we know the  $\mathcal{E}$  function, we can write the exit tracer concentration  $c(t)$  as the sum of the fluid I and fluid II contributions:

$$c(t) = c^* \cdot \int_0^t \mathcal{E}(x) dx + 0 \cdot \int_t^\infty \mathcal{E}(x) dx \quad (9.49)$$

Combining Eqs. (9.49) and (9.46) produces the desired relationship

$$\mathcal{F}(t) = \int_0^t \mathcal{E}(x) dx \quad (9.50)$$

which can be differentiated with respect to  $t$  to provide the alternative form

$$\frac{d\mathcal{F}(t)}{dt} = \mathcal{E}(t) \quad (9.51)$$

We note first from Eq. (9.51) that  $\mathcal{E}(t)$  can be obtained by differentiating an experimentally determined  $\mathcal{F}$  curve. Also, the theory of linear systems states that

<sup>†</sup> Standard terminology from statistics would indicate that  $\mathcal{E}$  is a density function with  $\mathcal{F}$  the corresponding distribution. The language above is so firmly embedded in the reaction engineering literature, however, that it would cause confusion to alter it here.

the time derivative of the unit-step response is the unit-impulse response, which reveals that  $\mathcal{E}(t)$  can be interpreted as the reponse of the vessel to the input of a unit tracer impulse at time zero. While an impulse is a mathematical idealization, we can approximate it experimentally by introducing a given amount of tracer into the vessel in a short pulse of high concentration.

In addition to the experimental methods just described for determining the RTD function, we can sometimes evaluate it if a mathematical or conceptual model of the mixing process is available. Considering the ideal CSTR as an example, the unsteady-state mass balance on (nonreactive) tracer is

$$\frac{dc}{dt} = \frac{F}{V_R}(c_0 - c) \quad (9.52)$$

To determine the result of an  $\mathcal{F}$  experiment for this system, we take

$$c(0) = 0 \quad (9.53)$$

$$c_0(t) = c^* \quad t \geq 0 \quad (9.54)$$

The solution to Eq. (9.52) under conditions (9.53) and (9.54) reveals

$$\mathcal{F}(t) = \frac{c(t)}{c^*} = 1 - e^{-(F/V_R)t} \quad (9.55)$$

Applying formula (9.51) to the result in Eq. (9.55) reveals that the RTD for a CSTR is

$$\mathcal{E}(t) = \frac{F}{V_R} e^{-Ft/V_R} \quad (9.56)$$

The physical perspective of the PFR introduced above readily reveals its RTD. If a tracer pulse is introduced in the feed, it flows through the vessel without mixing with adjacent fluid and emerges after a time  $L/u$ . Thus, the tracer pulse in the exit has exactly the same form as the pulse fed into the PFR, except that it is shifted in time by one vessel holding time. Deviation from such behavior is evidence of breakdown in the plug-flow assumption.

Often when dealing with distribution functions such as  $\mathcal{E}(t)$ , it is helpful to consider the moments of the distribution. The  $k$ th moment of  $\mathcal{E}(t)$  is defined by

$$m_k = \int_0^{\infty} t^k \mathcal{E}(t) dt \quad k = 0, 1, 2, \dots \quad (9.57)$$

Since a unit amount of tracer is introduced into a vessel to observe its  $\mathcal{E}$  curve, and since all tracer eventually must leave the vessel, we know that

$$m_0 = 1 \quad (9.58)$$

The first moment  $m_1$  is the mean of the RTD, or the *mean residence time*  $\bar{t}$ . Under the conditions of zero back diffusion stated at the start of this section, it can be proved [2] for a single phase fluid in an arbitrary vessel that

$$\bar{t} = m_1 = \frac{V_R}{F} \quad (9.59)$$

which says that the mean residence time is identical to the nominal holding time of the vessel. This relationship does not apply for a single phase in a multiphase mixture nor to a single phase in a vessel with heterogeneous catalyst or adsorbent. The second moment  $m_2$  is most often employed in terms of the distribution's variance  $\sigma^2 = m_2 - m_1^2$ , which is the average of the squares of deviations from the mean residence time.

Related functions useful in mixing and reactor analysis include the *internal age distribution* function  $I(t)$ , where  $I(t) dt$  denotes the fraction of fluid within the vessel which has been in the vessel for a time between  $t$  and  $t + dt$ . A mass balance can be applied to obtain

$$I(t) = \bar{t}^{-1}[1 - \mathcal{F}(t)]. \quad (9.60)$$

The intensity function  $\Lambda(t)$ , defined such that  $\Lambda(t) dt$  is the probability that a fluid element which has been in the reactor for time  $t$  leaves in the next short time interval  $dt$ , is especially useful in diagnosing deviations from ideal mixing regimes.  $\Lambda(t)$  is related to the functions introduced earlier by [16]

$$\Lambda(t) = \frac{\mathcal{E}(t)}{1 - \mathcal{F}(t)} = -\frac{d \ln [1 - \mathcal{F}(t)]}{dt} \quad (9.61)$$

For an ideal CSTR,  $\Lambda(t)$  is a constant. Figure 9.9 shows how  $\Lambda(t)$  behaves for several types of nonidealities in stirred vessels. In general, whenever  $\Lambda(t)$  has a maximum and subsequent decrease, the mixing vessel has stagnant regions or regions of fast and slow flows from inlet to effluent.

Although we cannot discuss all the details here, it is now well established that the RTD does not characterize *all* aspects of mixing (further discussion of this point from a variety of perspectives will be found in the references). The

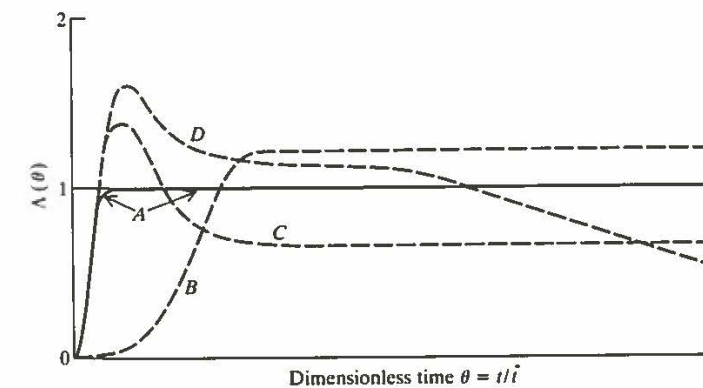


Figure 9.9 Intensity functions indicative of different types of imperfect mixing in stirred tank reactors (Ref. 16): A, Short delay between inlet and outlet (normal case); B, Delay between inlet and outlet due to insufficient stirring; C, Bypass between inlet and outlet; D, Bypass between inlet and outlet and stagnant regions due to insufficient stirring.

RTD indicates how long various "pieces" of effluent fluid have been in the reactor, but it does *not* tell us when fluid elements of different ages are intermixed in the vessel.

This point can perhaps be clarified by considering two limiting cases. In the first instance, suppose that fluid elements of all ages are constantly being mixed together. In other words, the incoming feed material immediately comes into intimate contact with other fluid elements of all ages. Such a situation, usually termed a state of *maximum mixedness*, prevails in the ideal CSTR. At the other extreme, fluid elements of different ages do not intermix at all while in the vessel and come together only when they are withdrawn in the effluent stream. In this case, which is called *complete segregation*, reaction proceeds independently in each fluid element: the reaction processes in one segregated clump of fluid are unaffected by the reaction conditions and rates prevailing in nearby fluid elements. Between these two limiting situations falls a continuum of small-scale mixing, or *micromixing*.

The RTD of a reactor is completely independent of its micromixing characteristics. Often, this is not a limitation because micromixing has a small effect on reactor performance. On the other hand, micromixing can influence reactor performance significantly in special situations. It has been suggested [16] that the sensitivity of reactor performance to micromixing can be usefully assessed by calculating reactor performance under the special cases of maximum mixedness and complete segregation. If substantial difference is obtained, the reactor is sensitive to micromixing and will be difficult to scale up. In such situations, predictability of scale-up will be enhanced by using a PFTR or something approximating it (see next section) because PFTR performance is micromixing insensitive regardless of the reaction network or kinetics.

In a reactor with complete segregation, each independent fluid element behaves like a small batch reactor. The effluent fluid is a blend of the products of these batch reactors, which have stayed in the system for different lengths of time. Restating this in mathematical terms, let  $c_{ib}(t)$  be the concentration of component  $i$  in a batch reactor after an elapsed time  $t$ , where the initial reaction mixture in the batch system has the same composition as the flow-reactor feed stream. So long as significant heating or volume change is not caused by the reaction(s), it makes no difference whether one or many different reactions are occurring. A fraction  $\mathcal{E}(t) dt$  of the reactor effluent contains fluid elements with residence times near  $t$  and hence concentrations near  $c_{ib}(t)$ . Summing over all these fractions gives the exit concentration  $c_i$  for the completely segregated reactor:

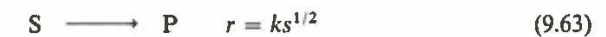
$$c_i = \int_0^{\infty} c_{ib}(t) \mathcal{E}(t) dt \quad (9.62)$$

In deriving Eq. (9.62), we assumed that reaction conditions ( $T$ , pH, dissolved oxygen, etc.) were effectively uniform in the "small-batch reactor" and in the mixing vessel characterized by the RTD. Here "effectively uniform" means that any differences in conditions which do exist have negligible or acceptably small effects on the bioreaction processes of interest. This assumption may well break

down in large-scale reactors in which substantial inhomogeneities in reaction conditions occur. The RTD for the vessel as a whole does not define how fluid within the vessel circulates through domains of different reaction conditions. Consequently, Eq. (9.62) can be used only to provide an estimate under conditions where appreciable nonuniformities exist in the bioreactor.

Certainly the individual cells or flocs of cells found in some biochemical reactors are segregated, so that application of Eq. (9.62) seems appealing. However, a rather subtle pitfall exists here. We must remember that living cells contain sophisticated control systems, with which they adapt and respond to their environment. Consequently, the changes which occur during batch culture reflect the combined and interactive influences of the medium and biological phases. Compositions in both of these phases change during the batch in a directly coupled fashion. Consequently, if a cell or floc in a flow system is to behave like the same small batch reactor observed in a batch experiment, it is necessary in general that the cell's environment (the surrounding fluid) also remain segregated in the flow system. If changes in medium composition do not play a critical role in the batch biological reactions, this requirement can be loosened and use of Eq. (9.62) can be better rationalized. Examples of such instances shall appear later in this chapter.

Returning now to the influence of micromixing, consider a single half-order irreversible reaction.



occurring in a stirred vessel which is completely segregated but has the same RTD as a CSTR. We might view the half-order reaction as an approximation to the Michaelis-Menten form over a rather narrow range of substrate concentrations. By computing  $s(t)$  for reaction (9.63) in a batch reactor and using this with Eq. (9.56) in Eq. (9.62) we find

$$s = s_0 \left\{ 1 - \frac{k\bar{t}}{s_0} \left[ 1 - \exp \left( -\frac{2s_0}{k\bar{t}} \right) \right] \right\} \quad (9.64)$$

On the other hand, if the same reaction takes place in an ideal CSTR, which has by definition micromixing at the maximum mixedness limit, the effluent substrate concentration is

$$s = s_0 \left\{ 1 - \frac{(k\bar{t})^2}{2s_0} \left[ -1 + \sqrt{1 + \frac{4s_0}{(k\bar{t})^2}} \right] \right\} \quad (9.65)$$

A general method for calculating conversion under maximum mixedness conditions in vessels with arbitrary residence times is described in Ref. 20.

From a practical design viewpoint, it is fortunate that reactor performance is often not too sensitive to micromixing. For example, for an irreversible second-order reaction in a CSTR, the maximum difference between the conversions at complete segregation and maximum mixedness is less than 10 percent. Thus, even in cases where it is known to be inexact, Eq. (9.62) may provide an adequate

approximation of reaction performance. [By series expansion of Eqs. (9.64) and (9.65), develop an expression for the relative difference,  $|1 - s(9.64)/s(9.65)|$ .]

For all single reactions with order less than unity, maximum substrate conversion is achieved at maximum mixedness. Complete segregation provides greatest conversions for reaction orders greater than one. As may be justified using the superposition principle for linear systems, the degree of micromixing does not influence first-order reactions. Thus, for one or more reactions with first-order kinetics, Eq. (9.62) may be used independent of micromixing state.

Another exploitation of RTD data is the evaluation of parameters in various nonideal-flow reactor models. A variety of such models is considered in the next section.

### 9.3.3 Models for Nonideal Reactors

Obviously the RTD contains useful information about flow and mixing within the vessel. One way the  $\mathcal{E}$  and  $\mathcal{F}$  functions can be used is to assess the extent of deviation from an idealized reactor. For example, we calculated  $\mathcal{E}$  and  $\mathcal{F}$  above for an ideal CSTR. By comparing these curves with those for a real vessel, we can get an idea of how well the actual system approximates complete mixing.

Different kinds of nonidealities often have distinctive manifestations in the observed response functions. We can gain some appreciation of them by constructing models representing various sorts of deviations from the idealized mixing system. Examples are shown in Fig. 9.10. Case (a) is the ideal CSTR, case (b)

Combined model schematic

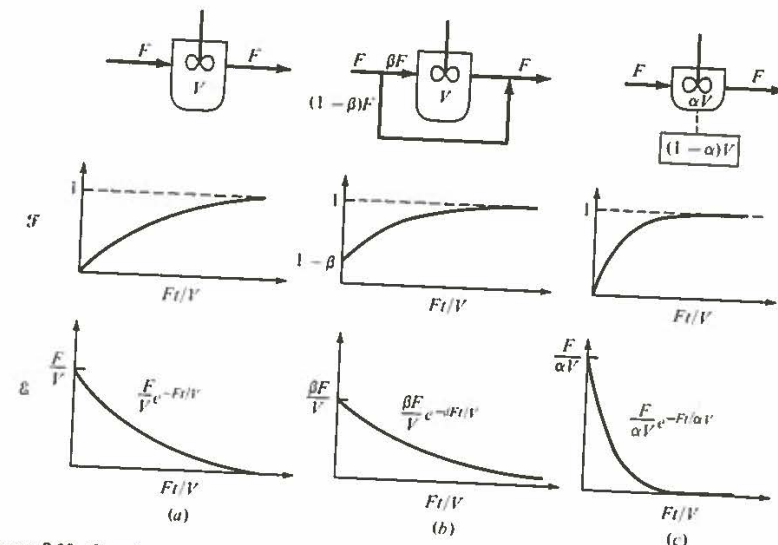


Figure 9.10  $\mathcal{F}$  and  $\mathcal{E}$  functions for (a) an ideal CSTR, (b) a CSTR with bypassing, and (c) a CSTR with a dead zone.

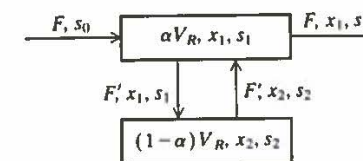


Figure 9.11 Model for an incompletely mixed CSTR with a stagnant region.

involves bypassing of the feed stream, and there is a dead volume  $(1 - \alpha)V_R$  in case (c). When there is bypassing, tracer appears immediately in the  $\mathcal{F}$  function, while a dead region results in faster decay of the  $\mathcal{E}$  curve than in the ideal case.

Another useful and commonly applied model for a nonideal continuous-flow stirred reactor uses two interconnected ideal CSTRs (Fig. 9.11). Here the reactor contents have been divided into two smaller, completely mixed regions. The feed and effluent streams pass through region 1, whose volume is a fraction  $\alpha$  of the total reactor volume. In turn, region 1 exchanges material with stagnant region 2 at volumetric flow rate  $F'$ . If we assume Monod growth kinetics with constant yield factor, the following mass balances describe steady-state conditions in this system:

$$x_1 = Y_{X/S}(s_0 - s_1) \quad \text{region 1 substrate} \quad (9.66a)$$

$$x_2 - x_1 = Y_{X/S}(s_1 - s_2) \quad \text{region 2 substrate} \quad (9.66b)$$

$$x_2 + \alpha\gamma\mu_{\max} \frac{s_1}{K_s + s_1} x_1 = (1 + \gamma D)x_1 \quad \text{region 1 cells} \quad (9.66c)$$

$$x_1 + (1 - \alpha)\gamma\mu_{\max} \frac{s_2}{K_s + s_2} x_2 = x_2 \quad \text{region 2 cells} \quad (9.66d)$$

where  $\gamma = \frac{V_R}{F'}$   $D = \frac{F}{V_R}$  = nominal dilution rate (9.67)

The dilution rate at washout for this model is obtained by setting  $s_0 = s_1 = s_2$  in Eqs. (9.66) to obtain

$$D_{\text{washout}} = \frac{\mu_{\max} s_0}{K_s + s_0} \left[ 1 + \frac{(1 - \alpha)^2 \gamma \mu_{\max} s_0}{K_s + s_0 - (1 - \alpha)\gamma \mu_{\max} s_0} \right] \quad (9.68)$$

Since the first expression on the right-hand side is identical to the washout dilution rate for the perfectly mixed system [Eq. (7.16)], the effect of incomplete mixing is to increase the value of  $D_{\text{washout}}$ . If the bracket on the right-hand side of Eq. (9.68) happens to be negative, it indicates that washout is impossible. (What does this mean physically?)

Figure 9.12 shows the effluent cell concentration  $x_1$  and biomass productivity  $x_1 D$  as functions of the dilution rate for  $\gamma = 0.5$  and a variety of volume fractions  $\alpha$ . In this figure, which was computed using the  $K_s$  and  $s_0$  values from Fig. 7.10, the change in the  $x$ -vs.- $D$  curve as  $\alpha$  changes from 1 (perfect mixing)

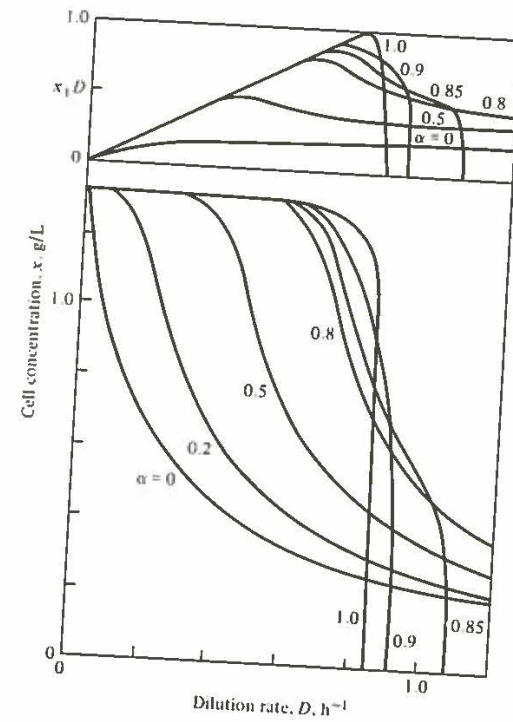


Figure 9.12 Exit cell concentration  $x_1$  as a function of dilution rate  $D$  and active zone volume fraction  $\gamma$  for dead zone model of Fig. 9.11. The upper portion of the figure shows biomass production rate  $x_1 \cdot D$  ( $\gamma = 0.5$ ).

to 0.9 or 0.85 (small stagnant zone) is very similar to the difference between the chemostat theoretical and experimental data given in Fig. 7.10. Moreover, the value  $\alpha = 0.9$  corresponds roughly to the vessel volume fraction above the impeller in the experimental reactor used to obtain Fig. 7.10.

In examining RTDs so far we have concentrated on reactors with continuous flow of medium and cells, but we should remember that a gassed-batch bioreactor has continuous throughput of gas. Thus, RTD measurements have been used to characterize gas holdup and mixing in batch reactors. These studies indicate major effects of type of contactor employed and reaction mixture rheology. For example, a CSTR in series with a PFR gives RTD behavior closely approximating measured gas RTDs in mechanically agitated tanks for water, water-salt, and *Saccharomyces cerevisiae* suspensions which all have low viscosities. On the other hand, in high viscosity solutions in agitated tanks, more complicated gas RTD behavior is evident. Figure 9.13 shows the measured internal age distribution for sparged gas flow through a 10 g/L suspension of *Penicillium chrysogenum* in an agitated vessel of standard dimensions. Here, a plug-flow element must be added to the model of Fig. 9.11 in order to fit the experimental result.

This type of model, commonly called a *combined model* or a *mixed model*, consists of interconnected idealized reactor types. It is but one of a wide class of

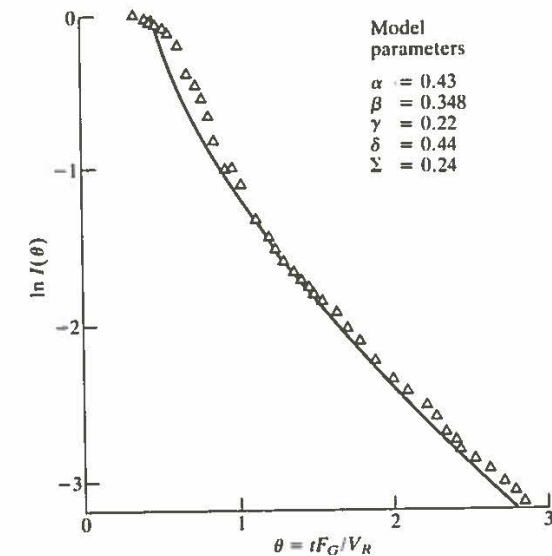
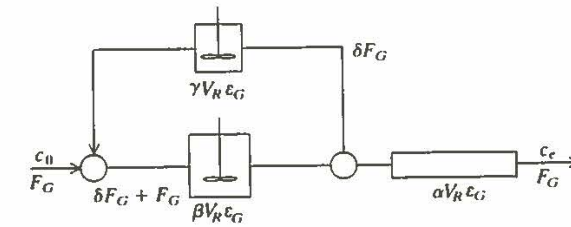


Figure 9.13 Experimentally measured internal age distribution for gas in an agitated vessel ( $\Delta$ ). The solid line is the internal age distribution calculated from the mixed model shown above with the parameter values indicated. (Reprinted by permission from M. Popović, A. Papalexiou, and M. Reuß, "Gas Residence Time Distribution in Stirred Tank Reactors," VI International Fermentation Symposium, London, Canada, 1980.)

possible representations of incomplete mixing. Combined models have the advantages of serving at once as a useful conceptual tool for thinking about flow and mixing in the reactor, as a basis for computing the performance of the nonideal vessel as a reactor, and as a guide for constructing laboratory reactors to study effects of nonidealities in large-scale equipment.

Once a combined model such as any of those shown above has been adopted to describe a particular nonideal bioreactor, the combined model can be used to calculate the performance of the vessel as a reactor. That is, the reaction kinetic expressions and material balances on substrates, products, and reaction effectors are written and solved in the context of the combined model network. This



procedure has already been illustrated above in Eqs. (9.66) for the combined model in Fig. 9.11 and simple Monod kinetics. However, we must be cautious and recognize the potential limitations in this approach, since a combined model, while adjusted to be consistent with the actual reactor RTD, will not in general possess identical micromixing and circulation characteristics compared to the real system. Accordingly, the combined model may fail to approximate reasonable system performance as a reactor. For example, the combined models shown in Fig. 9.11 will give the same RTD if the plug-flow tube element is put at the start rather than at the end of the network, but these two configurations will not give the same results for nonlinear kinetics. However, they will give the same output for a reaction network consisting entirely of first-order kinetics or for a first-order process such as mass transfer.

Although still subject to the limitations just described, mixed models can be extended in some situations to encompass nonuniform reaction conditions. Often there is a reasonable intuitive physical correspondence between the different ideal regions in a combined model and actual physical domains and environments within a bioreactor. For example, we have already mentioned in connection with the combined model of Fig. 9.11 that one region might represent the impeller zone and the other region the bulk of the tank. If air sparging enters the system near the impeller, it is reasonable to consider the dissolved oxygen level to be relatively high in that part of the combined model and the dissolved oxygen level to be relatively low in the bulk of the tank far from the impeller in a large-scale reactor. Thus, we could superimpose on the different interconnected tanks estimates or measured values of reaction conditions in different zones of a bioreactor and take these into account when calculating reactor performance.

In such situations, our knowledge of the biological kinetics may be inadequate to simulate reaction behavior properly under such fluctuating conditions. We shall return to this topic in the following section. To the extent that a combined model with different reaction conditions in different ideal elements is useful in describing the behavior of real, large-scale bioreactors, we can see now one approach to the problem of *scale-down*. Scale-down refers to a reasonable method for designing small-scale experiments in the laboratory to attempt to simulate and to study operation of nonideal large-scale reactors. Since the ideal systems, especially CSTRs, can be well approximated on a small scale, using a set of small reactors and pumps and interconnections, we can set up on a small scale in the laboratory the physical counterpart of the combined model. We can, in this model, scaled-down system, apply different levels of mixing intensity in different tanks, different aeration levels, different pH values, and other tank-to-tank variations in order to try to study and simulate the effects of such nonuniformities on performance and on biological reaction kinetics in large-scale systems. This approach is applicable to batch reactors as well as to continuous-flow reactors.

Different types of combined models involving a sequence of ideal CSTRs (Fig. 9.14) are usually used to simulate staged and column bioreactors and mixing configurations which more closely approximate plug flow. We can calculate the RTDs for these models by again setting up tracer mass balances on the

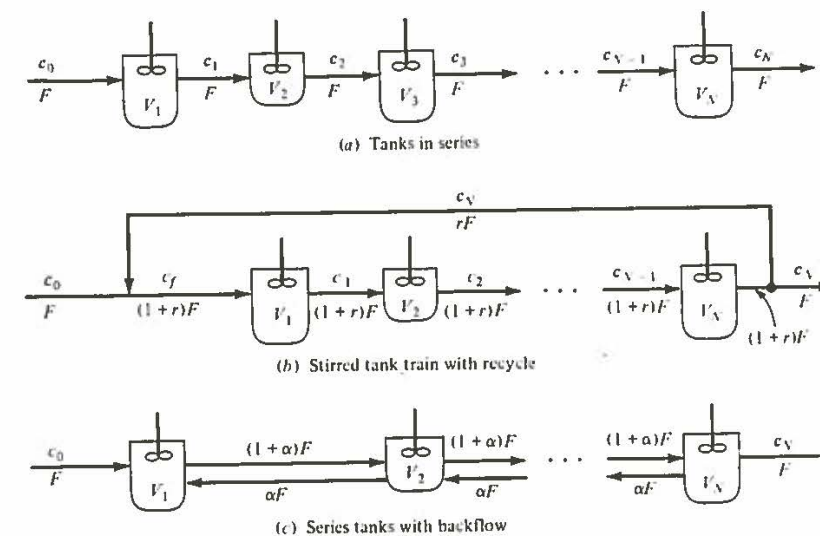


Figure 9.14 Schematic diagrams of different tanks in series designs and models: (a) tanks in series; (b) stirred tank train with recycle; and (c) series tanks with back flow.

stirred-vessel cascade and evaluating the response to a unit-impulse input. Carrying out the necessary algebra for the system of Fig. 9.14a subject to the usual assumption that the total reactor volume  $V_R$  is divided into  $N$  equally sized tanks

$$V_1 = V_2 = \dots = V_N = \frac{V_R}{N} \quad (9.69)$$

gives

$$\mathcal{E}(t) = \frac{N^N}{(N-1)!} \left( \frac{NF}{V_R} \right)^{N-1} t^{N-1} \exp\left(-\frac{NF}{V_R} t\right) \quad (9.70)$$

Plots of this function for a variety of  $N$  values are given in Fig. 9.15. The shift in  $\mathcal{E}(t)$  with increasing  $N$  from an exponential decay to a pulse at  $t = V_R/F$  is apparent.

The variance of the RTD in Eq. (9.70) is

$$\sigma^2 = \frac{1}{N} \quad (9.71)$$

This relationship is useful in developing a series CSTR model for an arbitrary vessel whose RTD has been experimentally determined. Taking the total staged-CSTR system volume  $V_R$  and flow rate  $F$  as in the actual process makes the mean residence time for the model match that of the real vessel. Taking  $N$  equal to the reciprocal of the experimentally measured variance for the real vessel RTD then

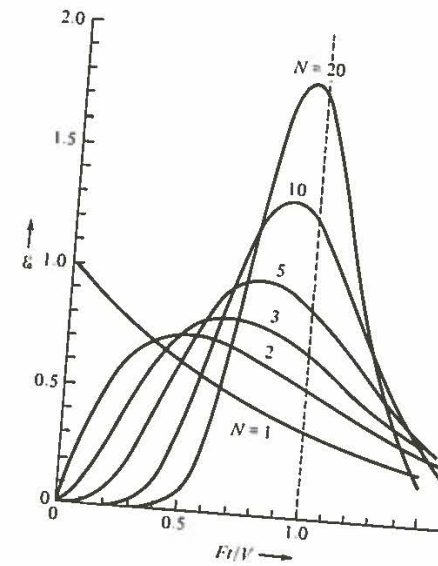


Figure 9.15 RTDs for  $N$  ideal CSTRs in series ( $V_R$  = total system volume, individual reactor volumes =  $V_R/N$ ).

ensures that the series-CSTR model RTD has the same second moment as the vessel of interest. If the vessel's RTD has a shape similar to those given in Fig. 9.15, the tanks-in-series model so derived will probably provide an adequate approximation of the real reactor's performance. (Remember that identical RTDs guarantee identical reactor performances only for total segregation or first-order kinetics). Notice as  $N \rightarrow \infty$ , the RTD for this model approaches that for an ideal PFR.

Figure 9.16 shows the results of experimental RTD studies of cocurrent perforated plate towers. In both experiments three plates separated the column into four sections, but in case 1 the plates had 3-mm holes; 2-mm holes were used in case 2, with the total hole area held at 10 percent in both instances. Comparing the experimental RTDs with the theoretical result for  $N = 4$  in Fig. 9.16 reveals that the plates with 2-mm holes provide good staging. Evidently there is some backflow through the plate perforations when they exceed the 2-mm size. Thus, in this case RTD data provide a useful design guideline for preserving the desired segregation in the tower.

Sometimes the addition of a growing microbial phase to a reactor dramatically alters its RTD. In the measured RTD of Fig. 9.17a, the eight-plate tower with no growing organisms exhibits a clear staging effect. When baker's yeast is grown in the same system, however, the RTD measured by a variety of tracers closely corresponds to an ideal CSTR (solid curve in Fig. 9.17b) rather than to an eight-CSTR cascade. This breakdown in staging effect is apparently due to sedimentation of the yeast suspension. By changing the column design so that four plates had only 3 percent hole area, the RTD with yeast growth became nearly that of a four-CSTR cascade.

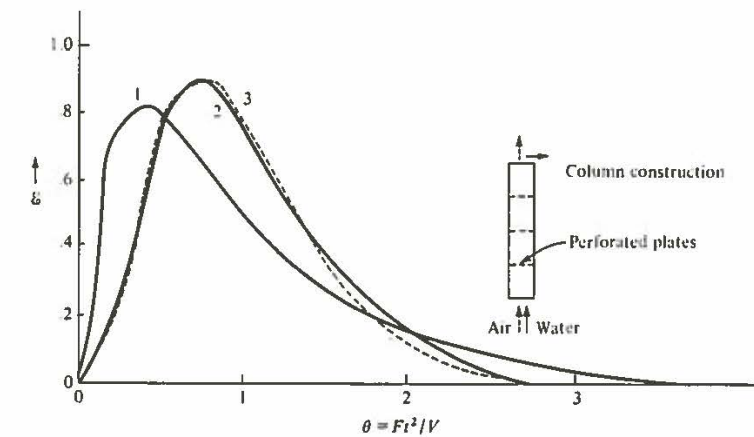


Figure 9.16 RTD data showing flow characteristics of a cocurrent perforated plate column. (1) Hole diameter = 3 mm, plate-area fraction = 0.0981, (2) hole diameter = 2 mm, area fraction = 0.0975, (3) calculated from four CSTRs-in-series model. (Reprinted from A. Ketai et al., "Performance of a Perforated Plate Column as a Multistage Continuous Fermentor," *Biotech. Bioeng.*, vol. 11, p. 911, 1969.)

Next we examine the performance of the CSTR cascades in Fig. 9.14 as bioreactors. The mass balance on an arbitrary component  $c$  in the  $j$ th tank is

$$F c_{j-1} - F c_j + V_j r_{fc} \Big|_{\text{tank } j} = 0 \quad (9.72)$$

For example, if we consider microbial growth in the tanks-in-series system with non-sterile feed ( $x_f \neq 0$ ), the biomass balances for tanks 1 through  $N$  are

$$\begin{aligned} F(x_f - x_1) + V_1 \mu_1 x_1 &= 0 \\ F(x_{j-1} - x_j) + V_j \mu_j x_j &= 0 \quad j = 2, 3, \dots, N \end{aligned} \quad (9.73)$$

These equations can be solved recursively to yield

$$x_1 = \frac{F x_f}{F - V_1 \mu_1} \quad (9.74)$$

and

$$x_j = \frac{F^{j-1} x_1}{(F - \mu_2 V_2)(F - \mu_3 V_3) \dots (F - \mu_j V_j)} \quad j = 2, \dots, N \quad (9.75)$$

For the case of equal volumes, the simpler form

$$\frac{D_1^{j-1} x_1}{(D_1 - \mu_2)(D_1 - \mu_3) \dots (D_1 - \mu_j)} \quad (9.76)$$

results from Eq. (9.75). Here  $D_1$  is the dilution rate of an individual tank ( $= F/V_1$ ).

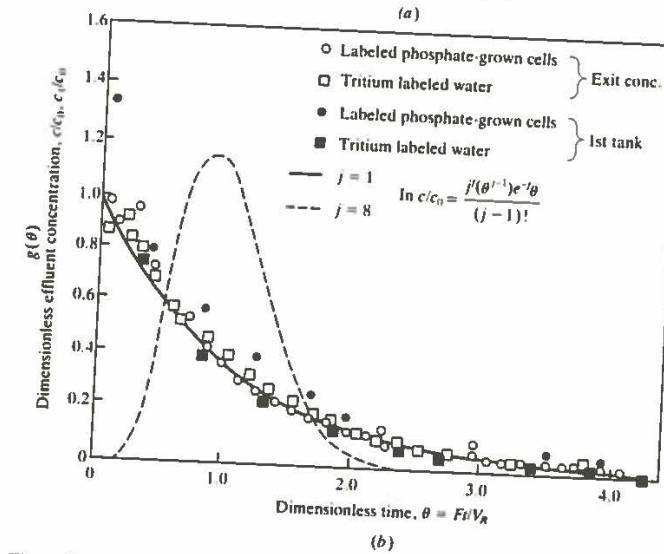
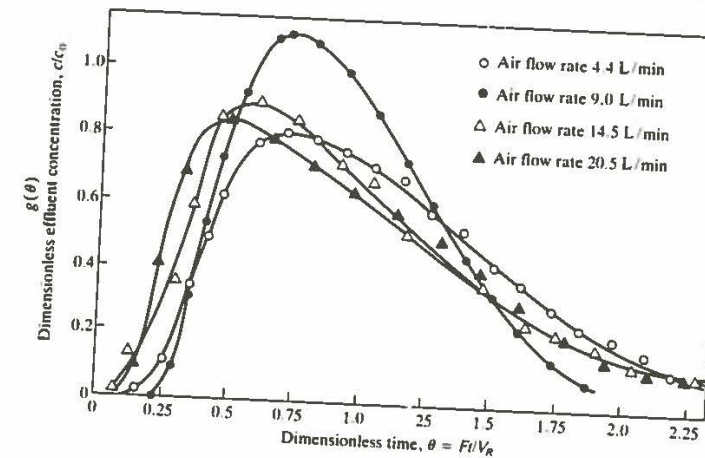


Figure 9.17 Measurement of RTD in an eight-plate tower (hole void fraction = 0.15) by different methods and under different operating conditions. (a) Salt tracer data show that the increased aeration flattens and broadens the residence time distribution. (b) Yeast cells present in the column; both labeled water and labeled cells used as tracers. (A. Prokop et al., "Design and Physical Characteristics of a Multistage, Continuous Tower Fermentor," Biotech. Bioeng., vol. 11, p. 945, 1969.)

We can deduce the effect of staging and recycle on the washout dilution rate  $D_{max}$  by examining the system of Fig. 9.14b. Assuming Monod growth kinetics with a maintenance term [Eq. (7.22)], sterile feed, equal volumes, and a constant yield factor, it has been shown that  $D_{max}$  satisfies

$$\frac{\mu_{max}}{D_{max}} = \frac{N(1 + K_s/s_0)\{1 - [r/(1+r)]^{1/N}\}}{1 - (k_e/\mu_{max})(1 + K_s/s_f)} \quad (9.77)$$

where as usual  $D$  is defined in terms of the overall process

$$D = \frac{F}{V_R} = \frac{F}{NV_1} \equiv \frac{D^*}{N} \quad (9.78)$$

Setting  $r = 0$  in Eq. (9.77) gives the critical dilution rate for the equal-volume cascade without recycle. If in addition to  $r = 0$ , we take  $k_e = 0$  so that the growth kinetics is of classical Monod form, Eq. (9.77) reduces to the familiar expression [see Eq. (7.16)].

$$D_{max}^* = \frac{\mu_{max}s_0}{K_s + s_0} \quad (9.79)$$

This result is expected on intuitive grounds: if washout occurs in the first tank in the equal-volume train, it will also prevail in the second, third, ..., and  $N$ th tank. (What happens in the nonequal-volume case if  $F > V_j D_{max}^*$  for  $j = 1, 2, \dots, k-1$  and  $F < V_k D_{max}^*$ ?)

A close conceptual analog of the CSTR cascade with backflow (Fig. 9.14c) is the dispersion model. A modification of the ideal PFTR, the dispersion model is derived by considering an axial diffusion process which is superimposed on the convective flow through the tube. Returning to the thin-section model described in Fig. 9.5, we add a dispersion flow  $A(D_z dc/dz)_z$  into the section and subtract a similar term  $A(-D_z dc/dz)_{z+\Delta z}$  for diffusion out of the thin slice on the left-hand side of Eq. (9.13). The same manipulations and limiting processes as followed that equation produce the dispersion-model mass balance

$$\frac{d(uc)}{dz} = \frac{d}{dz} \left( D_z \frac{dc}{dz} \right) + r_f c \quad (9.80)$$

Usually  $u$  and the effective axial dispersion coefficient  $D_z$  are approximately constant for liquids, so that Eq. (9.80) becomes

$$u \frac{dc}{dz} = D_z \frac{d^2c}{dz^2} + r_f c \quad (9.81)$$

Since Eq. (9.81) is a second-order differential equation, two boundary conditions are required. The generally accepted ones are

$$uc_f = \left( uc - D_z \frac{dc}{dz} \right)_{z=0} \quad (9.82)$$

$$\left. \frac{dc}{dz} \right|_{z=1} = 0 \quad (9.83)$$

When  $D_z$  is not too large, which is often the case, the complicated condition (9.82) can be replaced by

$$c \Big|_{z=0} = c_f \tag{9.84}$$

In this case the variance of the dispersion-model RTD is

$$\sigma^2 = \frac{2}{\text{Pe}} \left[ 1 - \frac{1}{\text{Pe}} (1 - e^{-\text{Pe}}) \right] \tag{9.85}$$

where the axial Peclet number  $\text{Pe}$  is defined by

$$\text{Pe} = \frac{uL}{D_z} \tag{9.86}$$

Physically  $\text{Pe}$  may be regarded as a measure of the importance of convective mass transport ( $\approx uc$ ) relative to mass transport by dispersion ( $\approx D_z c/L$ ). Considering the limits of Eq. (9.85) as  $\text{Pe} \rightarrow 0$  and  $\text{Pe} \rightarrow \infty$ , we see that the former case gives  $\sigma^2 = 1$ , which is identical to the ideal CSTR variance. In the limit of very large Peclet numbers,  $\sigma^2 \rightarrow 0$ , which corresponds to plug flow. As with the tanks-in-series model, Eq. (9.85) can be used to evaluate  $\text{Pe}$  for the dispersion model from an experimentally determined  $\sigma^2$ . When Monod kinetics with maintenance is used, the dilution rate  $D_{\text{max}}$  at washout for the dispersion model is given by

$$\frac{\mu_{\text{max}}}{D_{\text{max}}} = \frac{\frac{1}{4} \text{Pe} (1 + K_s/s_f)}{1 - (k_c/\mu_{\text{max}})(1 + K_s/s_f)} \tag{9.87}$$

As the relative influence of dispersion becomes vanishingly small ( $\text{Pe} \rightarrow 0$ ),  $D_{\text{max}}$  decreases to zero. This agrees intuitively with the notion that an ideal PFTR with sterile feed will not support a biological population.

It is important to realize that the axial dispersion coefficient  $D_z$  is *not* usually equal to molecular diffusivity. It is a modeling parameter which, when chosen properly, allows the dispersion model to represent some of the mixing effects of several physical phenomena. We shall mention three here: laminar flow in tubes, turbulent flow in pipes, and flow in packed beds.

If axial and radial diffusion characterized by diffusivity  $\mathcal{D}$  is superposed on axial convective transport by laminar flow, it can be shown that an effective axial dispersion coefficient is given by

$$D_z = \mathcal{D} + \frac{\bar{u}^2 d_t^2}{192\mathcal{D}} \tag{9.88}$$

Here  $\bar{u}$  denotes the average axial velocity ( $= \frac{1}{2}$  centerline velocity). The dispersion model with  $D_z$  given by Eq. (9.88) provides an excellent approximation to the RTD for laminar flow with diffusion provided the tube is long enough ( $L \gg d_t^2/40\mathcal{D}$ ).

In turbulent flow in pipes ( $\text{Re} > 2100$ ), motion of macroscopic eddies of fluid provides an important mechanism for mass, momentum, and energy transport. The effects of eddy transport closely resemble those of molecular-diffusion processes, but turbulent-diffusion fluxes are usually much greater in magnitude than their molecular counterparts. Consequently, the effective dispersion coefficient in this case depends mostly on the state of fluid flow. While the turbulent-flow Peclet number is typically of the order of 3, it falls with decreasing Reynolds number. This trend in turbulent flow as well as a variety of laminar-flow data are displayed in Fig. 9.18. Perhaps the most important biological reactor involving flow in empty tubes is the continuous liquid sterilizer, which is examined in detail in the following section.

In some reactors with immobilized biocatalysts the tube is packed with particles. These particles are fixed in the bed while the fluid flows around the particles and through the tube. Because fluid is constrained to flow in the interstices between pellets, a fluid element passing axially through the bed undergoes something like a random walk in the radial dimension. The effect of this particle-interrupted sojourn on the RTD of the system can be described by the dispersion

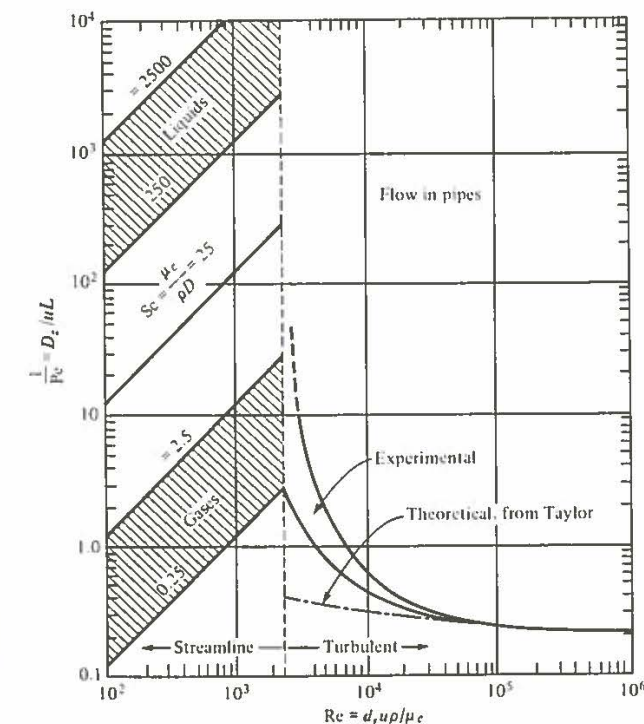


Figure 9.18 Correlations for the axial Peclet number ( $\text{Pe}$ ) in terms of the Reynolds ( $\text{Re}$ ) and Schmidt ( $\text{Sc}$ ) numbers for fluid flow in pipes.

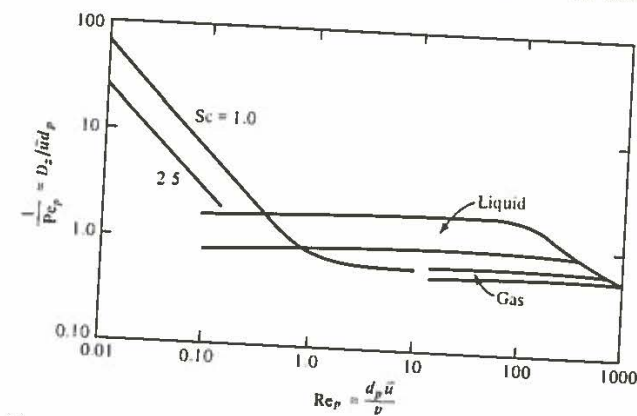


Figure 9.19 Correlations for the axial Peclet number  $Pe_p$  for flow in packed pipes. Notice that the dimensionless groups are based upon particle diameter  $d_p$  rather than the pipe diameter  $d_c$ .

model. Theory suggests that an axial Peclet number based on particle diameter,  $Pe_p$ , defined by

$$Pe_p = \frac{\bar{u}d_p}{D_z} \quad (9.89)$$

is approximately 2 in this instance, where  $d_p$  is the pellet diameter. Experimental studies confirm this result under some circumstances, but dependence of  $Pe_p$  on  $Sc$  and  $Re_p$  is apparent in Fig. 9.19.

In closing this discussion of dispersion-producing processes, we should note that there are many additional possibilities, including pipe bends and gradations in depth contours in rivers and streams. Theory is of little help in identifying  $D_z$  for these complicated flow situations, and we must consequently rely on measured RTD data to determine an appropriate  $D_z$  value.

The tanks-in-series and dispersion models are both one-parameter ( $N$  and  $D_z$ , respectively) nonideal mixing models. In different fashions each spans a continuum of mixing and segregation states ranging from ideal CSTR to ideal PFTR. Thus we are faced with a choice of which model to use. In terms of convenience of computation and analysis, the tanks-in-series representation is usually far superior. Also application of the dispersion model is prone to difficulty when backmixing ( $\sigma^2$ ) is large. However, Fig. 9.14 shows that a very large number of tanks is necessary to represent situations near plug flow. Consequently, as a general rule of thumb, the dispersion model is usually preferable for small deviations from plug flow (say  $\sigma^2$  of the order of 0.05 and smaller), while the tanks-in-series formulation is superior when there is substantial backmixing ( $\sigma^2 \geq 0.2$ ). This latter case is typical of fermentors and biological waste-treatment basins. The first is encountered in continuous sterilization of liquids, considered later in this chapter.

### 9.3.4 Mixing-Bioreaction Interactions

Flow and transport phenomena on different scales influence the kinetic behavior of cells. Effects imposed at a certain length scale (recall Fig. 9.2) can influence the observed kinetics of cell populations in different ways. It is important to recognize this connection so that kinetic measurements and models can be developed under conditions which will resemble in some senses those encountered in the large-scale reactor. In this section we examine some of the interactions of cellular kinetics and mixing in bioreactors.

We shall begin at the largest scale in which bulk circulation patterns carry the cells into different regions of the reactor which, as noted before, typically have different dissolved oxygen and turbulence levels in large-scale equipment. The role of bulk circulation in influencing overall cellular kinetics can be appreciated using a simple example. Suppose that oxygen is supplied locally at some region of the reactor (as occurs in a stirred tank) and that utilization of oxygen occurs in segregated fluid elements circulating in the reactor. This is not an unreasonable view for highly viscous fermentation situations. If one starts with a saturated oxygen concentration in water of  $0.3 \text{ mol m}^{-3}$  and considers reasonable oxygen uptake rates in the range of  $10\text{--}100 \text{ mol h}^{-1} \text{ m}^{-3}$ , oxygen will be exhausted in a segregated fluid element after 11 to 50 s. This is of the same order of magnitude as the mixing time in a large-scale reactor.

In order to put this impact of fluid circulation in a more quantitative and general perspective and to take into account the statistical distribution of circulation times, we shall examine the performance characteristics of a batch reactor in which the circulation time distribution is  $f_c(t)$ . Further, we assume that a zero-order reaction occurs in completely segregated fluid elements. Extension to other types of local reaction kinetics such as Michaelis-Menten kinetics is straightforward and only slightly complicates the calculations involved. The qualitative conclusions, however, remain the same. For such a zero-order reaction, with rate constant  $k_0$  and with initial reactant concentration  $s_0$ , the concentration in a fluid element varies with time according to

$$s(t) = \begin{cases} s_0 - k_0 t & t \leq t_e = k_0/s_0 \\ 0 & t > t_e \end{cases} \quad (9.90)$$

Here we define time  $t_e$  for nutrient exhaustion which is equal to  $k_0/s_0$ . We shall define  $F$  here as the fraction of time a fluid element spends in conditions where nutrient has been completely exhausted. This fraction can be computed using

$$F = \int_{t_e}^{\infty} f_c(t) \left( \frac{t - t_e}{\bar{t}} \right) dt \quad (9.91)$$

where  $\bar{t}$  denotes the mean circulation time. Assuming that  $f_c(t)$  is a log-normal distribution [Eq. (9.43)], Eq. (9.91) has been evaluated for different relative values of the parameters  $\bar{t}$ ,  $t_e$ , and the standard deviation  $\sigma$  of the mixing time distribution. Results indicated in Fig. 9.20 illustrate clearly that exposure of cells to starvation conditions increases as the mean circulation time and as the

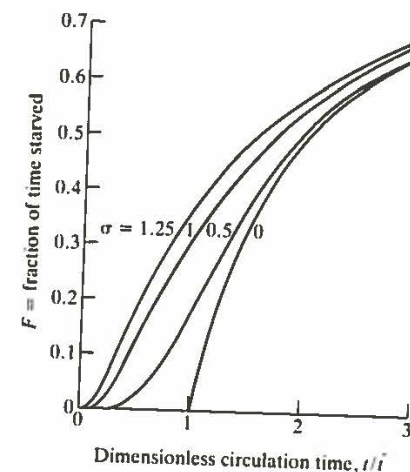


Figure 9.20 The fraction of time cells in circulating fluid elements are starved as a function of the dimensionless circulation time and the coefficient of variation of the circulation time distribution (Ref. 19).

standard deviation of circulation times increase. The quantity  $1 - F$  may be interpreted as the yield of the bioreactor relative to the yield that would have been obtained with nutrient provided at all points in the vessel. This calculation indicates that, for a given circulation time, it is preferable to design the reactor so as to minimize the dispersion of mixing times about the mean.

The model just considered, while informative, does not take into account the effects which transient environmental conditions encountered during sojourns around the reactor may have upon cellular kinetics. As noted in Fig. 9.1, the time scales for circulation in large scale bioreactors are comparable to the time scales for certain metabolic processes and adjustments, indicating that kinetic models developed under much different mixing conditions in a small reactor may not apply when greater mixing times and greater reaction environment fluctuations are encountered at larger scale.

Experiments conducted with the on-line fluorometer system described in Sec. 10.2 clearly illustrate the similarity of mixing and biological response times. Mixing times in an aerated (0.5% v/v) 70-L, mechanical agitated fermentor with 40-L working volume have been measured by injecting pulses of quinine in 0.05 M  $H_2SO_4$  solution and measuring transients in culture fluorescence. This measurement characterizes fluid circulation and mixing processes in the reactor. Subsequently, fluorescence responses were measured after pulse addition of glucose to a yeast culture. Here, the fluorescence is produced by intracellular reduced pyridine nucleotides, the levels of which are highly sensitive to the rate of glucose reaction in the cell. Thus, the second measurement provides information on the response time of the complete sequence of transport processes (bulk mixing  $\rightarrow$  diffusion to cells  $\rightarrow$  transport into cell) and metabolic reactions involved in nutrient use.

Table 9.3 shows the mixing time and the overall substrate utilization response time in this reactor at different stirring speeds. Interestingly, the biological

Table 9.3 Comparison of reactor mixing times and yeast glucose response time (all in seconds) as a function of mixing rate in a 70-L (40-L working volume) stirred bioreactor with 0.5 v/v/m aeration.

(Reprinted by permission from A. Einsele, D. L. Ristroph, and A. E. Humphrey, "Mixing Times and Glucose Uptake Measured with a Fluorometer," *Biotech. Bioeng.*, vol. 20, p. 1487, 1978.)

	200 rpm	500 rpm	700 rpm
Intracellular fluorescence response time	8.5	6.8	5.9
Bulk mixing response time	4.2	2.5	1.5
Difference = biological response time	4.3	4.3	4.4

response time for local glucose uptake and utilization is, as might be expected on intuitive grounds, essentially the same in all three cases, while the mixing time is reduced as agitation speed is increased. Another very significant fact indicated by these data is the similarity in order of magnitude for the response time for local glucose uptake and utilization and the mixing time for the reactor. This indicates that, as cells circulate in the reactor and encounter spatially inhomogeneous conditions, the metabolism of the cell may always be in a transient state since it does not respond much more rapidly than the characteristic time scale for environmental fluctuations due to liquid circulation.

Several experimental investigations have explored the influence of transient conditions on metabolism and noted significant effects. In a closed tubular-loop fermentor in which oscillations in dissolved oxygen levels are encountered around the loop, a culture of *Candida tropicalis* showed increased biomass yield based on substrate, reduced oxygen utilization for biomass production, and lower respiratory quotient. Opposite effects were observed in imposed oscillations in dissolved oxygen level in a continuous culture in *Pseudomonas methylotropha* ASI with methanol and carbon and energy source. In this case, decreased biomass to substrate yields and decreased growth rates were observed. In another experimental study, sinusoidal fluctuations of dissolved oxygen level with a period of 2 min. and a mean of 30% of air saturation were imposed on a culture of *Penicillium chrysogenum* P1. In this case, the specific penicillin production rate decreased significantly, resembling the effect expected at a lower mean dissolved oxygen level. This shift indicates a significant transient nonlinear effect on the bioreaction.

Turning now to the smaller scale of turbulent velocity fluctuations, we can expect important interactions between the turbulence intensity at different scales and the morphology (and thereby potentially the metabolic state) of certain organisms. This connection is expected to be most important for those organisms that grow to a size scale comparable to the turbulence scales expected. These scales range from the largest eddies, on the scale of the height of a turbine blade in an agitator, say 0.1 m, to the smallest eddies which are produced by the

cascade of transmission of turbulent energies (Sec. 8.3). In agitated bioreactor systems, this smallest eddy size is of the order of 20–100  $\mu\text{m}$ . To determine the biological structures influenced by velocity fluctuations on this scale, we can note in Fig. 9.2 that flocs of microorganisms and mycelial aggregates are intermediate in the size spectrum of turbulence and therefore will be substantially influenced by mixing intensity and the distribution of turbulence fields encountered in the reactor.

We have already discussed the effects which overall cellular aggregate size can have on overall rates due to diffusion limitation. Here we shall concentrate on more subtle effects which involve changes in morphological structure and metabolic state which substantially influence the fermentation. One interesting example of this class is the influence of mixing intensity upon growth, product formation, and nucleotide leakage from various mutants of *Aspergillus niger* which produce high levels of citric acid. As indicated in Fig. 9.21, the total biomass productivity increases with increasing agitation strength, but the dependence of citric acid production on agitation intensity is more complicated, exhibiting strong maxima with respect to agitation intensity for the three mutants considered. Parallel studies of nucleotide release as a function of agitation speed showed patterns which depended upon the strain. For some strains, increasing mixer speed gave higher levels of released nucleotides while for one strain the opposite and unexpected effect of decreasing nucleotide release at higher mixer speeds was noted. The effect of mixer speed on morphology of the mycelium for this unusual mutant is shown in Fig. 9.22. Here in micrographs of the organisms

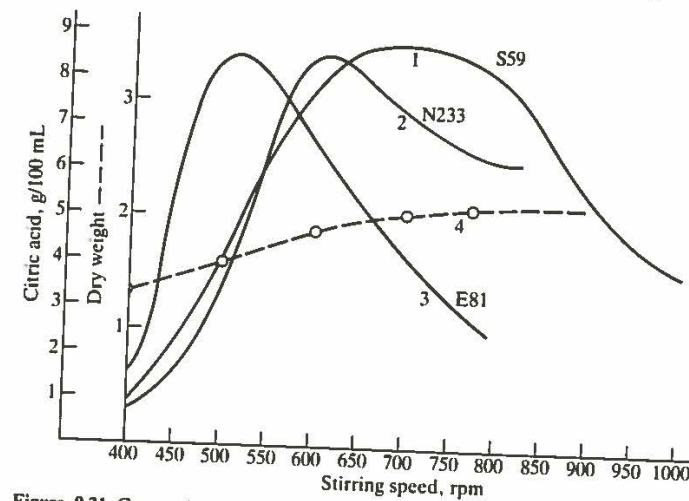
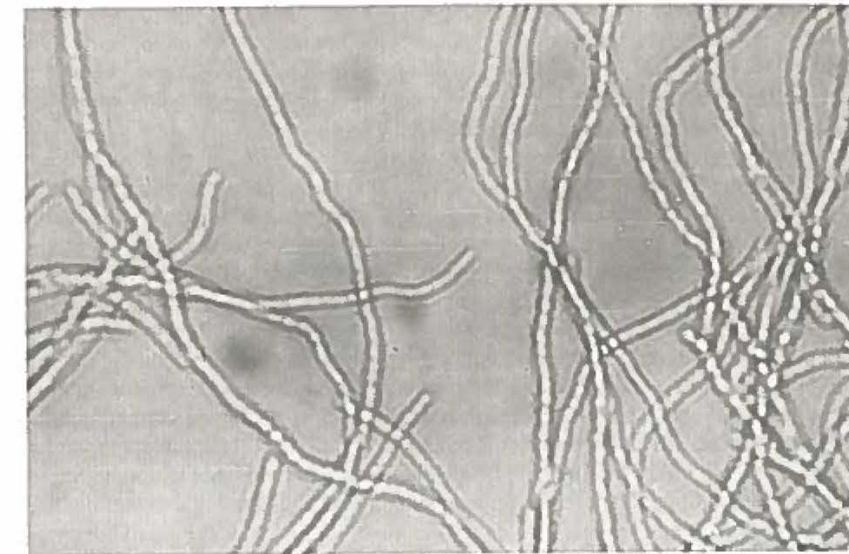
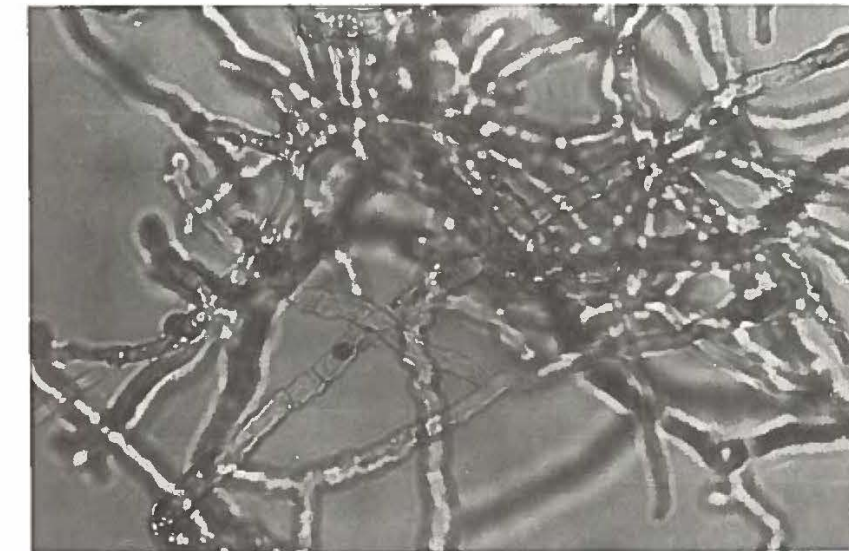


Figure 9.21 Curves 1 through 3 show citric acid accumulation after seven days' fermentation at different turbine agitation rates for *Aspergillus niger* strains S59, N233, and E81, respectively. Curve 4 is the corresponding biomass dry weight for strain S59. (Reprinted by permission from E. Ujcová, Z. Fencel, M. Musílková, and L. Seichert, "Dependence of Release of Nucleotides from Fungi on Fermentor Turbine Speed," *Biotech. Bioeng.*, vol. 22, p. 237, 1980.)



(a)



(b)

Figure 9.22 Microphotographs (400 $\times$ ) showing different mycelial morphology and septation in *A. niger* S59 cultivated at (a) 400 and (b) 1200 rpm. (Reprinted by permission from E. Ujcová, Z. Fencel, M. Musílková, and L. Seichert, "Dependence of Release of Nucleotides from Fungi on Fermentor Turbine Speed," *Biotech. Bioeng.*, vol. 22, p. 237, 1980.)

we see long, thin, and sporadically branched filaments with relatively few septa at low agitation speeds, while the hyphae are thicker, highly septated, and more densely branched and twisted at higher agitation speeds. This example points out that mixing intensity can have a profound effect on the organisms which influence process kinetics in a substantial way.

In the discussions and examples in this section, we have tried to indicate that, because of the potentially complicated response of growing cells to physical and chemical environment and our inability to develop a generally applicable kinetic model valid for all circumstances, we must be careful to recognize the interaction between chemical and physical environment provided in a certain bioreactor and the corresponding kinetic description which is appropriate and indeed necessary. The difficulty of reliable scale-up in cases of strong sensitivity of kinetic behavior to environmental fluctuations should be obvious. In such cases, we must look to reactor designs which provide reaction environments which are as well defined as possible—not necessarily uniform; this may be extremely difficult on a large scale. However, by use of some of the alternative bioreactor configurations considered in Sec. 9.7, we can reduce the variance of mixing times and the degree of environmental fluctuations in order to achieve a better defined contacting situation for which we can seek correspondingly valid kinetic descriptions. Basically, we cannot expect success in rational, predictable scale-up of bioreactors until we have better understanding of the transport processes at several scales and the bioreaction kinetics at several levels and can then synthesize these to calculate accurately reactor performance.

**Example 9.1: Reactor modeling and optimization for production of  $\alpha$ -galactosidase by a *Monascus* sp. mold** The enzyme  $\alpha$ -galactosidase may be useful in the beet-sugar industry because it can decompose raffinose, an inhibitor of sucrose crystallization. In a fascinating series of papers, Imanaka, Kaieda, Sato, and Taguchi<sup>1</sup> have investigated production of this intracellular enzyme by a mold they isolated from soil. Their original work deserves serious study: here we summarize some of the major results of their investigations.

As a first step in developing highly productive continuous processes for enzyme synthesis, batch and continuous cultures of the mold were cultivated under a variety of conditions. We list next the major findings from the batch experiments:

1. Among 20 different carbon sources including glucose, fructose, mannitol, and starch, only four sugars were effective in inducing high  $\alpha$ -galactosidase activity. The strong inducers are galactose, melibiose, raffinose, and stachyose.
2. Ammonium nitrate gave more enzyme production than the alternative nitrogen sources urea,  $\text{KNO}_3$ ,  $(\text{NH}_4)_2\text{SO}_4$ , and peptone. The optimal  $\text{NH}_4\text{NO}_3$  concentration in the medium is between 0.3 and 0.5 percent by weight.
3. When grown in a galactose medium, the cell mass is directly proportional to the  $\alpha$ -galactosidase activity. When a mixture of glucose and galactose was used as the carbon source, diauxic growth

<sup>1</sup> The material in this example is drawn chiefly from T. Imanaka, T. Kaieda, K. Sato, and H. Taguchi, " $\alpha$ -Galactosidase Production in Batch and Continuous Culture and a Kinetic Model for Enzyme Production," *J. Ferment. Technol. (Japan)*, 50:633, 1972, and T. Imanaka, T. Kaieda and H. Taguchi, "Optimization of  $\alpha$ -Galactosidase Production by Mold, II, III," *J. Ferment. Technol. (Japan)*, 51:423, 431, 1973.

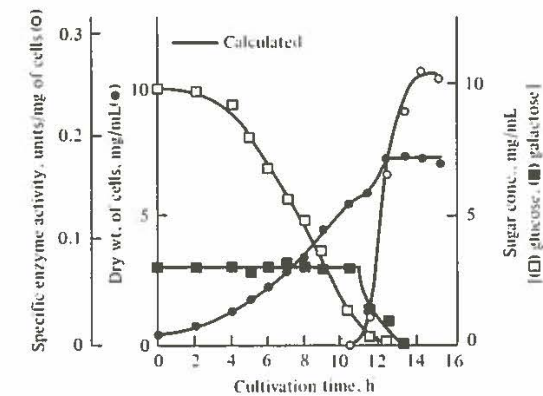


Figure 9E1.1 Results of batch cultivation of a *Monascus* sp. mold in a mixture of glucose and galactose [initial medium composition: glucose 1% (by weight), galactose 0.3%,  $\text{NH}_4\text{NO}_3$  0.5%,  $\text{KH}_2\text{PO}_4$  0.5%,  $\text{MgSO}_4 \cdot 7\text{H}_2\text{O}$  0.1%, yeast extract 0.01%]. The inoculum was grown in a glucose medium. The initial conditions used in the calculations were  $x = 5 \times 10^{-4}$  g/mL,  $s_1 = 1 \times 10^{-2}$  g/mL,  $s_2 = 3 \times 10^{-3}$  g/mL,  $s_{21} = 0$   $\mu\text{g}/\text{mg}$  cell,  $rs_{21} = 0.910$   $\mu\text{g}/\text{mg}$  cell,  $e = 0$  units/mg cell. [Reprinted from T. Imanaka et al., "Unsteady-state Analysis of a Kinetic Model for Cell Growth and  $\alpha$ -Galactosidase Production in Mold," *J. Ferment. Tech. (Japan)*, vol. 51, p. 423, 1973.]

was observed (see Fig. 9E1.1); almost no galactose is consumed until the glucose is nearly exhausted.

4. Figure 9E1.1 also shows that  $\alpha$ -galactosidase production does not start until the glucose is almost gone. Separate experiments revealed that glucose concentrations greater than 0.05 percent by weight repress synthesis of the enzyme.

Two different series of steady-state continuous-culture experiments were conducted in a single CSTR. In the first series, the dilution rate was initially at a very low level, and it was increased slowly in a stepwise fashion (shifted up) with observations of steady-state behavior at each  $D$  along the way. The data so observed are plotted in Fig. 9E1.2. Especially interesting is the discontinuous jump evident at  $D = 0.142 \text{ h}^{-1}$ . Below this dilution rate, galactose is being consumed and  $\alpha$ -galactosidase is synthesized. When  $D$  is increased above  $0.142 \text{ h}^{-1}$ , however, both these activities stop and glucose alone is utilized as the mold's carbon source. Evidently, this jump is a manifestation of the glucose effect, already seen in batch culture of this organism. When cultivated under relatively large specific growth rates (large  $D$ 's), the mold preferentially feeds on glucose.

Figure 9E1.3 illustrates the results of a similar series of experiments, except that here the CSTR was started up at a high dilution rate. Then, in a sequence of shift-down steps, the dilution rate was gradually decreased. While less sharp than the previous case, another discontinuity occurs, this time around  $D = 0.008 \text{ h}^{-1}$ . Below that critical dilution rate, enzyme is produced and galactose is assimilated, while no  $\alpha$ -galactosidase activity is evident for  $D > 0.008 \text{ h}^{-1}$ . This is in marked contrast to the shift-up experimental results, where enzyme production was apparent up to  $D = 0.142 \text{ h}^{-1}$ .

Replotting some of the data from the previous two figures in Fig. 9E1.4 clearly shows that this system exhibits multiple, stable steady states between  $D = 0.008$  and  $D = 0.142 \text{ h}^{-1}$ . For dilution rates between these limits, whether or not  $\alpha$ -galactosidase is produced depends upon how the reactor is started up. Shifting down into this range results in no enzyme synthesis, while shifting up will provide  $\alpha$ -galactosidase production.

Based upon these and other experiments, a mathematical model for substrate utilization, cell growth, and product synthesis was developed. In most respects, the individual model equations in



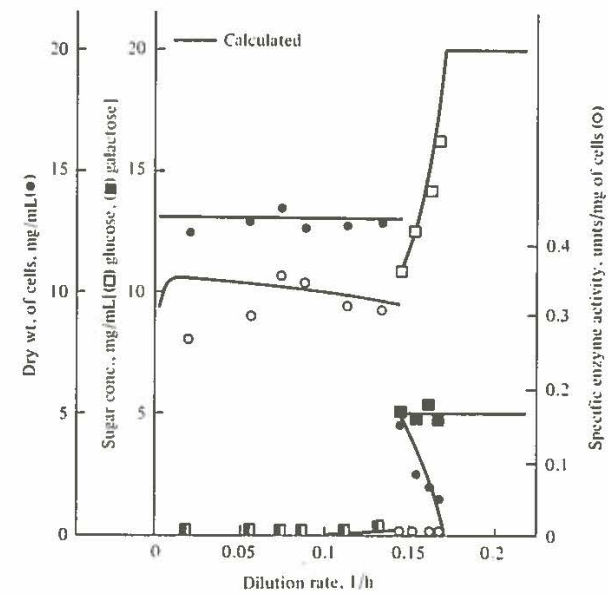


Figure 9E1.2 Steady-state cell and substrate concentrations and specific enzyme activity observed during gradual shift up of dilution rate for continuous culture (30°C). Initially the medium contains 2% glucose and 0.5% galactose. [Reprinted from T. Imanaka et al., "Optimization of  $\alpha$ -Galactosidase Production by Mold," *J. Ferment. Tech. (Japan)*, vol. 50, p. 633, 1972.]

Table 9E1.1 are familiar from our earlier studies: the specific growth rate  $\mu_2$  based on galactose is of Monod form, while the specific growth rate of glucose  $\mu_1$  includes competitive inhibition by galactose. All the constants in these growth-rate functions were evaluated for two different media from continuous-culture experiments. Parameters labeled  $G$  in Table 9E1.2 correspond to a glucose medium (20 g glucose, 5 g  $\text{NH}_4\text{NO}_3$ , 5 g  $\text{KH}_2\text{PO}_4$ , 1 g  $\text{MgSO}_4 \cdot 7\text{H}_2\text{O}$ , 0.1 g yeast extract in 1000 mL tap water at pH 4.5) while the  $p$  subscripts refer to a galactose medium advantageous for enzyme production (5 g galactose, 5 g  $\text{NH}_4\text{NO}_3$ , 5 g  $\text{KH}_2\text{PO}_4$ , 1 g  $\text{MgSO}_4 \cdot 7\text{H}_2\text{O}$  in 1000 mL tap water, pH 4.5).

The model for enzyme production is based upon the operon theory of induction, studied in Chap. 6. The specific rate of  $\alpha$ -galactosidase synthesis is proportional to the intracellular concentration of mRNA which codes for that enzyme. This mRNA is assumed to decompose by a first-order reaction and is produced provided the intracellular concentration of repressor  $R$  is smaller than a threshold value  $r_c$ . Below this threshold value, lower  $r$  values cause increased specific rates of mRNA synthesis. The repressor is formed at constant specific rate  $k_2$  and decomposes with first-order specific rate  $k_3 r$ . Repressor concentration is also reduced by complexing with the inducer, intracellular galactose.

The rate of galactose transport into the cell is given by the term in the intracellular galactose mass balance with coefficient  $U$ . To take into account the glucose effect this transport term is set equal to zero whenever the glucose concentration  $s_1$  exceeds a critical value  $s_{1c}$ , which is taken to be  $2.25 \times 10^{-4}$  g/mL.

Little information is available for direct evaluation of the rate constants in the operon model. Values for  $k_3$  and  $k_7$  were assigned based on the assumption that the repressor and mRNA half-lives are 40 and 5 min, respectively. The other parameter values listed in Table 9E1.2 were estimated by trial and error to achieve a reasonable fit to the experimental data.

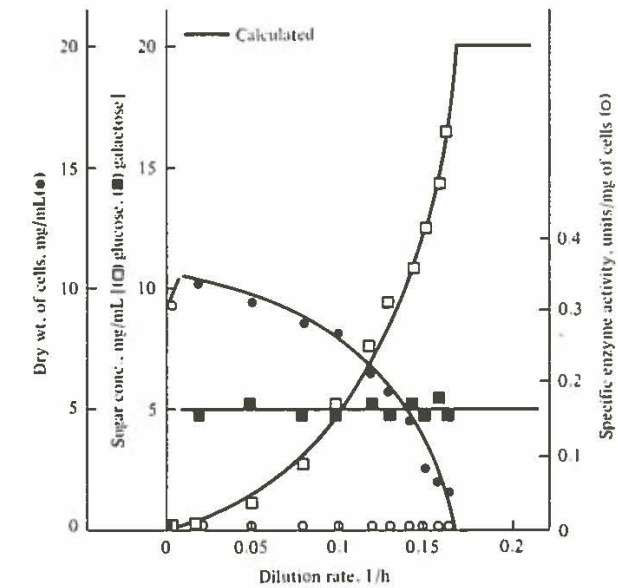


Figure 9E1.3 Steady-state cell and substrate concentrations and specific enzyme activity observed during gradual shift down of dilution rate for continuous culture (30°C). Initially the medium contains 2% glucose and 0.5% galactose. [Reprinted from T. Imanaka et al., "Optimization of  $\alpha$ -Galactosidase Production by Mold," *J. Ferment. Tech. (Japan)*, vol. 50, p. 633, 1972.]

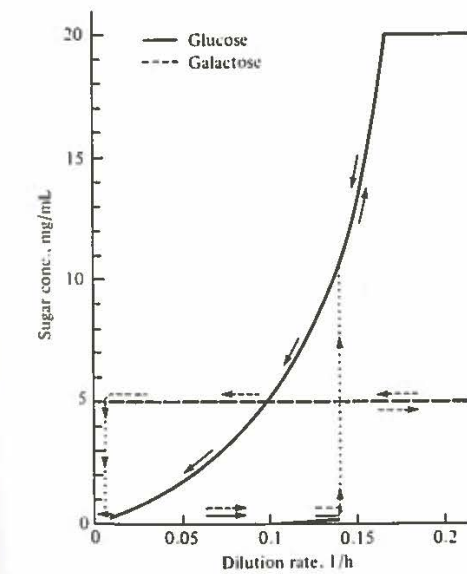


Figure 9E1.4 This replot of some of the curves from Figs. 9E1.2 and 9E1.3 displays steady-state multiplicity and hysteresis in continuous culture. Two stable steady states occur for dilution rates between 0.008 and  $0.142 \text{ h}^{-1}$ . Which is obtained depends on reactor start-up. [Reprinted from T. Imanaka et al., "Optimization of  $\alpha$ -Galactosidase Production by Mold," *J. Ferment. Tech. (Japan)*, vol. 50, p. 633, 1972.]

Table 9E1.1 Mathematical Model for  $\alpha$ -galactosidase production<sup>†‡</sup>

Substrate utilization	
$\frac{ds_j}{dt} = -\frac{1}{Y_j} \mu_j x$	for $j = 1(\text{glucose}), 2(\text{galactose})$ (9E2.1)
Biomass growth	
$\frac{dx}{dt} = (\mu_1 + \mu_2)x$	(9E2.2)
where	$\mu_1 = \frac{\mu_{\max, 1} s_1}{s_1 + K_1(1 + s_2/K_1)}$ (9E2.3)
and	$\mu_2 = \frac{\mu_{\max, 2} s_2}{s_2 + K_2}$ (9E2.4)
Operon model for enzyme production	
Intracellular galactose:	$\frac{d}{dt}(s_{2i} \cdot x) = Ux \left( \frac{G_2 s_2}{K_{m2} + s_2} - s_{2i} \right) - k_1 s_{2i} \cdot x$ for $s_1 < s_{1c}$ (9E2.5a)
	$= -k_1 s_{2i} \cdot x$ for $s_1 \geq s_{1c}$ (9E2.5b)
Repressor:	$\frac{d}{dt}(r \cdot x) = k_2 s - k_3 r \cdot x - k_4 r \cdot s_{2i} \cdot x + k_5 (rs_{2i})x$ (9W2.6)
Galactose-repressor complex:	$\frac{d}{dt}[(rs_{2i})x] = k_4 r \cdot s_{2i} \cdot x - k_5 (rs_{2i})x$ (9E2.7)
mRNA for galactosidase:	$\frac{d}{dt}(m \cdot x) = \begin{cases} k_6(r_c - r)x - k_7 m \cdot x & \text{for } r_c > r \\ -k_7 m \cdot x & \text{for } r \geq r_c \end{cases}$ (9E2.8a, 9E2.8b)
Enzyme:	$\frac{d}{dt}(e \cdot x) = k_8 m \cdot x$ (9E2.9)

<sup>†</sup> T. Imanaka, T. Kaieda, K. Sato, and H. Taguchi, *J. Ferment. Technol. (Japan)*, 50: 633, 1972.  
<sup>‡</sup> Concentration variables are  $x$  = biomass,  $s_1$  = glucose,  $s_2$  = extracellular galactose,  $s_{2i}$  = intracellular galactose,  $r$  = intracellular repressor,  $(rs_{2i})$  = intracellular inducer-repressor complex,  $m$  = intracellular mRNA, and  $e$  = intracellular  $\alpha$ -galactosidase. The remaining symbols are kinetic, yield, and transport parameters.

This model is certainly attractive because it includes substantial structure which is heavily based on established biological principles. On the other hand, we could object to the large number of adjustable parameters it contains. Several tests can be applied to investigate the suitability of this model. One is based on the following question: Can other models based on different assumptions but containing a similar number of adjustable constants fit the data equally well? If so, we cannot place much confidence in this particular form. Imanaka et al. conducted several such tests, including cases in which (1) intracellular galactose concentration is proportional to galactose concentration in the medium, or (2) repressor formation is proportional to intracellular glucose, or (3) rate of mRNA formation is inversely proportional to concentration of repressor. Any of these modifications in the model resulted in serious discrepancies with the experimental observations.

Table 9E1.2 Parameter values for the mathematical model of  $\alpha$ -galactosidase production<sup>†</sup>

Entries in the right column were evaluated experimentally; the remaining parameters were adjusted to fit the batch and continuous-culture results;  $G$  = glucose medium, 30°C,  $p$  = galactose medium, 35°C.

$k_1 = 40 \text{ h}^{-1}$	$\mu_{\max, 1G} = 0.215 \text{ h}^{-1}$
$k_2 = 1 \text{ mg}/(\text{mg cells} \cdot \text{h})$	$\mu_{\max, 2G} = 0.208 \text{ h}^{-1}$
$k_3 = 1 \text{ h}^{-1}$	$K_{1G} = 1.54 \times 10^{-4} \text{ g/mL}$
$k_4 = 0.1 \text{ mg cells}/(\text{mg} \cdot \text{h})$	$K_{2G} = 2.58 \times 10^{-4} \text{ g/mL}$
$k_5 = 1 \times 10^{-4} \text{ h}^{-1}$	$\mu_{\max, 1p} = 0.190 \text{ h}^{-1}$
$k_6 = 1 \text{ h}^{-1}$	$\mu_{\max, 2p} = 0.162 \text{ h}^{-1}$
$k_7 = 8 \text{ h}^{-1}$	$K_{1p} = 1.45 \times 10^{-4} \text{ g/mL}$
$k_{8G} = 3.2787 \text{ units}/(\text{mg mRNA} \cdot \text{h})$	$K_{2p} = 3.07 \times 10^{-4} \text{ g/mL}$
$k_{8p} = 5.0442 \text{ units}/(\text{mg mRNA} \cdot \text{h})$	$K_i = 1.39 \times 10^{-4} \text{ g/mL}$
$U = 100 \text{ h}^{-1}$	$Y_{1G} = 0.530$
$G_2 = 1 \text{ mg}/\text{mg cells}$	$Y_{2G} = 0.516$
$K_{m2} = 1 \times 10^{-8} \text{ mg}/\text{mg cells}$	$Y_{1p} = 0.377$
$s_{1c} = 2.25 \times 10^{-4} \text{ g/mL}$	$Y_{2p} = 0.361$
$r_c = 0.934 \text{ mg}/\text{mg cells}$	

<sup>†</sup> T. Imanaka, T. Kaieda, K. Sato, and H. Taguchi, *J. Ferment. Technol.*, 50: 558, 1972.

The other tests of the model which Imanaka et al. considered involved its ability to fit data collected under a wide variety of operating conditions. Indeed, this is the *raison d'être* for a complex, structured kinetic model, for if the model is sufficiently complete, it can be used to determine optimal operating conditions for the process. Here too the model performed extremely well. The solid curves in Fig. 9E1.1 were computed using this model with initial conditions as indicated in the figure, and the fit is very good.

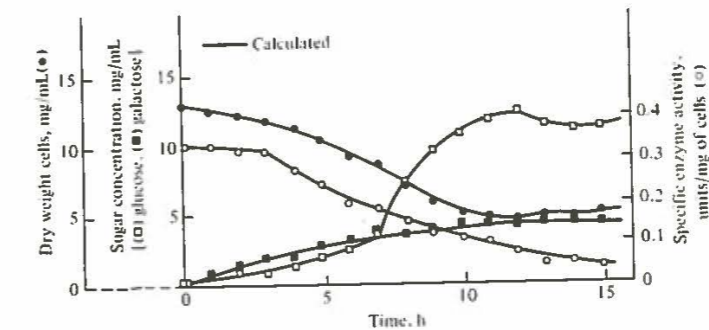
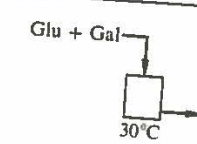
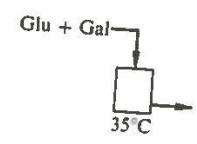
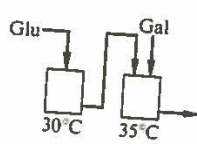
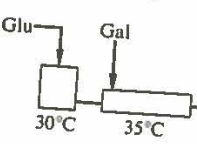
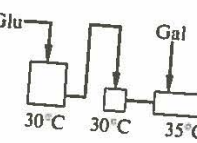
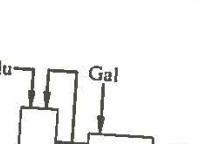


Figure 9E1.5 Transient behavior of CSTR continuous culture following a change in dilution rate from  $D = 0.140 \text{ h}^{-1}$  to  $D = 0.142 \text{ h}^{-1}$ . The medium contained two carbon sources: glucose (2%) and galactose (0.5%). Initial conditions used in the calculation were  $x = 1.30 \times 10^{-2} \text{ g/mL}$ ,  $s_1 = 2.23 \times 10^{-4} \text{ g/mL}$ ,  $s_2 = 5.01 \times 10^{-5} \text{ g/mL}$ ,  $s_{2i} = 2.5 \text{ } \mu\text{g}/\text{mg cell}$ ,  $r = 0.718 \text{ } \mu\text{g}/\text{mg cell}$ ,  $(rs_{2i}) = 1.28 \text{ } \mu\text{g}/\text{mg cell}$ ,  $m = 1.04 \times 10^{-2} \text{ } \mu\text{g}/\text{mg cell}$ ,  $e = 0.297 \text{ units}/\text{mg cell}$ . [Reprinted from T. Imanaka et al., "Unsteady-state Analysis of a Kinetic Model for Cell Growth and  $\alpha$ -Galactosidase Production by Mold," *J. Ferment. Tech. (Japan)*, vol. 51, p. 423, 1973.]

Table 9E1.3 Optimized operating conditions for six different continuous fermentor configurations<sup>†‡</sup>

System	Type of fermentation process	Optimum operating conditions, $D$ values in $h^{-1}$	Specific enzyme activity, units/mg of cells	Enzyme productivity, units/(L · h)
1		$D = 0.142$ Shift-up system	0.325	554
2		$D = 0.121$ Shift-up system	0.500	559
3		$D_1 = 0.200$ $D_2 = 0.250$ $\bar{D} = 0.118$	0.293	415
4		$D_1 = 0.133$ $D_2 = 0.286$ $\bar{D} = 0.097$	0.500	582
5		$D_1 = 0.193$ $D_2 = 2.342$ $D_3 = 0.286$ $\bar{D} = 0.117$	0.500	702
6		$D_1 = 0.178$ $D_2 = 0.286$ $\bar{D} = 0.117$ $C = 1.34$	0.500	702
		$D_1 = 0.266$ $D_2 = 0.286$ $\bar{D} = 0.145$ $C = 200$	0.500	870

<sup>†</sup> T. Imanaka, T. Kaieda, and H. Taguchi, *J. Ferment. Technol. (Japan)*, 51: 558, 1973.  
<sup>‡</sup> Glucose = 2 percent, galactose = 0.5 percent of the total medium.

The model equations for an unsteady-state CSTR can be obtained simply by adding terms of the form  $D$  (inlet concentration-concentration in the reactor) to each of the batch equations in Table 9E1.1. Steady-state CSTR mass balances are then obtained by setting all time-derivative terms equal to zero. With these equations, the solid lines in Figs. 9E1.2 and 9E1.3 were calculated. The hysteresis and jump phenomena observed experimentally are clearly well represented by the model. As a final test before turning to reactor optimization, the model was used to compute the transient behavior of the CSTR following shift-up. The results predicted by the model as well as experimental data are displayed in Fig. 9E1.5; here the agreement between measured and calculated responses, including the overshoot of glucose and undershoot of cell concentrations, is quite dramatic.

With the model of Table 9E1.1 thus well established, it was used to compute the enzyme productivity of a variety of continuous-reactor configurations (Table 9E1.3). For each design, the volumes of the various reactors were adjusted to maximize enzyme production. The overall dilution rate  $\bar{D}$  indicated in the table is defined as the total medium flow rate into the system divided by the total volume of all reactors in the process.

We shall examine a few details of systems 3 and 4. In these, as in systems 5 and 6, the basic idea is to grow a large cell concentration in the first part of the system using relatively cheap glucose only. Then a galactose medium is added at a later stage to induce enzyme production. Because enzyme induction takes some time, it is necessary to take into account adaptation of the intracellular reaction systems in the later stage. For this purpose, the induction stage is treated as a completely segregated system, and its effluent enzyme activity is computed using Eq. (9.62), which can be rewritten

$$e_e = \int_0^{\infty} e_b(t) \delta(t) dt \quad (9E1.1)$$

where  $e_b(t)$  is the enzyme concentration at time  $t$  computed from the batch-reactor model. In the batch calculations the initial conditions used are the concentrations in the feed to the induction stage.

Using this procedure, the enzyme productivity ( $= De_e x$ ) was computed for the two-stage system (3), with results shown in Fig. 9E1.6. The model revealed that maximum productivity would be obtained with  $D_1 = 0.20 h^{-1}$ , and experiments performed under that condition showed nearly exactly the same  $D_2$  dependence as predicted by the model. In system 4, a bioreactor designed to approximate plug-flow conditions was used for the second stage. Again, the model results (line) agreed very well with experimental data (dots) for this process (Fig. 9E1.7).

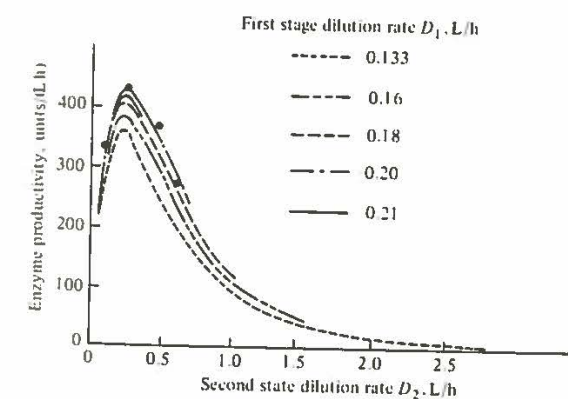


Figure 9E1.6 Calculated and experimental enzyme productivity in a two-CSTR continuous culture (System 3 from Table 9E1.3). [Reprinted from T. Imanaka et al., "Optimization of  $\alpha$ -Galactosidase Production in Multi-stage Continuous Culture of Mold, *J. Ferment. Tech. (Japan)*, vol. 51, p. 431, 1973.]

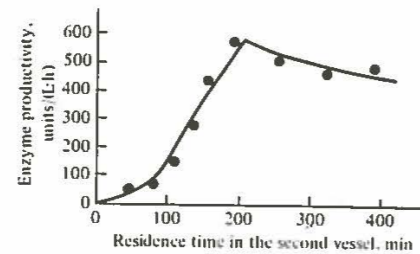


Figure 9E1.7 Productivity of enzyme in a CSTR-tubular fermentor cascade (system 4 from Table 9E1.3). [Reprinted from T. Imanaka et al., "Optimization of  $\alpha$ -Galactosidase Production in Multi-stage Continuous Culture of Mold," *J. Ferment. Tech. (Japan)*, vol. 51, p. 431, 1973.]

Returning now to Table 9E1.3, we see that well-chosen staged cultures provide substantially greater enzyme production than the best single process. For example, system 6 produces 55 percent more enzyme than the single CSTR. Clearly the availability of a sound kinetic model and the general tools of reactor design have here proved essential ingredients in formulating and optimizing a superior continuous-reaction process.

## 9.4 STERILIZATION REACTORS

Liquids, usually aqueous, can be sterilized by several means, including radiation (ultraviolet, x-rays), sonication, filtration, heating, and chemical addition. Only the last two are widely used in large-scale processes. However, small amounts of liquids containing sensitive vitamins and other complex molecules are sometimes sterilized by passage through porous membranes. In this section we shall concentrate on design of heat-treatment processes.

Requirements for destruction of viable microbes and viruses vary widely depending upon the material and its intended use. In some instances, e.g., sauerkraut manufacture and biological wastewater treatment, microorganisms naturally present in the process fluid are responsible for desirable reactions. Inhibitors for the growth of unwanted organisms are rapidly evolved in alcohol, vinegar, and silage production, so that here too sterilization requirements are not extreme. Milk pasteurization involves killing most but not all actively growing microbes. More severe treatment of milk is not practiced because degradation of desired components results. Trade-offs between destruction of useful compounds and death of unwanted organisms play a major role in choice and design of sterilization and pasteurization equipment.

Pure-culture fermentations, tissue culture, and some food products require more stringent measures. Essentially all contaminating microbial life must be excluded from the system, although the degree of "perfection" also varies somewhat. Economic considerations might indicate, for example, that a contamination probability [ $1 - P_0$  in Eq. 7.131)] of  $10^{-2}$  is acceptable for a batch fermentation process. In this case we would expect 1 batch out of every 100 to be lost due to contamination. We could accept this if the loss were comparable to the cost of additional sterilization capacity.

Much more severe requirements hold in the canning industry. A single surviving spore of *Clostridium botulinum* may cause lethal contamination, so that virtually complete elimination is required. Typically, a design criterion in this

situation specifies that the spore survival probability  $1 - P_0$  be reduced to less than  $10^{-12}$ . This example illustrates the importance of small deviations from essentially complete conversion of substrate (spores and vegetative cells) into products (inactive spores, dead cells) in sterilization reactors. Thus, careful sterilization-reactor design can clearly be critical. Continuous sterilization processes are examined after analysis of the batch case.

### 9.4.1 Batch Sterilization

Let us begin by considering a well-mixed closed volume containing a cell or spore suspension. The fluid is to be sterilized by heating, and then cooled to a suitable temperature for subsequent processing. The concentration of surviving organisms resulting from this process can readily be computed starting from Eqs. (7.125) and (7.126):

$$\frac{dn}{dt} = -k_{d0} e^{-E_d/RT(t)} n \quad (9.92)$$

where we have explicitly included time variations in the fluid temperature. Separating the variables in Eq. (9.92) and integrating, we find

$$\ln \frac{n_0}{n_f} = \int_0^{t_f} e^{-E_d/RT(t)} dt \quad (9.93)$$

where the  $f$  subscript denotes final conditions.

Common batch-sterilization designs include one or more of the following heat sources: steam sparging (bubbling of live steam through the medium), electrical heating, and heating or cooling with a two-fluid heat exchanger. Deindoerfer and Humphrey<sup>†</sup> have associated with each heating or cooling mode a particular time-temperature profile; these functions are shown in Table 9.4. The integral on the right-hand side of Eq. (9.93) can be evaluated by segmentation into three intervals of heating, holding, and cooling. A total of four integral forms arise: constant temperature and each of the three transient modes (hyperbolic, linear, and exponential).

Constant temperature

$$\ln \frac{n_0}{n_f} = \int_0^{t_f} k_{d0} e^{-E_d/RT} dt = k_{d0} t_f e^{-E_d/RT} \quad (9.94)$$

Hyperbolic

$$\ln \frac{n_0}{n_f} = \frac{k_{d0} a (E_d/RT_0)}{(a+b)^2} e^{-(E_d/RT_0)[b/(a+b)]} \times \left[ E_2 \left\{ \frac{E_d}{RT_0} \left[ \frac{1+bt_f}{1+(a+b)t_f} - \frac{b}{a+b} \right] \right\} - E_2 \left( \frac{E_d}{RT_0} \frac{a}{a+b} \right) \right] \quad (9.95)$$

<sup>†</sup> F. H. Deindoerfer and A. E. Humphrey, "Analytical Method for Calculating Heat Sterilization Times," *Appl. Microbiol.*, 7:256 (1959).

Table 9.4 Temperature-time profiles in batch sterilization†

Type of heat transfer	Temperature-time profile	Parameters
Steam sparging	$T = T_0 \left( 1.0 + \frac{at}{1 + bt} \right)$ hyperbolic	$a = \frac{hs}{MT_0 C_p}$ $b = \frac{s}{M}$
Electrical heating	$T = T_0(1.0 + at)$ linear	$a = \frac{q}{MT_0 C_p}$
Steam (heat exchanger)	$T = T_N(1 + be^{-at})$ exponential	$a = \frac{UA}{McC_p}$ $b = \frac{T_0 - T_N}{T_N}$
Coolant (heat exchanger)	$T = T_{e0}(1 + be^{-at})$ exponential	$a = \frac{wc'}{M\rho C_p} (1 - e^{-UAc/wc})$  $b = \frac{T_0 - T_{e0}}{T_{e0}}$

where  $h$  = enthalpy differences between steam at sparger temperature and raw medium temperature (per kg steam)

$s$  = steam mass flow rate

$M$  = initial medium mass

$T_0$  = initial medium temperature (°K)

$q$  = rate of heat transfer, kcal per unit time

$U$  = overall heat-transfer coefficient, kcal/(m<sup>2</sup>·h·°C)

$A$  = heat-transfer area, m<sup>2</sup>

$T_N$  = temperature of heat source (°K)

$w$  = coolant mass flow rate

$c'$  = coolant specific heat

$T_{e0}$  = coolant inlet temperature (°K)

$\rho$  = medium density

$C_p$  = medium heat capacity

† After F. H. Deindoerfer and A. E. Humphrey, *Appl. Microbiol.*, 7: 256, 1959.

#### Linear increasing

$$\ln \frac{n_0}{n_f} = \frac{k_{d0} E_d}{RT_0 a} \left( E_2 \left( \frac{E_d}{RT_0} \right) - E_2 \left( \frac{E_d}{RT_f} \right) \right) \quad (9.96)$$

#### Exponential

$$\ln \frac{n_0}{n_f} = \frac{k_{d0}}{a} \left[ E_1 \left( \frac{E_d}{RT_H} \right) - E_1 \left( \frac{E_d}{RT_f} \right) \right] - \frac{k_{d0}}{a} e^{-E_d/RT_H} \left[ -E_1 \left( \frac{-E_d}{RT_H} \frac{b}{1+b} \right) + E_1 \left( \frac{-E_d}{RT_f} \frac{b}{1+b} \right) \right] \quad (9.97)$$

where  $E_n$  is the exponential integral

$$E_n(z) = \int_z^\infty \frac{e^{-w} dw}{w^n} \quad (9.98)$$

a tabulated function available in many handbooks and computer packages. The result for cooling is obtained by substituting  $T_{e0}$  for  $T_H$  and using the definitions of  $a$  and  $b$  appropriate for cooling (Table 9.4).

In each case, the final result yields  $\ln(n_f/n_0)$ , the logarithm of the ratio of final to initial concentrations. If, for example, electrical heating is followed by holding at an elevated temperature and subsequent liquid-coolant heat exchange, we can write the ratio of final to initial viable-cell concentrations in the form

$$\ln \frac{n_f}{n_0} = \ln \left[ \frac{n_f}{n_0(\text{coolant})} \frac{n_f(\text{holding})}{n_0(\text{holding})} \frac{n_f(\text{electrical})}{n_0(\text{electrical})} \right] \quad (9.99)$$

since  $n_0(\text{coolant}) = n_f(\text{holding})$  and  $n_0(\text{holding}) = n_f(\text{electrical})$ . Rewriting Eq. (9.99) as

$$\ln \frac{n_f}{n_0} = \ln \frac{n_f(c)}{n_0(c)} + \ln \frac{n_f(h)}{n_0(h)} + \ln \frac{n_f(e)}{n_0(e)} \quad (9.100)$$

we see that the overall result  $\ln(n_f/n_0)$  is obtained by adding the three appropriate individual solutions above, each evaluated for the particular time interval in that mode of operation.

Another situation which may be usefully examined analytically is thermal sterilization of solids or stagnant fluids. Such processes are important from several perspectives. One significant application is destruction of toxic organisms in sealed food containers. Also, it is necessary to minimize all viable microorganisms in the closed container which could decompose or otherwise spoil the product. Solid particles or microbial aggregates are often found suspended in liquids to be sterilized. We should recognize that these forms tend to protect organisms in their interior from thermal destruction and that more extensive heating is therefore required when such solids are present.

Analysis of both of these processes, at least for simple container and particulate geometries, can be reduced to a two-step recipe analogous to the procedure followed above. First, we solve a transient heat-conduction problem to determine the temperature in the solid as a function of position and time. Assuming constant thermal conductivity  $k$ , this problem has the general form

$$\rho C_p \frac{\partial T}{\partial t} = k \nabla^2 T \quad (9.101)$$

where  $\nabla^2$  is the Laplacian operator and  $\rho C_p$  is as defined in Table 9.4. In addition to the partial differential equation (9.101),  $T$  is specified as a function of position within the solid at time zero, and the temperature at the external solid surface is known as a function of time for  $t > 0$ .

Considering a spherical solid, for example, the following equations must be solved to determine the interior temperatures for  $t > 0$ :

$$\frac{\partial T}{\partial t} = \frac{k}{\rho C_p} \frac{1}{r^2} \frac{\partial}{\partial r} \left( r^2 \frac{\partial T}{\partial r} \right) \quad (9.102)$$

$$T(r, 0) = f(r) \quad 0 \leq r \leq R \quad (9.103)$$

$$T(R, t) = g(t) \quad t > 0 \quad (9.104)$$

where  $r$  is distance from the sphere's center and  $f$  and  $g$  are prescribed functions. If the sphere is initially at a uniform temperature  $T_0$ , and if the surface temperature  $T(t, R)$  is maintained at a constant value  $T_1$  for  $t > 0$ , this problem can be solved by separation of variables to obtain

$$T(r, t) = T_1 + \frac{2R(T_1 - T_0)}{\pi r} \sum_{n=1}^{\infty} \frac{(-1)^n}{n} \sin \frac{n\pi r}{R} \exp \left( -\frac{k}{\rho C_p} \frac{n^2 \pi^2 t}{R^2} \right) \quad (9.105)$$

The temperature at the center of the sphere ( $r = 0$ ) can be deduced from Eq. (9.105) by taking the limit  $r \rightarrow 0$ . This result is

$$T(0, t) = T_1 + 2(T_1 - T_0) \sum_{n=1}^{\infty} (-1)^n \exp \left( -\frac{k}{\rho C_p} \frac{n^2 \pi^2 t}{R^2} \right) \quad (9.106)$$

Figure 9.23 shows temperature distributions computed from these formula for a variety of elapsed times. In the context of sterilization, it is critical to note that there is a time lag between the imposition of a high temperature at the

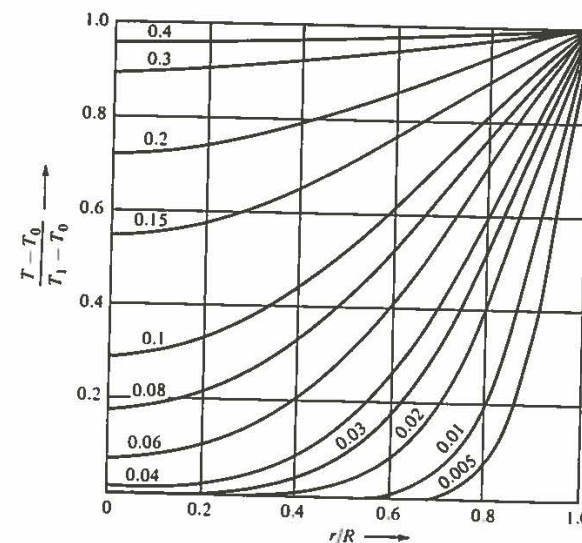


Figure 9.23 Temperature profiles within a sphere of radius  $R$  as a function of dimensionless time  $kt/\rho C_p R^2$  (given as a parameter on the curves). Initially the sphere temperature is  $T_0$  throughout, and the outer-surface temperature for  $t > 0$  is  $T_1$ .

surface and achievement of similar temperatures everywhere within the solid. Consequently, the kill of organisms at the sphere's center will generally be less complete than near the surface. This observation remains qualitatively correct for many other geometries and initial and boundary conditions. While we cannot delve further here into the details of transient heat conduction under various conditions, a wealth of additional information, theory, and analytical solutions is available in Carslaw and Jaeger [29].

Once the time-temperature-position relationship has been determined, the resulting destruction of microbes and spores can be calculated. Two different design approaches have been used in the food-processing industry. In the first, the organism concentration at the center is considered. Since the center heats most slowly, presumably if the center is adequately treated, the remainder of the solid is sufficiently sterilized. To compute the surviving organisms at the center we need only insert the temperature-time function evaluated at that position into Eq. (9.93) and compute the integral. For this step, numerical or graphical means are often necessary since  $T(t)$  is usually a rather complex expression, such as Eq. (9.106).

Another approach is to conduct the previous calculations many times in order to determine survivor concentrations at each point within the solid. Then by integrating these concentrations over the volume, the number of survivors or probability of survivors can be evaluated. Obviously, this calculation is somewhat tedious although it is straightforward in principle. Consequently, several shortcut design procedures based on this whole-container philosophy have been developed for use in the food industry. Since their explanation requires substantial additional vocabulary and definitions, we refer the interested reader to Charm [30] for a thorough discussion.

While batch sterilization enjoys the advantages of being a relatively simple process, it suffers from several drawbacks. One is the time required for heating and cooling. Related to this disadvantage is another: the extent of thermal damage to desirable components. Many vitamins are destroyed by heating, and proteins can be denatured at elevated temperatures. While the destruction of these components often follows the same kinetics as organism death [Eq. (9.92)], it is important to recognize that the activation energies for these undesirable side reactions are typically much smaller than for the sterilization "reaction." The values listed in Table 9.5, for example, are less than the 50 to 100 kcal/g mol magnitudes which usually characterize spore and cell destruction.

Since the desired reaction here has a higher activation energy than the side reaction, increasing the temperature has the beneficial effect of increasing the ratio of desired rate to undesired rate. This means that if unfavorable Browning reactions or damage to susceptible compounds are to be avoided, the sterilization process should operate at the highest feasible temperature and for the shortest time (HTST = high temperature, short time) which provides the necessary organism death. The slow heating and cooling portions of batch sterilization do not achieve these objectives. Continuous sterilization, considered next, is much better suited for achieving HTST conditions.

**Table 9.5 Approximate activation energies for some undesirable side reactions resulting from heat treatment**

Reaction	Activation energy $E$ , kcal/g mol
Browning (or Maillard) reaction between proteins and carbohydrates	31.2
Destruction of vitamin B <sub>1</sub>	21.0
Destruction of riboflavin (B <sub>2</sub> )	23.6
Denaturation of peroxidase	23.6

**9.4.2 Continuous Sterilization**

Two basic types of continuous-sterilizer designs are shown schematically in Fig. 9.24. In Fig. 9.24a, direct heating is provided by steam injection, with the heated fluid then passing through a holding section before cooling by expansion. The system in Fig. 9.24b features indirect heating using a plate heat exchanger. A number of variations in each type are possible with most featuring high ratios of heat-exchange surface to process volume. Consequently, continuous sterilizers provide relatively rapid heating and cooling so that HTST conditions can be realized.

Two different design approaches are available if we assume that the temperature in the continuous sterilizer is approximately uniform. This may be valid at least in the holding sections. In the first method we apply the dispersion model

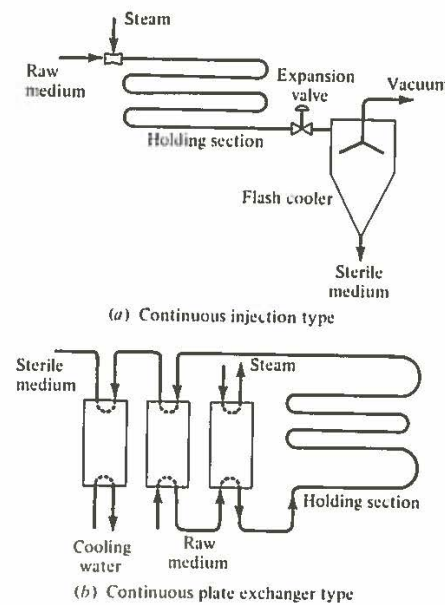


**Figure 9.24** Two different continuous sterilizer designs: (a) direct steam injection (b) plate heat exchanger. (Reprinted from S. Aiba, A. E. Humphrey and N. F. Millis, "Biochemical Engineering," 2d ed., p. 257, University of Tokyo Press, Tokyo, 1973.)

described earlier. After  $c$  in Eqs. (9.81) to (9.83) has been identified with  $n$ , we take  $r_{fn} = -k_d n$ ; then the organism concentration throughout from the tubular reactor with dispersion can be determined analytically. The resulting value of  $n$  at the sterilizer effluent is given by

$$\frac{n(L)}{n_0} = \frac{4y \exp [Pe/2]}{(1+y)^2 \exp [(Pe)(y)/2] - (1-y)^2 \exp [-(Pe)(y)/2]} \quad (9.107)$$

with

$$y = \left(1 + \frac{4 Da}{Pe}\right)^{1/2} \quad (9.108)$$

where here the Damköhler number  $Da$  is defined by

$$Da = \frac{k_d L}{u} \quad (9.109)$$

For small deviations from plug flow ( $Pe^{-1}$  small), Eq. (9.107) reduces to the simpler form

$$\frac{n(L)}{n_0} = \exp \left(-Da + \frac{Da^2}{Pe}\right) \quad (9.110)$$

These solutions are conveniently displayed as a plot of remaining viable fraction  $n(L)/n_0$  vs. the dimensionless group  $Da$  for various values of the Peclet number (Fig. 9.25). From this plot we can see that, as  $Pe \rightarrow \infty$  so that ideal plug flow is approximated, the desired degree of medium sterility can be achieved with the shortest possible sterilizer. Consequently, the flow system should be designed to keep dispersion at a minimum.

If flow through the isothermal continuous sterilizer cannot be well represented with the dispersion model, we can make use of general RTD theory. It is difficult to think of a better example of a completely segregated reactor than a suspension of cells or spores subjected to heat treatment. Consequently, provided back diffusion of organisms into the sterilizer feed line is negligible, we can compute the effluent surviving-organism concentration  $n$  using Eq. (9.62). Rewriting this equation in terms of organism concentration, we have

$$n = \int_0^{\infty} n_b(t) \mathcal{E}(t) dt \quad (9.111)$$

where  $\mathcal{E}(t)$  is the RTD of the continuous sterilizer. Recalling that  $n_b(t)$  is the organism concentration at time  $t$  in a batch sterilizer with  $n_b(0) = n_0$ , we can use Eq. (7.125) in Eq. (9.111) to obtain

$$\frac{n}{n_0} = \int_0^{\infty} \mathcal{E}(t) e^{-k_d t} dt \quad (9.112)$$

In some instances evaluation of the right-hand side of Eq. (9.112) is facilitated by noting that it is formally identical to the Laplace transform of  $\mathcal{E}$  with the usual Laplace transform parameter  $s$  replaced by  $k_d$ .

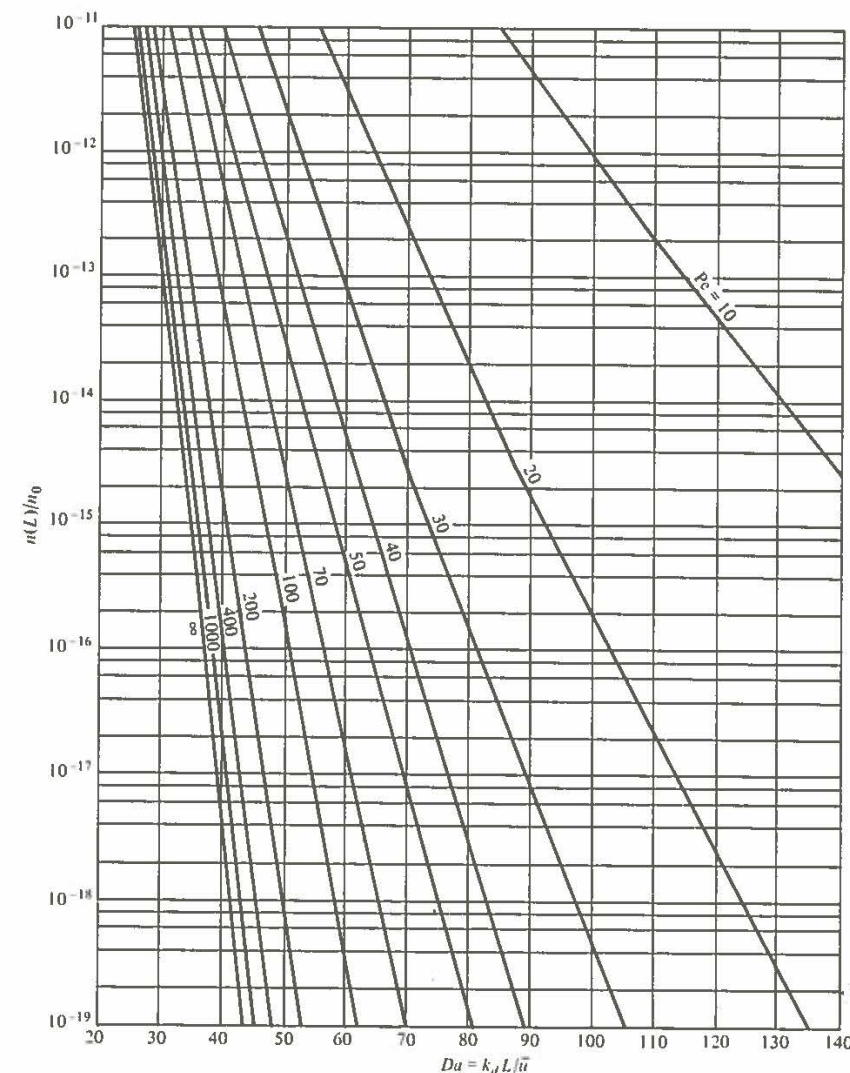


Figure 9.25 Effect of axial dispersion on organism destruction in a continuous sterilizer. (Reprinted from S. Atba, A. E. Humphrey, and N. F. Millis, "Biochemical Engineering, 2d ed., p. 263, University of Tokyo Press, Tokyo, 1973.)

Before leaving the topic of continuous sterilization, we should mention its several advantages in addition to the HTST feature already discussed. First, continuous processing typically requires less labor than batch operations. Also, continuous treatment units provide a more uniform, reproducible effluent than batch sterilization. This is extremely important in the food industry, where small changes in treatment can change the taste of the product.

When practiced in the fermentation industry, batch sterilization is usually done in the fermentor itself (*in situ*). Heating and cooling rates here depend upon the surface-to-volume ratio of the fermentor, and this ratio in turn usually changes during scale-up. The sensitivity of sterilization effects on organisms and medium components to equipment size can be reduced by using continuous sterilization. If continuous sterilization is used, it is not necessary to design the fermentor also to fulfill the requirements of a good batch sterilizer.

Of course there are some drawbacks to continuous sterilization: direct steam heating can add excess water to the medium, and heat exchangers used for indirect heating or cooling can be fouled by suspended solids. Also, continuous sterilization tends to cause foaming of fermentation media. Additional details on the operation trade-offs of sterilizers are available in Ref. 33 of Chap. 7.

## 9.5 IMMOBILIZED BIOCATALYSTS

Performance of a bioreactor depends directly and critically upon the properties of the biocatalysts employed. Earlier, we discussed different ways in which enzymes can be applied to provide useful catalytic functions. Also, we have already examined genetic modification of cells in order to improve their productivities for desired compounds. Now, before investigating additional reactor types, we must introduce another form of biocatalyst application.

Our main topic in this section is immobilized cell catalysis. The central feature of immobilized cell systems is the use of some confining or binding structure to constrain the cells in a particular region of the reactor. As we have already seen for immobilized enzymes, such immobilization methods for cells may involve entrapment in or attachment to small particles or might be achieved by use of larger-scale barriers to cell transport.

Before considering methods to achieve cell immobilization and some of the experiments conducted to date with immobilized cell catalysts, we will review some of the motivations for cell immobilization. One benefit of cell immobilization is attainment of higher cell densities than in suspended cell systems. There are several other additional reasons for using immobilized cells in batch bioreactors. Some mammalian cell lines grow only if attached to a surface. For these types of cells, immobilization is a rule rather than an option. Second, immobilized cells can be used as the basis for specific electrodes to measure concentrations of nutrients, metabolites, drugs, and toxic chemicals in bioreactors and in other process and clinical contexts. In addition, immobilization can be used to control cell morphology and broth rheology. By confining microbial growth to



the interstices and surfaces of support particles, the rheological and mass-transfer properties of the broth are relatively well defined and do not change as much during the batch process as occurs with some organisms during batch growth. Cell immobilization offers continuous processing without organism washout or genetic drift and also allows in some cases continuous separation of product and removal of reaction inhibitors. As with other immobilized catalysts, the costs of immobilization may be appreciable and may more than offset these cited advantages.

In the case of continuous-flow bioreactors, the motivation for using immobilized cells is to extend the time which the catalytic functions of the cells can be employed to accomplish a desired chemical reaction or chemical reaction sequence. In contrast to immobilized enzyme catalysis, immobilized cell catalysts can be used to achieve a broad spectrum of catalytic functions varying substantially in complexity. As sketched in the diagram in Fig. 9.26, immobilized cell catalytic activities can be classified based upon the level of metabolism that remains active and which is applied to achieve process objectives. When cells are used in a suspended state and leave the reactor with the effluent stream, some ongoing growth of cells is required in order to prevent washout. Indeed, the increase in washout dilution rate achieved with cell concentration and recycle discussed earlier in this chapter represents a macroscopic form of partial cell immobilization. By this means, the throughput of the process can be increased in a way that is partially decoupled from the rate of growth of the organisms. If the cells are completely retained within the reactor, however, the complete spectrum of catalytic complexity diagrammed in Fig. 9.26 may possibly be available since there is no requirement for growth. In fact, growth is often undesired in some of

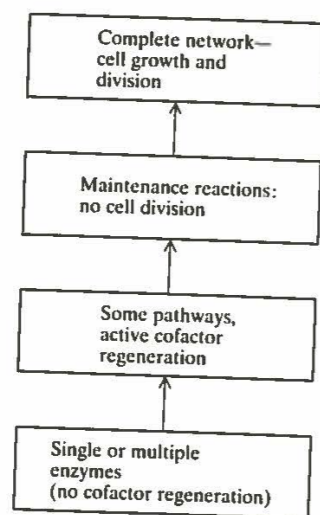


Figure 9.26 Levels of reaction network complexity encountered in immobilized cell catalysis.

these cases since growth can lead to reduced yields and since accumulated cells can cause mechanical and flow disruptions in the reactor.

The simplest level of catalysis provided by immobilized cells is activity of one or several enzymes but without any involvement of cofactors. Here, the immobilized cell essentially serves as an immobilized enzyme catalyst, with the entire cell used in order to minimize treatment and processing costs in formulating the immobilized enzyme catalyst. However, possible difficulties with extra mass-transfer resistance provided by the cell envelope and with degradation of the desired enzyme by intracellular proteases must be considered in such applications. On the other hand, some enzymes may be stabilized by remaining in their native cellular environment.

Next, a nongrowing immobilized cell system can provide catalysis through a multistep pathway involving cofactor utilization and regeneration. In principle, so long as all cofactors, enzymes, substrates, and regenerating chemicals are present, there is no reason why associated synthetic reactions and cell growth need to occur. If the desired cofactor-using pathway already exists in an organism, it may be advantageous to consider using the existing functional pathway rather than attempt to engineer a different type of cofactor utilization and regeneration process.

In the next level of catalytic complexity considered, biosynthesis and maintenance reactions occur, but there is insignificant cell growth and cell division. Finally, the most complicated situation is the one in which the full metabolic network is active and the cells are growing and dividing. This case arises, for example, in the immobilized cell batch applications mentioned earlier. It might also be employed in a continuous reactor context as a means of regenerating the biocatalyst, since some organisms do not respond well to a nongrowth environment and lose activity rapidly under such conditions. As we shall see later in examples, alternating reaction conditions between one of the less complex catalytic levels and full growth conditions is a useful strategy for obtaining extended catalyst service.

There are two different advantages in using a catalyst which carries out the desired functions without a large number of additional reactions. First is the consideration of yield. Clearly, if a substrate can be converted stoichiometrically to a certain product by action of a specific microbial pathway without concomitant growth of cells or production of other end products, yields will be increased. Another potential advantage is higher overall reaction rate. The characteristic times to achieve significant conversion of a substrate increases dramatically as one progresses from the simplest, single enzyme level in Fig. 9.26 to the most complex, full-growth state. In the former situation, rates are characterized by rates of single enzyme-catalyzed steps, with time scales on the order of minutes, typically. On the other hand, cell doubling times, which characterize the complete network reaction time, are in the range of hours to days for all but the most rapidly growing bacteria. Thus, as one moves up the ladder of metabolic complexity displayed in Fig. 9.26, the residence time required in the reactor to achieve substantial substrate conversion will also in general tend to increase

significantly. Therefore, it is a substantial potential advantage to be able to use the enzymes and cofactors needed to accomplish a particular conversion and to design the reactor residence time accordingly.

With this background framework in mind, we turn next to formulation and characterization of immobilized cell catalysts, after which some examples illustrating the spectrum of catalytic possibilities with these systems will be examined.

### 9.5.1 Formulation and Characterization of Immobilized Cell Biocatalysts

In this section, we review methods which have been applied to immobilize cells and the characteristics of the resulting catalysts that are important in different process contexts. Entrapment in polymeric networks is the most commonly applied method for cell immobilization. Table 9.6 lists different mechanisms which have been used to form the entrapping network. By far the most widely used cell entrapment method involves ionic cross-links in a layer or bead of alginate, a natural polysaccharide material. The gentleness of this gellation procedure, in contrast to chemical polymerizations, results in much higher initial viability of the immobilized cells. Fig. 9.27 illustrates schematically one protocol for preparation of spherical calcium-alginate beads containing immobilized cells.

When selecting a network entrapping method and the particular conditions applied to formulate the network, the resulting properties of the immobilized cell catalyst must be considered. Some of the major parameters of process interest are listed in Table 9.7. Both the chemical and mechanical characteristics of the network can influence its permeability to substrates, inhibitors, products, and other medium components. The mechanical properties of the network may constrain the type of catalyst particle geometries that are possible. Compressibility and other attributes of mechanical strength are much more important in large-scale practice than in laboratory study. Many of the polysaccharide beads commonly applied in laboratory research because of their biocompatibility are not well suited for large-scale application because of their high compressibility which limits the utility of these materials to shallow columns. Similarly, particles which are impact sensitive are not suitable for use in contacting schemes such as agitated slurry reactors in which the catalyst beads must withstand exposure to collisions without substantial attrition or breakage.

Table 9.6 Polymeric networks used for cell immobilization

Network formation	Cross-links	Examples
Precipitation	Nonspecific	Collagen, polystyrene, carrageenan
Ion-exchange gelation	Ionic	Al-alginates
Polycondensation	Covalent-heteropolar	Epoxy resins
Polymerization	Covalent-homeopolar	PAAm, PMAAm

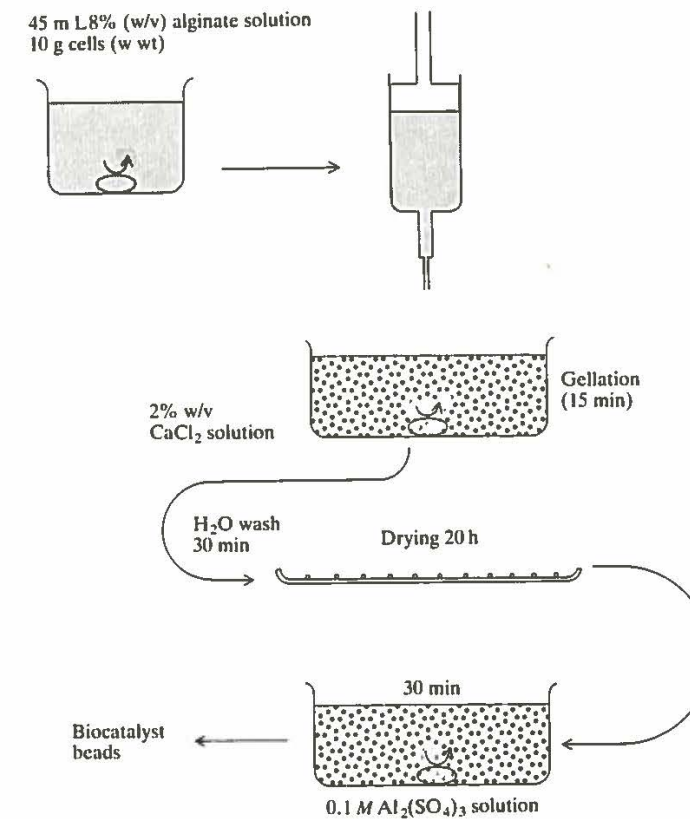


Figure 9.27 Summary of one protocol for entrapping cells in alginate beads.

Table 9.7 Important parameters of polymer networks used for cell entrapment

Mechanical	Chemical
Permeability	
Geometry	Toxicity
Compressibility, strength	Hydrophobic/philic
Shear sensitivity	Ionic composition

The chemical properties listed may influence catalyst activity directly through action on the cell's metabolic controls and indirectly by influence on the local microenvironment of the cells. For example, if the polymeric network contains toxic chemicals, degradations in cellular activities can be expected. The charge, ionic composition, and hydrophobicity of the network may all influence the partition coefficients of reaction mixture components and alter the concentrations in contact with the cells relative to the concentrations delivered in the bulk reaction mixture solution at the exterior of the catalyst particles.

Another method of cell entrapment is entanglement in convoluted or porous structures. Compressed stainless steel screens have been used to support the growth of microorganisms. Also, mold spores inoculated into autoclaved beads of porous filter aid material have been used as an inoculum for batch fermentations. Cells have also been entrapped within the macroporous regions in asymmetric hollow fibers. In addition to these local entrapment methods, we should remember that complete or partial cell entrapment can be achieved on a macroscopic scale by use of cell separation and recycle to the reactor. Alternatively, relatively small substrates and products may be added to or removed from a cell suspension through a dialysis or other type of ultrafiltration membrane placed in the cell suspension.

Many different types of cells have been immobilized by adsorption or covalent attachment to the surfaces of various solid support materials. Examples of immobilization of cells ranging from bacteria to mammalian tissue cells on natural and synthetic materials are summarized in Table 9.8. Further information on these and other immobilization methods may be found in the general immobilized cell references listed at the end of this chapter and in the specific references associated with the examples presented next.

**Table 9.8** Examples of cells immobilized by attachment to surfaces

Cells	Support
Adsorption adhesion	
<i>E. coli</i> , <i>Cl. acetobutylicum</i>	Ion exchange resin
<i>Asp. oryzae</i>	Modified cellulose
<i>Streptomyces</i>	Modified Sephadex
<i>Lactobacilli</i> , yeast	Gelatin
<i>S. carlsbergensis</i>	PVC
<i>Pseudomonas</i> sp.	Anthracite
Tissue cells	Polysaccharide
Covalent bonding	
<i>B. subtilis</i>	Agarose and carbodiimide
<i>E. coli</i>	Ti(IV) oxide

### 9.5.2 Applications of Immobilized Cell Biocatalysts

In this summary of examples illustrating the different levels of immobilized cell catalysis, we shall proceed from the simplest to the most complicated situation. By immobilizing whole cells which have been suitably permeabilized [by treatment with lytic enzymes, by exposure to alcohols or dimethylsulfoxide (DMSO)], individual enzymes in approximately their natural environment may be immobilized for continuous process use. Many such immobilized enzyme/immobilized cell catalysts have been prepared and some are now in commercial use. This strategy for enzyme immobilization has the advantage of being relatively simple compared to isolation of enzyme from the cells and subsequent immobilization, and, perhaps of greater practical significance, this method may enhance immobilized enzyme stability.

Shown in Fig. 9.28 is experimental data on deactivation of aspartase and fumarase enzyme activity in immobilized *E. coli* cells and in suspended intact cells. For both enzymes, loss of activity is greatly retarded in the immobilized cell formulations. There is a possibility that some of this apparent stability may be due to mass-transfer limitations as was discussed in Sec. 4.4; that is, if the immobilized enzyme/cell catalyst is operating under severely diffusion-limited kinetics, observed deactivation will be substantially slower than actual deactivation. However, in this particular system, further experiments by Chibata and colleagues point to a true stabilizing effect of enzyme retention in the native cellular environment. Intact *E. coli* cells were sonicated and the soluble and precipitate fractions were subsequently separated and immobilized. The aspartase activity in the immobilized soluble fraction decayed much more rapidly than the aspartase activity in the immobilized precipitate fraction. Furthermore, intact cells treated

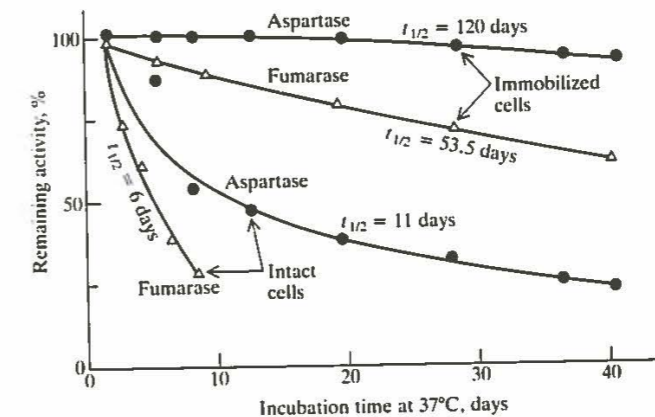


**Figure 9.28** Comparison of deactivation of aspartase and fumarase in suspended cells and in immobilized cells (Reprinted by permission from I. Chibata (ed.), "Immobilized Enzymes," p. 140, Kodansha Ltd., Tokyo, 1978.)

with solubilizing agents for membrane-bound enzymes (deoxycholate or Triton X-100) yielded precipitate and soluble fractions which both lost activity rapidly after immobilization. These experiments suggest that aspartase is stabilized by binding or association with cellular membranes or granules. However, it should be noted that the opposite effect has been observed in whole-cell enzyme immobilization. Glucose isomerase in permeabilized immobilized cells of some organisms loses activity more rapidly than the same enzyme isolated from the cells. This phenomenon has been attributed to proteolytic attack on the enzyme by intracellular enzymes.

The subject of intracellular hydrolytic activities is very important across the entire spectrum of immobilized cell applications. As discussed in Chap. 6, cells require for efficient function certain intracellular hydrolytic activities. Loss of enzyme activity by intracellular hydrolysis as well as loss of cellular membrane and transport integrity by other degradative processes clearly play key roles in determining the useful lifetime of an immobilized cell catalyst. Greater understanding of these intracellular degradative processes, along with other types of deactivation events due to protein unfolding and membrane damage due to chemical attack from medium components, is required in order to optimize the cells genetically and to formulate the best immobilized cell preparation and corresponding reactor configuration and operating conditions. Indeed, we should note here parenthetically that decades have been invested in developing useful strains within the context of suspended cell cultivation and that long-term efforts may be needed to achieve the genetic modifications required to yield especially useful organisms for immobilized cell applications.

At the next level of catalytic complexity is multistep bioconversion involving cofactor use and regeneration. The most widely studied systems of this type involve transformation of glucose to economically important end-products in anaerobic environments. Glucose conversion to ethanol by immobilized yeast (*Saccharomyces cerevisiae*) or bacteria (primarily *Zymomonas mobilis*) have been studied extensively, and at least one process based upon immobilized cell biocatalysis has been demonstrated at pilot scale [34].

Studies of glucose to ethanol conversion using immobilized cells originated with investigations of continuous brewing, in which highly flocculent yeast strains permit retention of cells which could be effectively immobilized in a fluidized-bed reactor (Sec. 9.6.4). Subsequently, yeast immobilized by adsorption on a gelatin film, and by entrapment in  $\kappa$ -carrageenan, alginate, or polyacrylamide have been reported. Experiments with a column of *Saccharomyces carlsbergensis* cells immobilized in  $\kappa$ -carrageenan showed a startup transient period of around seven days after which the concentration of viable cells in the gel was constant as were the effluent glucose and ethanol concentrations. Subsequent process improvements have led to increased product concentrations exceeding 100 g ethanol/L.

The Kyowa Hakko Kogyo Company of Japan has announced a pilot-scale process for ethanol production using immobilized yeast cells in fluidized-bed reactors (Sec. 9.6.4). The flow sheet for this process is given in Fig. 9.29. Results

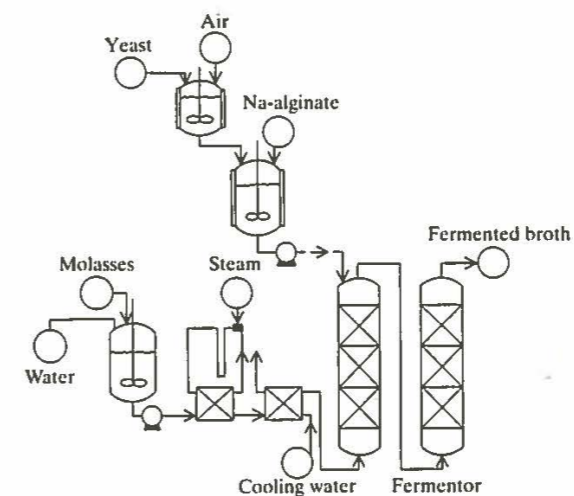


Figure 9.29 Process schematic for ethanol production using immobilized yeast [34].

of three months of initial trials include production of 8.5% v/v of ethanol from diluted cane molasses feed (14% glucose concentration) at 30°C at a space velocity (volume feed · volume gel<sup>-1</sup> · h<sup>-1</sup>) of 0.4 to 0.5 h<sup>-1</sup>. Sugar-to-ethanol yield was 95% of the theoretical maximum and the ethanol productivity based on total column volume was ca 20 g L<sup>-1</sup> h<sup>-1</sup>.

A more complicated situation arises in conversion of glucose to acetone, butanol and ethanol using the bacterium *Clostridium acetobutylicum* and related strains. This organism possesses a complex regulatory system for its catabolic pathways, details of which remain incompletely understood in spite of long experience with this organism in traditional suspended culture fermentations. Under certain environmental and cell states, organic acids are the primary end-products of glucose metabolism, while in other situations the desired organic solvents are produced. Consequently, this is a more complicated and difficult system than the glucose to ethanol conversion accomplished by yeast, since here we must consider how to manipulate the final product selectivity in the desired fashion.

The feasibility of continuous, long-term bioconversion of glucose to organic solvents has been demonstrated in research by Förberg and coworkers [35]. In this study, *Cl. acetobutylicum* entrapped in calcium alginate gel was fed with a glucose medium which lacked essential growth factors. Intermittently, at intervals starting at two to four hours and subsequently increased to eight hours, the culture was fed a complete growth medium in order to regenerate deactivated catalyst. Using this operating strategy, which combines the multistep bioconversion, nongrowth operation with brief intervals of full cell growth, stable operation of the system for an interval of eight weeks was reported. Overall biomass production was greatly suppressed and the yield of butanol per unit amount of

**Table 9.9 Comparison of butanol formation yields and productivities for immobilized<sup>†</sup> and suspended<sup>‡</sup> cells of *Clostridium acetobutylicum***

	$Y_{p/x}$ $\left(\frac{\text{g butanol}}{\text{g cells (dry wt)}}\right)$	$Y_{p/s}$ $\left(\frac{\text{g butanol}}{\text{g glucose}}\right)$	$r_{fp}$ $\left(\frac{\text{g butanol}}{\text{L} \cdot \text{day}}\right)$
Growing immobilized cells (full medium)	1.3-1.9	0.11	
Immobilized cells (intermittent dosing of full nutrient medium)	50	0.20	16.8
Batch culture, suspended cells	3.6	0.19	6.9

<sup>†</sup> C. Förberg, S.-O. Enfors, and L. Haggström, *Eur. Appl. Microbiol. Biotech.* 17: 143, 1983.

<sup>‡</sup> A. R. Moreira, D. C. Ulmer, and J. C. Linden, *Biotech. Bioeng. Symp.* no. 11: 567, 1981.

glucose consumed was increased significantly relative to a comparison case in which immobilized cells were exposed to full growth medium. Listed in Table 9.9 are representative parameters of the immobilized cell experiments with full growth medium, for immobilized cells with intermittent dosing of growth medium alternating with only conversion medium, and results from a conventional batch fermentation using the suspended bacterium.

While further research and development is needed to improve the immobilized cell system, this example clearly indicates the opportunity for altering kinetic and stoichiometric behavior by appropriate choice of cell formulation and medium manipulation, providing additional options for engineering manipulation and optimization of a biocatalytic process.

These fermentation examples introduce the challenging problem of gas transport in immobilized cell catalysts and associated reactors. Here we shall consider only the local problem of transport in the catalyst. Suppose that the bioconversion can be described stoichiometrically as a single chemical reaction and that the transport of substrate S and product P in the catalyst can be characterized by effective diffusivities  $D_s$  and  $D_p$ , respectively. It is easy to show using the governing material balances and boundary conditions on the catalyst that the concentration of product  $c_p$  and concentration of substrate  $c_s$  within the catalyst formulation are related by the following equation, in which  $\alpha$  denotes the number of moles of product formed for each mole of substrate consumed

$$c_p = c_{p0} + \frac{\alpha D_s}{D_p} (c_{s0} - c_s) \quad (9.113)$$

Here subscripts 0 denote conditions at the external boundary of the catalyst. Several useful observations can be made simply by setting  $c_s$  equal to zero and calculating thereby, based only on stoichiometric and transport considerations, the maximum level of product concentration which can be obtained in such a catalyst.

This simple equation has important ramifications in cases of gas consumption and production. First, supposing that the substrate is a sparingly soluble gas

such as oxygen, we see from Eq. (9.113) that only a small increase in product concentration can be expected in reaction in a single catalyst particle. Considering now the case of formation of a moderately soluble gas such as  $\text{CO}_2$ , it is evident that, using a highly soluble substrate such as glucose, a concentration of  $\text{CO}_2$  may be obtained within the catalyst which exceeds the saturation concentration, giving rise to nucleation and growth of gas bubbles within the catalyst. This phenomenon has been reported to cause severe mechanical difficulties in immobilized cell reactors, resulting in bursting of networks containing entrapped  $\text{CO}_2$ -producing cells and of cartridges containing yeast cells immobilized in hollow fibers.

Accordingly, we have problems with limitations on product formation for sparingly soluble substrates and with removal of sparingly soluble products. These concerns dictate use of small thicknesses of catalyst in order to avoid ineffective use of interior catalyst in the case of a sparingly soluble gas and in order to avoid excessive buildup of sparingly soluble products in that situation. This short catalyst thickness can be achieved either by use of small particles or by formulation of the catalyst so as to contain supported cells or entrapped cells only in a thin outer film on the outer surface of a larger particle or object which facilitates mechanical retention in the process. Addressing requirements for supply and removal of sparingly soluble compounds is a major consideration also at the reactor design level.

Interestingly, experimental studies of ethanol production from glucose using immobilized yeast have indicated different overall conversion rates in immobilized cells compared to suspended cells incubated under similar conditions. In some of these investigations, diffusion limitations and their effects are possibly implicated, but enhancements in specific rates of ethanol production of the order of 30-50 percent have been observed in carefully controlled comparison experiments under identical reaction conditions and with no mass-transfer limitations. Alteration in local water activity by the presence of the supporting matrix or surface has been hypothesized as one cause of such phenomena. Other possibilities include altered chemical microenvironments due to the support as mentioned earlier.

However, it would not be surprising to encounter substantial metabolic adjustments to the unusual environments which cells encounter in the immobilized state. Binding or adherence to a solid surface may be recognized by specific receptors on the cell which alter metabolic function. Similarly, interference with normal morphological development by multipoint binding to a surface, by fibers of the entrapment matrix, or by cell-cell contact may elicit metabolic responses not evident in relatively unconcentrated suspended cell environments. Furthermore, certain extracellular products will be present in such dense immobilized matrices at much higher concentrations than in suspended cell systems. Certainly, we might expect that microbial cells ordinarily functioning in a relatively independent state may exhibit altered catalytic properties when grown in a more dense, tissue-like form in an immobilized cell preparation. Therefore, it is necessary to characterize carefully the intrinsic kinetics of immobilized cell catalysts

**Table 9.10** Examples of biosynthesis processes conducted by immobilized cells

Substrates	Immobilized cells	Product	Comments
Glucose, inorganic ammonia, metal ions	<i>Corynebacterium glutamicum</i> <sup>†</sup>	Glutamic acid	15 g product/L in 144 h
Pantothenic acid, cysteine, ATP, MgSO <sub>4</sub>	<i>Brevibacterium ammoniagenes</i> <sup>†</sup>	Coczyme A	500 µg product/mL
Glucose medium	<i>Penicillium chrysogenum</i> <sup>†</sup>	Penicillin	1.5 units mL <sup>-1</sup> h <sup>-1</sup>
1% peptone medium	<i>Bacillus</i> sp (KY 4515) <sup>†</sup>	Bacitracin	16–19 units mL <sup>-1</sup>
1% meat extract, 0.05% yeast extract medium	<i>Bacillus subtilis</i> FERM-P No. 2040 <sup>†</sup>	α-Amylase	15,000 units/mL
LB broth	<i>Escherichia coli</i> C600 (pBR322) <sup>‡</sup>	β-Lactamase	1 × 10 <sup>-11</sup> units/cell/h 8 units/mL/h

<sup>†</sup> Entrapped in polyacrylamide gel.

<sup>‡</sup> Entrapped in hollow-fiber membranes.

and to anticipate possible kinetic alterations due to immobilization. Kinetics based upon suspended cell studies under identical conditions may not be applicable. Even more complicated cellular adjustments in terms of morphology and biochemical activities can be expected as we consider more complicated biocatalytic functions.

In view of the complexities and early stage of development of immobilized cell catalysis for multistep conversions, it is not surprising that relatively little has been done so far on use of immobilized cells to achieve biosynthesis of metabolites and biological polymers. Features of some of the experimental studies of biosynthesis by immobilized cells are indicated in Table 9.10. In some cases, there was little cell growth, while in other cases, intermittent full growth medium feeding was employed to extend useful activity of the cells. Full cell growth was allowed in some of these studies. Of course, if the cells are growing at some finite rate, either washout or lysis of cells must occur at a rate which balances the growth rate in order to maintain a steady-state level of functioning cells. In the case of animal cells cultivated on solid surfaces, regulatory mechanisms built into the cells arrest growth approximately at the stage of monolayer development and switch the metabolism of the cells from growth to product formation. There is much still to be learned to achieve the feasible ideal of immobilized cell systems for synthesis of complex products at high yields and high rates in continuous reactors.

## 9.6 MULTIPHASE BIOREACTORS

Under many circumstances it is approximately valid to treat bioreactors, which almost always contain multiple phases in the form of cells, low solubility sub-

strates or products, gas bubbles, or catalyst particles, as effectively homogeneous. There are several situations, however, in which it is important to take the multiphase nature of the reactor contents into account when designing the bioreactor or analyzing its performance. Our focus in this section is on such reactors and some of the approaches which may be applied to describe them conceptually and mathematically.

### 9.6.1 Conversion of Heterogeneous Substrates

Bioreactors containing heterogeneous substrates are encountered in utilization of starch and cellulose particles, in conversion of steroids, and in growth on paraffinic hydrocarbons. In such cases, we must establish or make assumptions about the location of the reaction—with the major possibilities being either at the phase interface or in bulk solution using a very small amount of dissolved substrate. In some cases, both situations arise. For example, digestion of cellulose particles begins by adsorbed cellulase enzymes followed by conversion of glucose in solution by microorganisms. In reactors involving heterogeneous substrates, the interfacial area per unit reactor volume is typically a central parameter which depends on substrate pretreatment in some cases and most directly upon reactor operating conditions in others. The following example of microbial growth on an insoluble carbon source provides a specific illustration of the different types of considerations which are frequently necessary in analysis, design, and operation of such reactors.

**Example 9.2: Agitated-CSTR design for a liquid-hydrocarbon fermentation**<sup>†</sup> Some microorganisms, e.g., the yeast *Candida lipolytica*, will grow on dodecane and other paraffinic hydrocarbons which are practically insoluble in water. Two alternative mechanisms have been proposed for microbial growth at the hydrocarbon-aqueous-phase interface; (1) cells (characteristic diameter  $D_c$ ) much smaller than dispersed hydrocarbon droplets (diameter  $D_h$ ) cluster around the paraffin drops; on the other hand, (2) if  $D_h \ll D_c$ , we may presume that droplets adsorb onto the outer surfaces of the relatively large microorganisms.

The closing observations in Sec. 8.4 on aerated microbial hydrocarbon fermentations indicate that the adsorption and flocculation relations between air bubbles, cells, and hydrocarbon droplets change over the course of a batch fermentation. For a continuous process, however, we may expect to operate in one particular growth mode, thus a single bubble-cell-hydrocarbon droplet configuration may be predominant, rendering quantitative description easier.

Moo-Young and coworkers have considered these two situations and have proposed the following modified Monod growth-rate equations which include the effect of surface-area availability:

Case 1,  $D_c \ll D_h$

$$\mu = \mu_{\max} \frac{s/D_h}{K_s + s/D_h} \quad (9E2.1)$$

<sup>†</sup> Drawn from M. Moo-Young, "Microbial Reactor Design for Synthetic Protein Production," *Can. J. Chem. Eng.*, 53: 113, 1975.

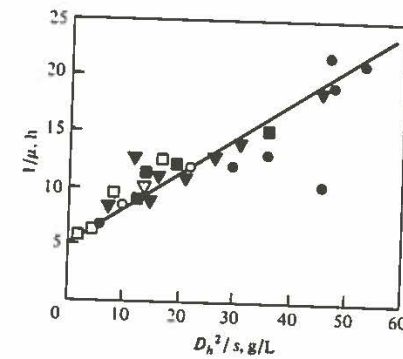


Figure 9E2.1 This double-reciprocal plot of experimental data for growth rates of *C. lipolytica* yeast on dodecane is consistent with the model assuming hydrocarbon droplet attachment to microorganisms. (Reprinted from M. Moo-Young, "Microbial Reactor Design for Synthetic Protein Production," *Can. J. Chem. Eng.*, vol. 53, p. 113, 1975.)

Case II,  $D_c \gg D_h$

$$\mu = \mu_{max} \frac{s(D_h)^2}{K_s'' + s(D_h)^2} \quad (9E2.2)$$

where  $K_s'$  and  $K_s''$  are modified  $K_s$  values. As the Lineweaver-Burk plot in Fig. 9E2.1 indicates, experimental data for the *C. lipolytica*-dodecane system support the second hypothesized mechanism. Equations useful for CSTR design can be developed by relating input agitator power to dispersed hydrocarbon drop size (Chap. 8). If the diameter  $D_h$  of the substrate hydrocarbon droplets is determined by shear at the impeller-tip region, the correlations in Example 8.2 predict that

$$D_h = C \left( \frac{P}{V} \right)^{-0.4} \quad (9E2.3)$$

which was found to fit the experimental data of this study when  $C = 0.023$ . Substitution of this formula into Eq. (9E2.2) yields

$$\mu = \mu_{max} \frac{s(P/V)^{0.8}}{K_s''' + s(P/V)^{0.8}} \quad (9E2.4)$$

Using this specific growth rate in the ideal CSTR model with constant yield factor gives for sterile feed

$$x = Y \left[ s_0 - \frac{DK_s'''}{\mu_{max} - D} \left( \frac{P}{V} \right)^{-0.8} \right] \quad (9E2.5)$$

and

$$D_{max\ output} = \mu \frac{K_s'''}{K_s''' + s_0 \left( \frac{P}{V} \right)^{0.8}} \quad (9E2.6)$$

Figure 9E2.2 shows the biomass production rate  $Dx$  computed using Eq. (9E2.5). Those plots, as well as Eqs. (9E2.5) and (9E2.6), clearly show the importance of considering interactions between biological reactions and fluid mechanics in the design and analysis of microbial reactors.

In spite of the changing adsorption patterns in batch hydrocarbon fermentations referred to in Sec. 8.4 and Fig. 8.14, a model assuming that the cells of *C. lipolytica* growing on hydrocarbon droplets adsorb continuously on the hydrocarbon-droplet surface until a cell monolayer is formed gives some agreement with batch-fermentation data (See L. E. Erickson, A. E. Humphrey, and A. Prokop, "Growth Models of Cultures with Two Liquid Phases. I. Substrate Dissolved in Dispersed Phase," *Biotech. Bioeng.*, 11: 449, 1969).

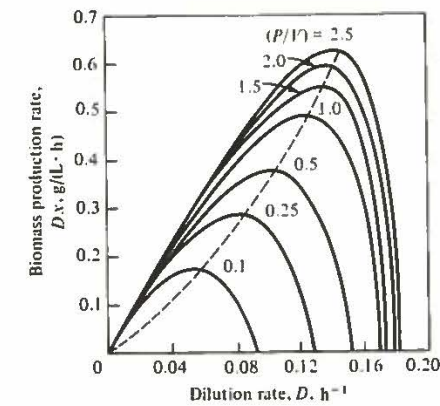


Figure 9E2.2 Biomass productivity for liquid-hydrocarbon fermentation as a function of dilution rate and agitator power input per unit volume  $P/V$  ( $\text{hp}/\text{m}^3$ ).

### 9.6.2 Packed-Bed Reactors

Columns packed with immobilized biocatalyst particles currently enjoy several applications and additional uses are expected. In such reactors, which are called packed-bed or fixed-bed reactors, immobilized enzymes are used for glucose isomerization, for selective penicillin hydrolysis, and for selective reactive separation of racemic mixtures of amino acids. Many immobilized cell systems have also been examined in packed-bed configurations.

The simplest and often quite useful description of packed-bed reactor performance uses a plug-flow reactor model modified to account for the influence of the packed catalyst on flow and kinetics features. The superficial flow velocity through the reactor is equal to the volumetric flow of the feed divided by the void cross-sectional area which is the total cross-sectional area times the void fraction  $\epsilon$ . The appropriate rate expression for use in the tubular reactor material balance is based upon use of effectiveness factors as described in Chap. 4. For example, considering a single reaction  $S \rightarrow P$  with intrinsic rate  $v = v(s, p)$  the rate of product formation per unit volume of immobilized biocatalyst pellet at a point in the reactor is:

$$v \Big|_{\text{overall/unit volume of pellet}} = \eta(s_s, p_s)v(s_s, p_s) \quad (9.114)$$

where  $s_s$  and  $p_s$  are the substrate and product concentrations at the exterior pellet surface at that position inside the reactor. In general, the effectiveness factor  $\eta$ , which accounts for intraparticle diffusion, and the rate expression  $v$  depend upon both  $s_s$  and  $p_s$ , as indicated.

If mass-transfer resistance between the bulk liquid phase and the pellet surface is next examined, a steady-state material balance on substrate over the pellet gives for a spherical catalyst pellet of radius  $R$ :

$$\begin{aligned} \text{Rate of substrate diffusion out of bulk liquid} \\ = \text{rate of substrate disappearance by reaction within pellet} \end{aligned}$$

or

$$4\pi R^2 k_s (s - s_s) = \frac{4}{3}\pi R^3 \eta(s_s, p_s) v(s_s, p_s) \quad (9.115)$$

With this equation and reaction stoichiometry,  $s_s$  and  $p_s$  can be evaluated in terms of the bulk liquid concentration  $s$ . Substituting these expressions into Eq. (9.114) then gives the total rate of substrate disappearance per unit volume of catalyst pellets in terms of the bulk fluid substrate concentration.

In writing the material balance on a differential slice of the plug-flow packed-bed reactor, we must remember that bulk fluid exists only in a fraction  $\epsilon$  of this volume and catalyst particles occupy a fraction  $1 - \epsilon$  of this volume. The substrate concentration  $s$  used in this equation is the concentration per unit fluid volume. Accordingly, the material balance on substrate becomes

$$u \frac{ds}{dz} = - \left( \frac{1 - \epsilon}{\epsilon} \right) \eta(s_s, p_s) v(s_s, p_s) \quad (9.116)$$

where, as noted above, the quantities on the right-hand side can be evaluated in terms of  $s$ , allowing integration of Eq. (9.116) for given values of feed substrate and product concentration.

The situation is greatly simplified if intraparticle and external mass-transfer resistances are negligible, since these conditions imply  $\eta \rightarrow 1$  and  $s_s \rightarrow s$ , respectively. In such circumstances, the governing mass balances can be integrated analytically, with results as indicated previously in Table 9.2 for plug-flow reactors.

As mentioned earlier in connection with our discussions of the dispersion model for flow reactors, flow around the particles in a packed bed and mixing in the interstitial voids of the reactor create a small amount of backmixing which may cause deviations from ideal plug-flow behavior. In these cases, the dispersion model with dispersion coefficient evaluated as discussed earlier or a tanks-in-series model may be applied. The effect of a small amount of dispersion on reactor performance relative to ideal plug-flow behavior was discussed already in connection with sterilization reactors. Other approaches to mathematical modeling of packed-bed systems with different levels of backmixing and different interactions between the fixed and flowing phases are available in the chapter references.

### 9.6.3 Bubble-Column Bioreactors

By bubble-column bioreactors we mean reactors with large aspect ratio (height to diameter ratio) which take the form of columns instead of more squat tanks typical of agitated vessels. Also, in such reactors, mixing is supplied entirely by forcing compressed gas into the reactor which then rises through the liquid. Reactors of this type have been used for many years in the chemical industry because of their advantages of relatively low capital cost, their simple mechanical configuration, and reduced operating costs based on lower energy requirements. While relatively unfamiliar in the biological processing industries, tower bioreac-

tors have been used on a large scale for beer production and for vinegar manufacture. Also, related tower designs are essential elements of very large scale processes which have emerged for cultivation of microorganisms (single-cell protein or SCP) for use as animal feed.

In some cases a single column, which may contain internal plates or even agitators in some or all stages, is used. The reactors may be used in a batch mode or operated continuously with cocurrent or countercurrent flow of liquid relative to the rising gas. In several recent designs, called air lift or pressure cycle reactors, an external loop is used to provide fluid circulation. Such loops have the advantages of permitting high efficiency heat exchange, a major need for large-scale microbial cultivation on paraffinic or methanol substrates. Also, the circulation loop enhances definition of the flow and mixing properties in the vessel. Properties of bubble columns with and without external loops and single or multiple stages have been extensively investigated and described in a series of studies by Schügerl and colleagues [36, 37]. Here we shall only introduce some of the concepts which can be applied to formulate equations for designing such reactors and for analyzing experimental data obtained in such systems.

We saw in Chap. 8 that for a sufficient density of rapidly growing aerobic organisms, the overall growth rate is typically limited by the rate of oxygen transfer from the gas bubbles into the liquid phase. Analysis of this limiting rate process requires knowledge of liquid and gas mixing within the tower. Studies on air-water sparged columns without any recycle loops have shown that if (a) gas flow rates are large relative to the liquid and (b) column height  $L$  and diameter  $d_t$  are of similar magnitude, both liquid and gas phases are well mixed. Conversely, for the more typical long columns, Eq. (8.115) gives the column height  $L (= z \text{ there})$  to obtain a desired amount of  $O_2$  transfer.

For the integrated form (8.115) to be valid, it is necessary to maintain the interfacial area factor  $a$  nearly constant along the tower. This in turn requires that the gas remain in bubbling flow. Air-water experiments reveal that the gas bubbles rising through the liquid will coalesce into slugs if the gas volume fraction  $\epsilon$  exceeds a critical value  $\epsilon_{\max}$ , which is roughly 0.3. The requirement that the gas volume fraction remain less than  $\epsilon_{\max}$  can be translated into a design specification for column diameter by noting that any point in the tower

$$F_G = u_G \epsilon \frac{\pi d_t^2}{4} \quad (9.117)$$

where  $F_G$  and  $u_G$  are the gas volumetric flow rate and linear velocity, respectively. We may reasonably assume  $u_G$  is the terminal velocity  $u_t$  of a single gas bubble in a stagnant liquid and that  $F_G$  is roughly the same as the feed gas flow rate  $F_{Gf}$ . The latter assumption is rationalized on the grounds that  $O_2$  consumed from the bubbles is at least partially replaced by  $CO_2$ . Under these conditions Eq. (9.117) reveals that  $\epsilon$  is smaller than  $\epsilon_{\max}$  so long as

$$d_t \geq 2 \left( \frac{F_G}{u_G \epsilon_{\max}} \right)^{1/2} \quad (9.118)$$



which can be used to estimate sizing of the tower. Not considered in this elementary analysis is rising bubble growth due to reduction in hydrostatic head. This may increase  $u_r$  and, in the extreme, cause a transition to cap-shaped bubbles.

Other means of providing small gas bubbles throughout the tower include insertion of perforated plates and/or impellers or other internal devices. These internals break up any coalesced gas slugs and thereby preserve a large gas-liquid contact area. Further details on alternative mechanical designs for bioreactors are presented in Sec. 9.7.3.

Figure 9.30 illustrates schematically the conceptual framework applied to formulate a 2-phase mathematical model for a concurrent flow tower-loop reactor (airlift bioreactor). In the tower section on the right-hand side, two-phase flow of gas and liquid occurs. After gas separation at the top of the column, a liquid stream is recycled through the loop on the left to the bottom of the column, which is also the point of gas sparging into the system. The system is described by treating the liquid and gas as separate phases which ascend the tower section with different linear velocities  $u_L$  and  $u_G$ , respectively. The volume fractions occupied by liquid and gas are designated  $\epsilon_L$  and  $\epsilon_G$ , respectively, and these values are determined from use of gas holdup correlations or measurements. Superimposed on bulk convective axial transport in plug flow is axial dispersion in both the gas and liquid phase with different dispersion coefficients. Substrate and oxygen utilization occurs due to microbial reactions in the fluid phase and oxygen is depleted from the gas phase by virtue of oxygen transfer into the liquid.

Examining now a differential slice of the tower section between position  $z$  and position  $z + dz$  (see Fig. 9.30b), we can derive the following material balances on oxygen concentration in the liquid phase and oxygen mole fraction in the gas phase by extensions of the methods already illustrated for treating steady-state plug-flow reactors. The final forms of these mass balances are given by

Liquid phase

$$\frac{\partial c_l(z, t)}{\partial t} = D_l(t) \frac{\partial^2 c_l(z, t)}{\partial z^2} - u_L(t) \frac{\partial c_l(z, t)}{\partial z} - r_f(x, s, c_l, z, t) + k_l(z, t) a(z, t) [c_l^*(z, t) - c_l(z, t)] \quad (9.119)$$

Gas phase

$$p(z, t) \frac{\partial x_g(z, t)}{\partial t} = D_g(t) \frac{\partial}{\partial z} \left( p(z, t) \frac{\partial x_g(z, t)}{\partial z} \right) - \frac{\partial}{\partial z} \left( p(z, t) x_g(z, t) u_G(z, t) - \frac{RT \epsilon_L(t)}{M_{O_2} \epsilon_G(t)} \right) - k_l(z, t) a(z, t) [c_l^*(z, t) - c_l(z, t)] \quad (9.120)$$

Combined with analogous material balances for substrate consumption and cell growth, and similar balances for the liquid phase in the recycle loop, these equations can be used for description of unsteady-state mass-transfer experiments, batch operation of the bioreactor, or steady-state and dynamic behavior of the

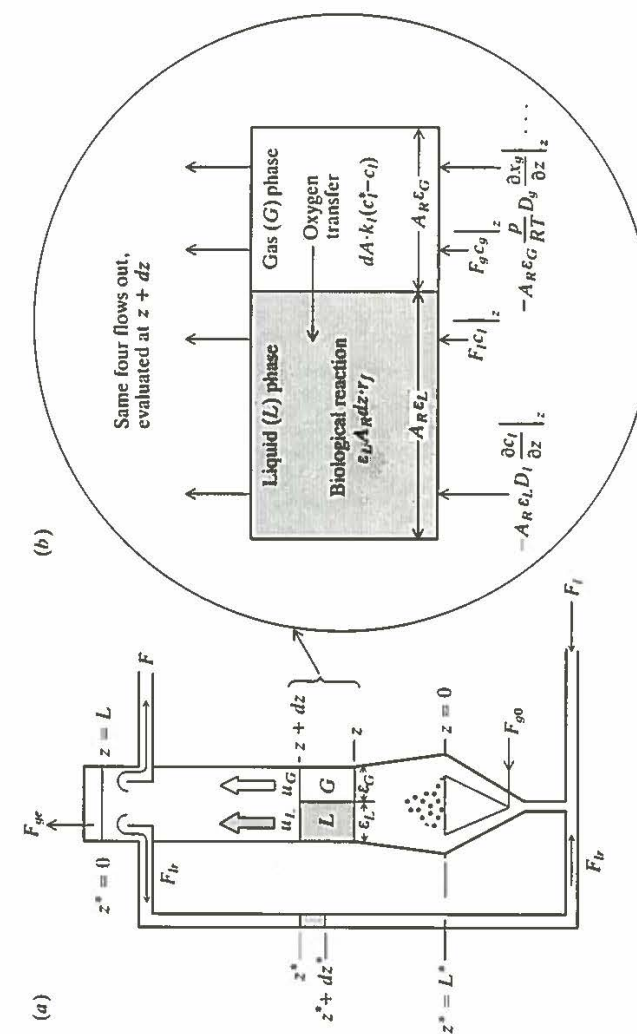


Figure 9.30 (a) Schematic diagram showing framework of a mathematical model for a bubble column reactor with recycle and (b) detail of a differential section showing terms considered in deriving gas (g, G) and liquid (l, L) phase material balances (Ref. 37).

tower bioreactor with continuous feed and product removal. Extensive experimental studies and parameter evaluation for this model are described in Ref. 37.

#### 9.6.4 Fluidized-Bed Bioreactors

Fluidized-bed reactors generally are column geometries as considered in the last section and, if gas supply or removal is involved, require consideration of gas flow and mass transfer similar to those just discussed. However, in a fluidized-bed reactor an additional catalyst phase appears.

In a fluidized-bed tower reactor like the one shown in Fig. 9.31, liquid flows upward through a long vertical cylinder. Heterogeneous biocatalyst particles (floculated organisms, pellets of immobilized enzymes or cells) are suspended by drag forces exerted by the rising liquid. Entrained catalyst pellets are released at the top of the tower by the reduced liquid drag at the expanding cross section and fed back into the tower. Thus, by a careful balance between operating conditions and organism characteristics, the biocatalyst is retained in the reactor while the medium flows through it continuously.

Fluidized-bed biological reactors are considerably more complex than the CSTR and PFTR varieties so far examined. For example, in tower fermentors used for continuous beer production, there is a gradient of yeast flocs through the unit. Near the bottom, the organism concentration (centrifuged wet weight per weight of broth) may reach 35%, while the yeast concentration drops to 5 or 10% at the top of the tower. Moreover, there is a progressive change in medium characteristics along the reactor. Easily fermented sugars (glucose, fructose, sucrose, some maltoses) are consumed first, near the feed point, thereby lowering the medium density. In the middle and upper portions of the tower, the yeast flocs ferment maltotriose and additional maltose. This scenario of rapid initial fermentation followed by slower reactions involving less desirable substrates is consistent with the experimental data shown in Fig. 9.32.

A rudimentary model for such fluidized reactors can be developed by assuming that (1) the biological catalyst particles (microbial flocs or immobilized-enzyme pellets) are uniform in size, (2) the fluid-phase density is a function of substrate concentration, (3) the liquid phase moves upward through the vessel in plug flow, (4) substrate-utilization rates are first-order in biomass concentration but zero-order in substrate concentration, and (5) the catalyst-particle Reynolds number based on the terminal velocity is small enough to justify Stoke's law (recall Example 1.1). Assumptions (4) and (5) are reasonable for many applications, and (1) to (3) may be adequate approximations.

Under these assumptions, the substrate conservation equation follows the form of Eq. (9.15):

$$\frac{d(su)}{dz} = -kx$$

or

$$u \frac{ds}{dz} + s \frac{du}{dz} = -kx \quad (9.121)$$

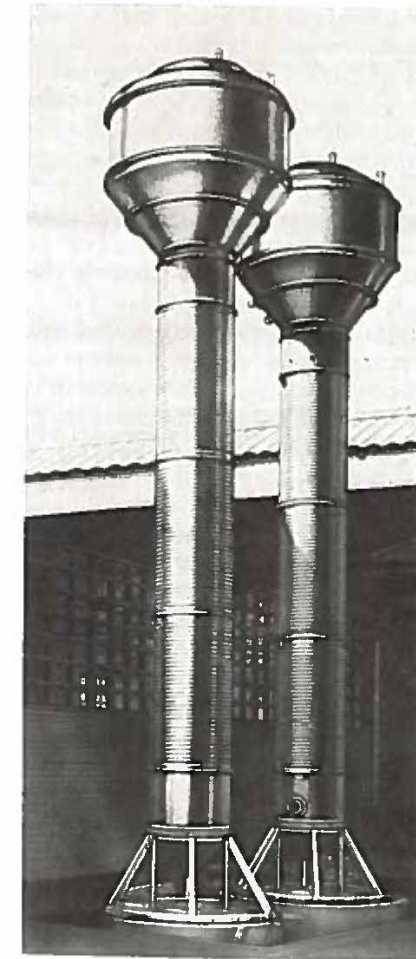


Figure 9.31 A tower fermentor used for continuous brewing. (Courtesy of A. P. V. Co., Ltd.)

For Stoke's flow, the concentration of the suspended biomass can be related to the liquid flow velocity in a fluidized bed by

$$x = \rho_0 \left[ 1 - \left( \frac{u}{u_t} \right)^{1/4.65} \right] \quad (9.122)$$

where  $\rho_0$  is the microbial density on a dry weight basis and  $u_t$  is the terminal velocity of a sphere in Stoke's flow (Eq. (8.34)). (Should the dry-weight or wet-weight biomass density be used in the terminal-velocity formula?) Note that in the context of the fluidized bed we assume that local biomass concentration is

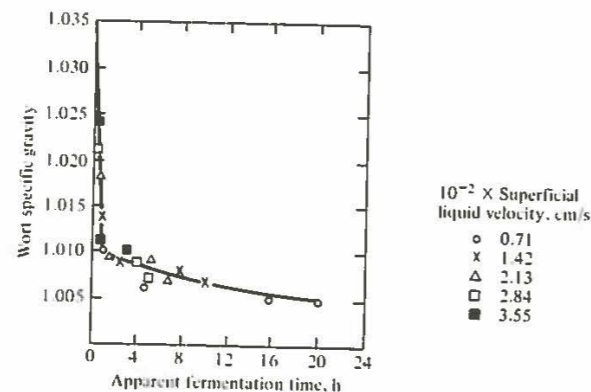


Figure 9.32 Column fermentor data for yeast growth on a sugar mixture show an initially rapid rate of substrate utilization (as revealed by change in wort specific gravity), followed by a period of much slower utilization rates. (Reprinted from R. N. Greenshield and E. L. Smith, "Tower-Fermentation Systems and Their Applications," *The Chemical Engineer*, May 1971, 182.)

dictated entirely by hydrodynamic factors rather than the biochemical-reaction-metabolism features emphasized for other reactor types. Substituting Eq. (9.122) into (9.121) leaves two unknowns,  $s$  and  $u$  as functions of position  $z$  in the tower.

We complete the model by applying Eq. (9.15) to total mass ( $r_f = 0$ ) to reveal

$$\frac{d}{dz}(\rho u) = 0 \quad (9.123)$$

Expanding (9.123) and using  $\rho = \rho(s)$  gives

$$\rho(s) \frac{du}{dz} + \left(u \frac{d\rho}{ds}\right) \frac{ds}{dz} = 0 \quad (9.124)$$

To cast the model in standard form suitable for numerical integration, we may now view Eqs. (9.121) and (9.124) as simultaneous algebraic equations in the unknowns  $ds/dz$  and  $du/dz$ . Solving this algebraic set, which need not be written out in full here, gives  $ds/dz$  and  $du/dz$  in terms of  $s$  and  $u$ : a set of two simultaneous differential equations to be integrated with the initial conditions

$$s(0) = s_f \quad u(0) = u_f = \frac{F_f}{A_f} \quad (9.125)$$

where  $A_f$  is the tower cross section at the bottom. The effluent substrate concentration  $s_e$  is  $s(z = L)$ .

All this is much simplified if we assume that whatever fluid density changes occur do not affect  $u$  significantly. With  $u$  independent of position, Eq. (9.121) integrates directly, with the result

$$s_e = s_f - k\rho_0 \left[ 1 - \left(\frac{u}{u_t}\right)^{1/4.65} \right] \frac{L}{u} \quad (9.126)$$

where  $x$  from Eq. (9.122) has been inserted and  $L$  is the tower height. Such linear dependence of substrate concentration on mean reaction time  $L/u$  is apparent in at least portions of Fig. 9.32 (if we also assume a linear relationship between  $s$  and  $\rho$ ).

Unfortunately, however, the data in Fig. 9.32 suggest that our most serious error in this model is lumping of many substrates: the various sugars consumed during the anaerobic alcohol fermentation have been grouped together into a single hypothetical or average substrate in our model. In doing this, we have no way to include the glucose effect, which plays a very important role in the operation of continuous tower fermentors for brewing.

It is usually desirable to attempt to maintain plug flow of the reaction mixture through the fluidized bed. Instabilities in the flow patterns within the bed can in some situations cause significant backmixing which results in deterioration of reactor performance. Increased backmixing is more likely as the reactor capacity increases by increasing diameter and as the fluid-flow rate through the reactor is decreased. In many instances in biological fluidized-bed reactors, relatively small fluid linear velocities are necessary because small catalyst particles are used and the density difference between the fluid and the catalyst particles is low. Also, lower fluid velocities give greater catalyst concentrations in the reactor. It has been shown that insertion of static mixing elements into a fluidized-bed bioreactor can substantially improve the bed expansion characteristics and reduce undesired fluid backmixing [44].

Since packed-bed reactors provide a closer approximation to plug-flow, the question may arise as to the advantages and motivations for use of fluidized-bed bioreactors. One major consideration in this connection is contacting of the reaction mixture with gases. It is very difficult to provide effective aeration of packed-bed reactors at significant scale, and, in cases where gaseous products such as  $\text{CO}_2$  are produced, to prevent excessive buildup of gas in later portions of the reactor. A fluidized-bed reactor provides a less constrained flow environment for gas-liquid-solid contacting and mass transport. Providing good gas and liquid supply to biocatalysts is also a major advantage of trickle-bed reactors, our final topic in this section.

### 9.6.5 Trickle-Bed Reactors

Trickle-bed reactors are three-phase systems containing a packed bed of heterogeneous catalyst and flowing gas and liquid phases. One (or more) reactant is provided in each feed liquid and gas phase, so that biochemical reaction depends on contacting of liquid, containing the sparingly soluble reactant from the gas phase, with the catalyst surface. Accordingly, the performance of such reactors is substantially influenced by the physical state of gas-liquid flow through the fixed bed and by the associated mass-transfer processes.

The important physical characteristics of such a reactor are the surface area of the packing, the efficiency of wetting of the catalyst by the flowing liquid phase, the gas-liquid flow pattern, mass transfer of sparingly soluble reactants

from the gas to the liquid phase, mass transfer of both reactants to the catalyst surface, and, in the case of a porous or permeable catalyst, diffusion of reactants to the intraparticle catalytic sites.

One of the first applications of trickle-bed bioreactors which remains in practice today is the trickling biological filter used for wastewater treatment. In this system, which is described in more detail in Chap. 14, a rotating distributor sprays the liquid waste stream over a circular bed of gravel on which microbial films adhere. The liquid trickles down and through the packed bed in approximately laminar flow, while air rises through the bed by natural convection due to heat generated by the microbial reaction. A very similar operating design has been used for manufacture of vinegar (biological oxidation of ethanol to acetic acid) in a rectangular column packed with wood chips. For such a laminar liquid flow case, assuming a simplified geometry such as a plane sheet, a detailed model of the flow and transport processes can be formulated and solved. This problem is addressed further in the case study presented by Atkinson [5].

In applying biocatalysts in industrial practice, other trickle-bed reactor configurations involving cocurrent upflow or downflow of the two phases can be employed. Such reactors have long been used in the petroleum and petrochemical industry for hydrocracking, hydrotreating, and other multiphase reaction processes. When specifying operating conditions and formulating design models for such reactors, it is important to remember that, depending upon the gas and

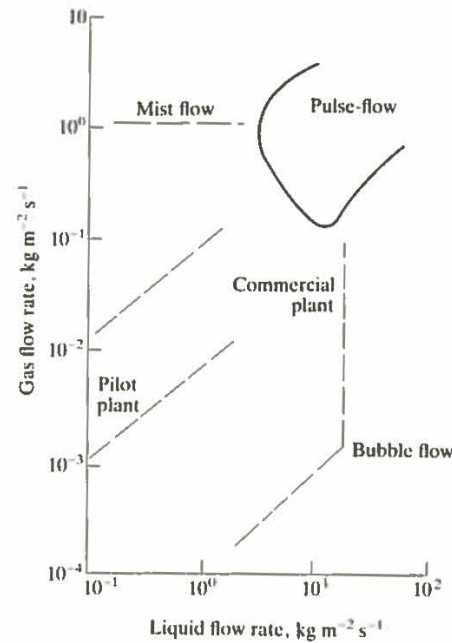


Figure 9.33 Two-phase flow regimes for cocurrent gas-liquid flow in packed beds. (Reprinted by permission from J. G. van de Vusse and J. A. Wesselingh, "Multiphase Reactors," p. 561 in "Chemical Reaction Engineering: Survey Papers" (4th International/6th European Symposium on Chemical Reaction Engineering), DEHEMA, Frankfurt, 1976.)

liquid flow rate (and to some degree on other properties of the fluids), a broad spectrum of two-phase flow regimes ranging from continuous liquid phase with dispersed bubbles to continuous gas phase with dispersed droplets or mist can be obtained (Fig. 9.33). Also, an unstable flow regime in which pulses of gas and liquid alternatively pass as slugs through the reactor is evident. The regions in Fig. 9.33 labelled pilot plant and commercial plant are taken from experience in petroleum processing. Some bioreactor operating regimes involve slow air flow rate. In trickling-filter biological waste treatment, for example, the small exothermicity of the reaction drives aeration upflow by natural convection.

The types of reactor models applicable here resemble those considered earlier in this section. Typically, the system is divided conceptually into a solid phase in contact with a covering liquid film in contact with the gas phase. This is a direct extension of the two-phase bubble-column already mentioned. Then, transport between and through the phases is considered along with any diffusion limitations on reaction rates. An excellent case study illustrating engineering treatment of a biological trickle-bed reactor has been reported by Briffaud and Engasser based on their studies of a trickle-flow fixed-film bioreactor for conversion of glucose to citric acid [46].

As is always the case in selecting a certain reactor configuration, many design, construction, and operating properties must be considered. Table 9.11 lists the comparative advantages and disadvantages of trickle-flow, stirred-slurry, and sparged-slurry-column or fluidized-bed reactors for achieving three-phase contacting and reaction.

Table 9.11 Comparison of design and operating characteristics of different three-phase reactor configurations.

(Reprinted by permission from J. F. van de Vusse and J. A. Wesselingh, "Multiphase Reactors," p. 561 in "Chemical Reaction Engineering: Survey Papers" (4th International/6th European Symposium on Chemical Reaction Engineering), DEHEMA, Frankfurt, 1976.)

Problem areas	Reactor		
	Trickle-flow	Stirred slurry	Sparged slurry column
Staging	++	-	+
Pressure drop	-	+	+
Maximum flow rates	-	+	++
Heat removal	(+)	+	+
Catalyst replacement	-	+	+
Catalyst attrition	(+)	-	(+)
Catalyst utilization	-	+	+
Ease of construction	+	-	++
Scaling-up	(+)	+	-

## 9.7 FERMENTATION TECHNOLOGY

In order to gain some appreciation of different practical aspects of bioreactor design and operation and the process context in which such reaction processes occur, we shall consider in this section some aspects of industrial practice in use of microbial bioreactors (which are traditionally called fermentors). Our primary emphasis will be on standard materials and methods used in batch-fermentation processes. At the close of this section, we will examine some of the alternative reactor designs which have been evaluated in small scale and in some cases have been implemented on extremely large scales.

Figure 9.34 is a schematic illustration of the important components of a typical fermentation process. Selection of a suitable medium has already been mentioned (Sec. 7.1.2), as have means of sterilizing it (Sec. 9.4) and any necessary gases (Chap. 8). Additional comments on medium formulation are provided in the following section. Although some influences of the inoculum on process behavior were discussed in Chap. 7, the microbiological problems encountered in this step require further investigation here. Section 9.7.2 will concentrate on the design of the fermentation vessel itself. Instrumentation and control are examined in Chap. 10; cell and product recovery operations are considered subsequently in Chap. 11.

### 9.7.1 Medium Formulation

A variety of factors must be considered when formulating a fermentation medium. One relates to cellular stoichiometry and the desired amount of biomass to be produced. The basic concept here is simply a material balance: during the

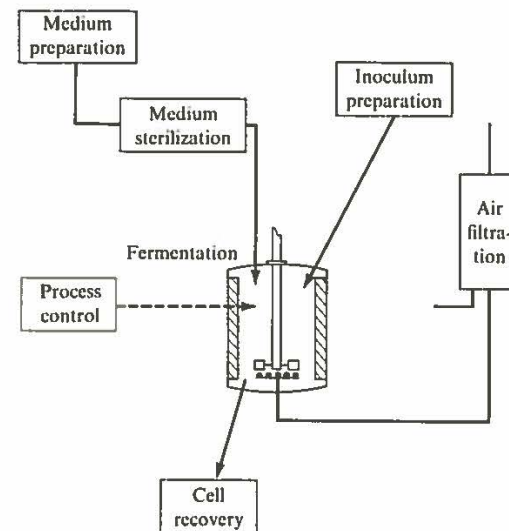


Figure 9.34 The basic operations involved in a typical aerobic fermentation.

course of cellular growth, small organic and inorganic molecules such as glucose and ammonia are converted into biomass. Nutrients (reactants) must be provided in sufficient quantities and proper proportions for a specified amount of biomass (products) to be synthesized. Computation of the necessary amounts of various substrates clearly requires knowledge of the product (biomass) composition. Typical elementary compositions of several different microorganisms were listed in Table 5.10. Also important in medium formulation is provision of necessary minerals (Table 9.12).

Once the elemental requirements have been calculated, choices still remain of the chemical compounds used to supply the necessary elements. Many commercially important microorganisms are chemoheterotrophs whose energy and carbon needs are satisfied by simple sugars. Instead of purified sugars, crude sources such as beet, cane, or corn molasses (50 to 70 percent fermentable sugars) are frequently used as carbon and energy sources in industrial fermentation media. In some instances process wastes like whey and cannery wastes provide cheap yet satisfactory carbon sources for fermentations. For example, one type of food yeast is grown commercially using a byproduct of papermaking, sulfite waste liquor, which contains about 2 percent fermentable hexoses and pentoses.

A variety of possible nitrogen sources are available including ammonia, urea, and nitrate. If the microorganism produces proteolytic enzymes, however, it can obtain necessary nitrogen from a variety of relatively crude proteinaceous sources. Among the possibilities for such crude sources are distiller's solubles, cereal grains, peptones, meat scraps, soybean meal, casein, cereal grains, yeast extracts, cottonseed meal, peanut-oil meal, linseed-oil meal, and corn-steep liquor. Especially important in penicillin fermentation media, corn-steep liquor is a

Table 9.12 Inorganic constituents of different microorganisms

Element	g/100 g dry weight		
	Bacteria	Fungi	Yeast
Phosphorus	2.0-3.0	0.4-4.5	0.8-2.6
Sulphur	0.2-1.0	0.1-0.5	0.01-0.24
Potassium	1.0-4.5	0.2-2.5	1.0-4.0
Magnesium	0.1-0.5	0.1-0.3	0.1-0.5
Sodium	0.5-1.0	0.02-0.5	0.01-0.1
Calcium	0.01-1.1	0.1-1.4	0.1-0.3
Iron	0.02-0.2	0.1-0.2	0.01-0.5
Copper	0.01-0.02	.....	0.002-0.01
Manganese	0.001-0.01	.....	0.0005-0.007
Molybdenum	.....	.....	0.0001-0.0002
Total ash	7-21	2-8	5-10

<sup>†</sup> From S. Aiba, A. E. Humphrey, and N. F. Millis, *Biochemical Engineering*, 2d ed., p. 29, Academic Press, Inc., New York, 1973.

concentrated (50 percent solids) aqueous waste resulting from the steeping of corn to make corn starch, gluten, and other products.

We have mentioned in earlier chapters that some microorganisms require an external source of some amino acids and growth factors. Other microbes which do not have a strict requirement for such medium adjuncts are frequently more productive if nonessential growth factors and nitrogen and carbon sources are provided. In industrial practice growth factors are typically provided by some of the crude-medium components already mentioned, e.g., corn-steep liquor or yeast autolysate. Similarly, these crude preparations often supply many of the minerals necessary for cell function. Other minerals are added to the medium as necessary.

When product formation is the major objective of a fermentation, *precursors* may be added to the medium to improve yield or quality. Generally the precursor molecule or a closely related derivative is incorporated into the fermentation product molecule. Specific examples of precursor applications include benzoic acids for production of novobiocins, phenylacetic acid for manufacture of penicillin G, and 5,6-dimethylbenzimidazole for vitamin B<sub>12</sub> fermentation. In addition to these well-defined precursors, crude media components like corn-steep liquor may also provide useful precursor compounds.

Additional detail on selection and formulation of fermentation media are given in the References. We now turn our attention to other aspects of fermentation technology.

### 9.7.2 Design and Operation of a Typical Aseptic, Aerobic Fermentation Process

While common features are evident among most commercial fermentation processes, significantly different process designs as well as operating practices arise, often as a result of varying sensitivity to contamination by undesirable organisms. If it is necessary to avoid any intrusion, the fermentation must be operated on an *aseptic* basis so that a pure culture is maintained. In some situations, e.g., yeast growth at low pH or fermentation of hydrocarbons by carefully selected bacterial strains, aseptic precautions can be relaxed somewhat since operating conditions discourage growth of many potential contaminants.

This section will concentrate on aseptic practices since they impose the greatest demands on the ingenuity and thoroughness of the biochemical engineer. Our discussion follows the general sequence of events in the operation of a batch fermentation, beginning with development of an inoculum from a stock culture.

Preparation of an inoculum requires careful proliferation of relatively few cells to a dense suspension of from 1 to 20 percent of the volume of the production fermentor. This involves a stepwise procedure of increasing scale. The starting point is a *stock culture*, a carefully maintained collection of a particular microbial strain. Since the strain may be the result of extensive screening and mutation searches and may constitute a significant competitive advantage in the industry, it is imperative that the integrity of the production species be preserved. The usual strategy for achieving maximal genetic stability in a stock strain is to minimize its metabolic activities during storage. Microorganisms are usually

maintained in the desired dormant state by *lyophilization* (freeze-drying) of a liquid cell suspension or by thoroughly drying dispersions of spores or cells on sterile soil or sand. Highly mutated stock organisms are frequently susceptible to *back mutation* and other types of undesirable genetic instability. Thus, constant checks on stock cultures are essential.

If we take lyophilized culture as an example, the next step in inoculum preparation is suspension of the cells in a sterile liquid. A drop of this suspension is then transferred to the surface of an agar *slope* or *slant*, made by solidifying a sterile nutrient medium in an inclined test tube using agar, a polysaccharide derived from seaweed. After incubation to obtain sufficient growth, the cells are again suspended in liquid and added either to a larger agar surface in a flat-sided Blake or Roux bottle or transferred to a shake flask. These flasks are agitated in machines which shake them in rotary or reciprocal patterns to promote submerged growth with adequate transport of gases to and from the organisms. Several successive steps with increasingly larger flasks usually are required before proceeding to the next step. All the transfers described above must be accomplished under sterile conditions. Rooms especially designed to permit sterilization and maintenance of aseptic conditions and controlled temperature are used in the fermentation industry for these delicate operations.

Further proliferation of the culture is next accomplished in one or more seed vessels, small fermentors with many of the instrumentation and control systems typical of large production units. Conditions in these reactors are chosen to maximize growth of the culture.

Since at this point we have moved from conditions typical of a microbiology laboratory into the plant environment, it is well to pause and consider some of the special design features required to maintain aseptic conditions. First, the system must be arranged to permit independent sterilization of its components. As an example of the extreme care this requires in design and operations, consider the problem of transferring the inoculant from the seed tank to the production fermentor. The schematic in Fig. 9.35 illustrates the required services and

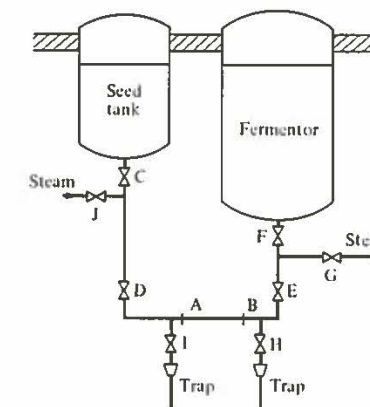


Figure 9.35 Valve and piping configuration for aseptic inoculation of a large-scale fermentor. Operation sequence: (1) install pipe section AB; (2) sterilize connection with 15 lb/in<sup>2</sup> gauge steam for 20 min valves D to J open; valve C remains closed; condensate collects in steam traps in branches H and I; (3) cool fermentor under sterile air pressure with valves C, G, H, I, J closed and valves D, E, F left open; sterile medium fills connection; (4) increase pressure in seed tank to 10 lb/in<sup>2</sup> gauge; lower fermentor pressure to 2 lb/in<sup>2</sup> gauge; (5) transfer inoculum by opening valve C; (6) steam-seal fermentor-seed-tank connections by closing C and F and opening G and J; steam and condensate is bled from partially open D and E.

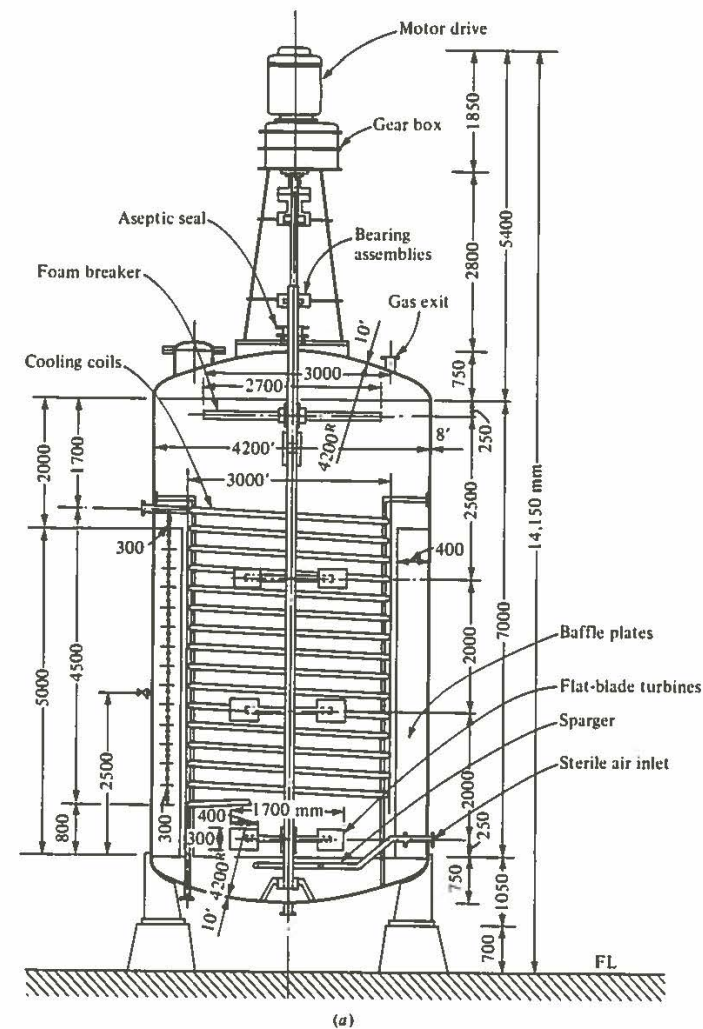


Figure 9.36 (a) Cutaway diagram of a 100,000-liter fermenter used for penicillin production. (b) Photograph looking down into a large production fermenter. [(a) Reprinted from S. Aiba, A. E. Humphrey and N. F. Millis, "Biochemical Engineering," 2d ed., p. 304, University of Tokyo Press, Tokyo, 1973. (b) Reprinted from R. Müller and K. Kieslich, "Technology of the Microbiological Preparation to Organic Substances," *Angew. Chem. Intl. Edit. Eng.*, vol. 5, p. 653, 1966.]



Figure 9.36 (Continued)

sequence of events. All valves in the system must be easy to maintain, clean, and sterilize. For these reasons ball valves are quite popular. Several other general principles of aseptic process design are shown in Fig. 9.35. Specifically, all vessel connections should be steam-sealed: no direct connections between sterile and nonsterile portions of the system should be allowed. Maintenance of a positive pressure on the system ensures that leakage will be outward rather than inward.

The physical characteristics of a typical commercial fermentation vessel are shown in Fig. 9.36. These vessels are usually constructed from stainless steel to minimize corrosion problems and contamination of the fermentation broth by unwanted metallic ions (recall the discussion in Sec. 5.9.2 on the influence of iron ions in the citric acid fermentation). Care must be taken here and elsewhere in the overall process to avoid dead spaces, crevices, and other niches where solids resistant to sterilization can accumulate and where microbial films can grow. All-welded vessel construction with polished welds helps to minimize these problems.

The agitator assembly is designed to meet the mixing and aeration requirements already discussed in Chap. 8. Special attention to the design and maintenance of the aseptic seal is essential to avoid contamination. Although only one impeller is required in laboratory-scale fermentation, several may be necessary in a large commercial vessel.

Typically only 70 to 80 percent of the vessel volume is filled with liquid, with a gas space occupying the top portion of the tank. Often the combined action of aeration and agitation of the liquid promotes the formation of a foam on the liquid surface, especially if the medium contains high concentrations of peptides. Foam impedes gas mass transfer from the broth to the head space, forcing foam

out of the vessel and contaminating the system when collapsed foam reenters the fermentor. In Fig. 9.36, a supplementary agitator located in the head space serves to destroy the foam. For especially persistent foams, chemical agents called *anti-foams* are added to the broth. These compounds destabilize the foam by reducing surface tension. As noted in Chap. 8, the interfacial characteristics of antifoams can decrease the rate of oxygen transfer.

Several functions can be served by the heat-transfer coils within the vessel. If the medium is to be sterilized batchwise within the fermentor, these coils must have adequate capacity for the necessary heating and cooling. The heat-exchange system must also be able to handle the peak process load, which includes the combined effects of microbial activity and viscous dissipation from mixing (Sec. 8.10). Typical heat-transfer coefficients for uninoculated medium are about the same as for water, while a dense mycelial broth may exhibit a coefficient more typical of a paste.

Fermentation in the production vessel may take from less than 1 day to more than 2 weeks, 4 to 5 days being typical of many antibiotic manufacturing processes. During this interval, operating conditions must be carefully maintained or varied in a predetermined manner. More details on this operating practice will be provided in Chap. 10. Nevertheless, it should be evident from the general review already given that aseptic fermentation is an expensive, time-consuming proposition. Obviously, loss of product from one batch cycle can be extremely costly, so that the previous emphasis accorded sterilization is well taken.

9.7.3 Alternate Bioreactor Configurations

A number of factors, summarized in Table 9.13, have motivated development of new types of bioreactors. Many of these factors were encountered in the development by ICI of an extremely large-scale SCP process. This reactor has a total volume of 2300 m<sup>3</sup> (a column of 7-m diameter and 60-m height within an effective reactor volume of 1560 m<sup>3</sup>). Furthermore, in this reactor organisms are grown on methanol, resulting in extremely large heat release. A conventional

Table 9.13 Factors motivating development of new types of reactors [50]

1. Construction of very large reactors
  - 1.1. Design problems
  - 1.2. High power requirement ( $P/V = \text{constant}$ )
  - 1.3. High costs of energy and cooling water
  - 1.4. Problems of heat removal
2. Reduction of specific capital costs
3. Reduction of specific energy costs
4. Avoidance of cell damage
5. Reduction of substrate losses (due to evaporation and respiration)
6. Increase of substrate conversion

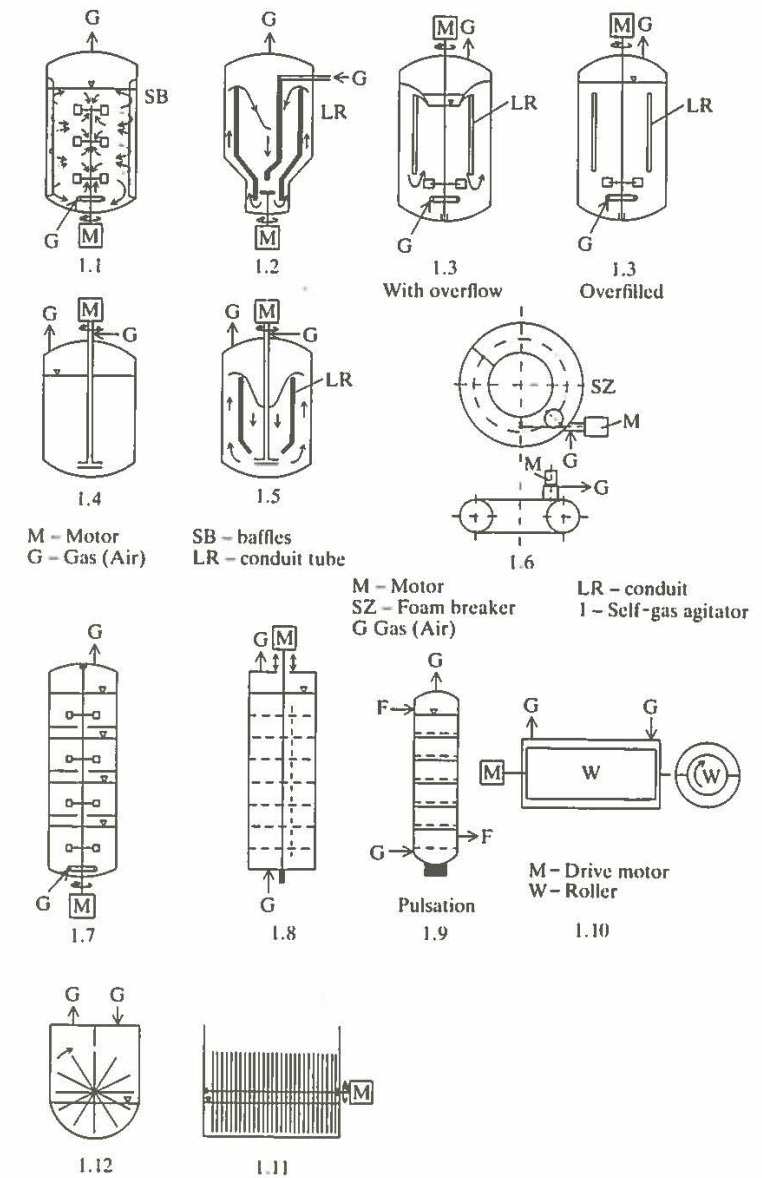


Figure 9.37 Bioreactor configurations using mechanically moved internals for energy input [50].



sparged, mechanically agitated stirred-tank fermentor is completely impractical on this scale. This led to the development of a new airlift design mentioned in the previous section.

A number of other alternative reactor configurations have been proposed and examined in various scales ranging from laboratory to pilot to full scale. An excellent summary of many of these designs and their properties with respect to efficiency of energy use for gas dispersion and mixing have been presented in a

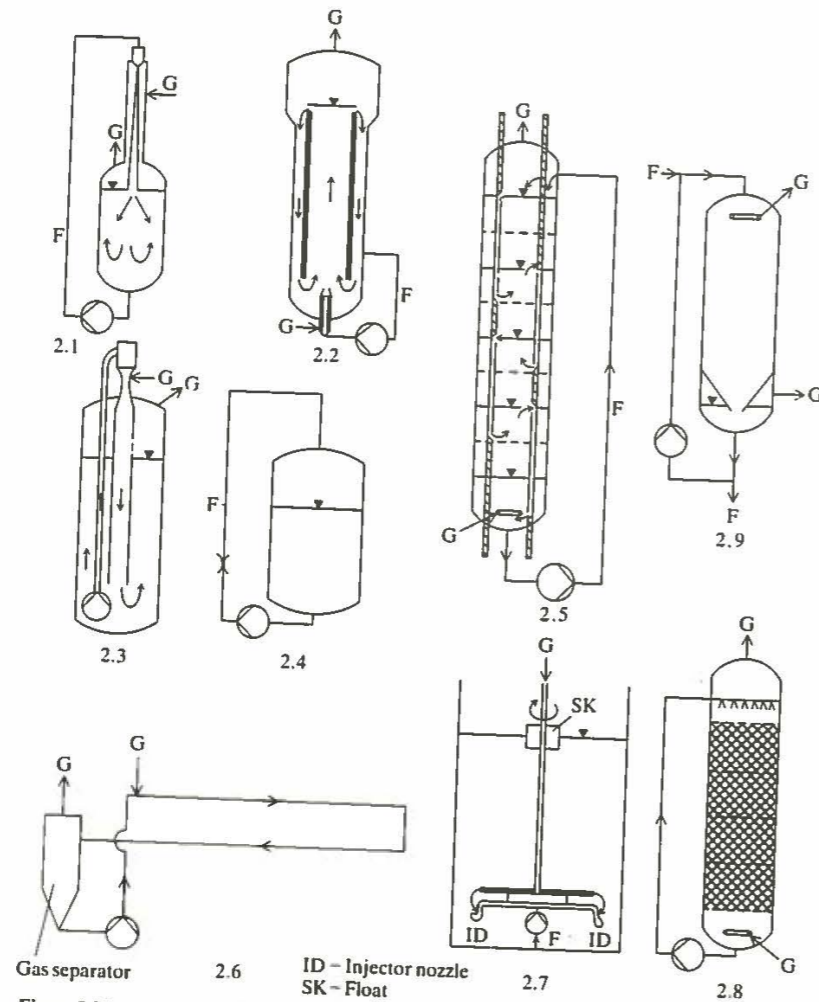


Figure 9.38 Circulation driven by an external pump provides energy input in these types of reactors [50].

review article by Schügerl [50]. In that review, bioreactors have been classified according to three main classes of energy input.

One class of bioreactors employs mechanically moved internals for energy input (Figure 9.37). In several of these designs an internal draft tube provides a defined circulation pattern to achieve loop flow patterns. Design 1.6 is a horizontal loop with foam separator which is completely filled with the gas-liquid mixture. In case 1.9, pulsation of the liquid flow occurs, and in configuration 1.11, viewed here from the side, disks on a rotating shaft are intermittently dipped into the liquid contents at the bottom of the reactor.

Figure 9.38 shows another set of reactor configurations in which energy is provided by liquid circulation using an external pump. In design 2.1 the liquid jet is injected downward and plunges into the liquid reactor contents, while in design 2.7 the injection nozzles for fluid are at the tips of a rotating bar.

The final group of reactor types, where energy input is provided in the form of compressed gas, are sketched in Fig. 9.39. In most of these designs, reactor

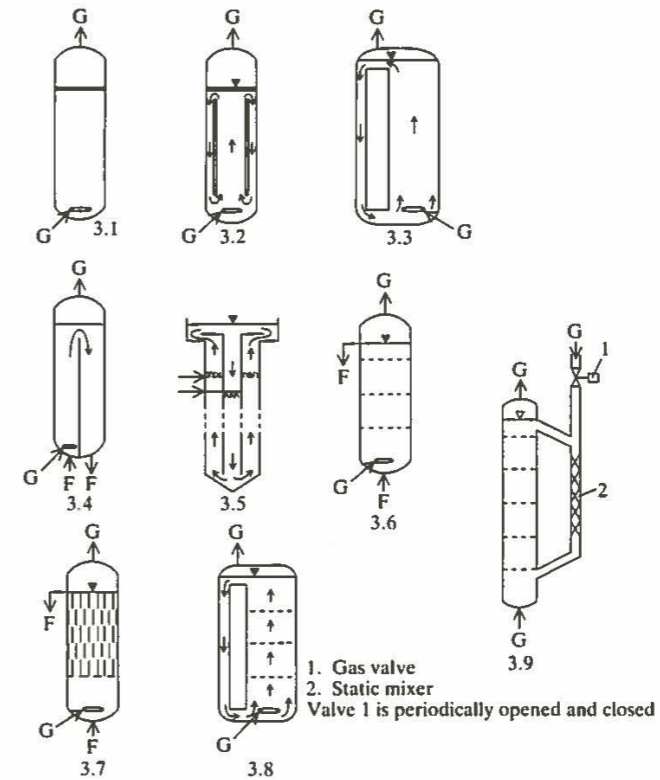


Figure 9.39 Submerged-type reactors with energy input by compression [50].

internals are provided for redispersion of gas and several different loop-flow configurations are evident. Further details on all of these reactor configurations and additional references are available in Schügerl's review [50].

## 9.8 ANIMAL AND PLANT CELL REACTOR TECHNOLOGY

Growth of animal cells in culture is currently used for manufacture of several products including vaccines, the proteolytic enzyme urokinase, monoclonal antibodies, and interferons. Such processes also have substantial potential for production of other lymphokines (a group of proteins which regulate certain aspects of the immune system), other enzymes, growth factors, clotting factors, and hormones. The advent of recombinant DNA technology introduces competition with animal cell cultivation for some of these products but also presents new possibilities for product manufacture using animal cell culture. On one hand, the opportunity of expressing foreign proteins in microorganisms means that microbial processes can now be used to manufacture these proteins in significant quantity. However, as explained in section 6.4.4, protein naturally synthesized in animal cells are often subjected to several different types of posttranslational modifications which are not accomplished in procaryotes. This means that for molecules requiring such posttranslational modification for activity or stability, eucaryotic hosts are necessary. Furthermore, problems with proper protein folding and proteolytic attack makes expression of some eucaryotic proteins difficult in procaryotic hosts. With improving methods for expression of foreign genes in animal cells, the prospects for industrial recombinant host-vector systems using animal cells are increasing.

Many useful and interesting chemicals can conceivably be synthesized in cultures of plant cells. Also, cultivation of plant cells may facilitate genetic engineering of plants and may ultimately allow the regeneration of whole crop plants from tissue originated in culture.

There are several common features in cultivation of plant and animal cells which complicate reactor design for their cultivation and for manufacture of their products. Many of the cell types of interest exist naturally as dense packings of similar cells. Such cell tissues in their native state are contacted with fluids of the organism of specific composition and containing a variety of regulatory molecules which can strongly influence cellular function. Growth rates of the cells may naturally be very low. The challenges faced in submerged cultivation of these cells is to provide an acceptable environment for growth of the cells—many types of plant and animal cells when placed in culture do not grow at all. Once this obstacle has been surmounted, the goal is to determine cultivation conditions which allow growth of cells to high densities in the shortest possible time, while retaining the metabolic capability of the cells to carry out the desired reactions.

In this section, we will concentrate primarily on approaches to environmental support of animal cells and a brief summary of some experiences with these organisms. Developments in plant cell culture are at a relatively early stage and

will be more briefly summarized at the end of this section. Because of the expense of animal cell cultivation, because of slow growth rates which prolong experimental studies, and because of some neglect, quantitative characterization of the kinetic properties of animal cells is practically nonexistent. In many cases, limiting nutrients are not known, and descriptions of growth and product formation kinetics as functions of nutrient and inhibitor concentrations, pH, temperature, and other environmental variables are not generally available. Although the influence of mechanical forces on animal and plant cell cultures is recognized as a critical factor in reactor design, controlled studies designed to characterize in engineering terms the connection between mechanical forces and cell survival, growth, and morphological state are lacking. Instead, hardware and catalyst configurations have been invented which provide enhancements in growth rates, greater cell densities, or more product. Although substantial advances have been accomplished based on this empirical approach, there is room for great improvement based on new and improved designs once the kinetic behavior and engineering properties of these cells are more thoroughly understood.

### 9.8.1 Environmental Requirements for Animal Cell Cultivation

Culture media for animal cells is relatively complicated and expensive compared with microbial media. Antibiotics are usually included to reduce problems with microbial contamination. Animal serum is included in most media at concentrations from 5 to 20 vol % in order to promote cell replication. Some but not all of the functions provided by serum in animal cell growth medium have been identified. Serum helps to generalize the utility of the given medium for growth of different types of animal cells which may have different nutritional and growth factor requirements. It has been observed that nutritional requirements can depend upon cultivation conditions, and in these cases use of a rich and very abundant medium component helps to compensate for uncertainties in particular nutritional requirements. For reasons not yet understood, cells grown in media with greater serum content tend to be more resistant to mechanical damage.

There are, however, a number of problems associated with serum use in cell cultivation media. First, serum is the major cost in large-scale cell production. For example, serum, which can cost up to \$300/L, contributes 80 percent of the material cost when used at a level of 10 percent. Serum also represents a major source of contamination to the culture by viruses, mycoplasma (parasitic or pathogenetic gram-negative procaryotes), and bacteria. Serum can contain inhibitors which interfere with virus replication (for vaccine production) or enzyme production. As in the undefined natural complexes added to microbial growth media, serum represents a variable and somewhat unpredictable medium component. Finally, serum introduces pyrogenic (fever-producing) contaminants into the medium which complicate product recovery. The albumin protein background contributed by serum also interferes with recovery of protein products present in low concentrations such as monoclonal antibodies, motivating the use of serum-free medium in order to facilitate recovery of the desired product.

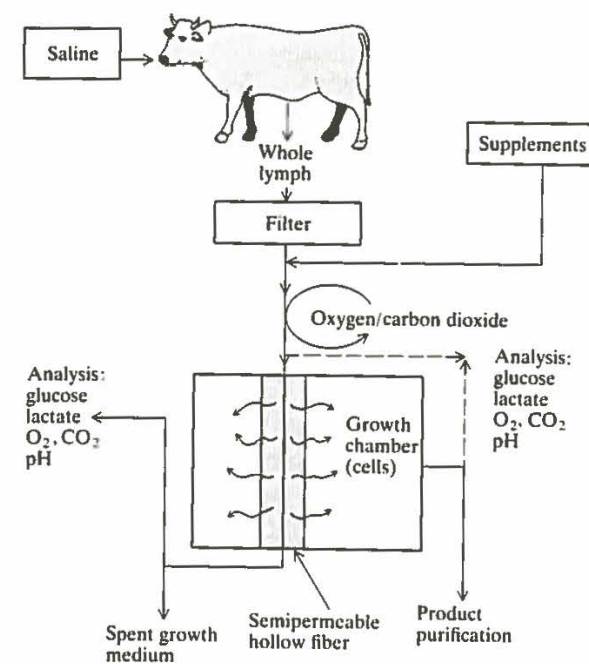


Figure 9.40 Schematic diagram of a cell culture technique which uses filtered cow lymph to provide medium components. (Reprinted by permission of Bio-Response, Inc.)

One novel strategy which has been proposed for reducing the cost of complex adjuncts for cell culture media is illustrated in Fig. 9.40. Here, whole lymph from a live cow is filtered and subsequently contacted with cells in the growth chamber using a hollow fiber ultrafilter. Provisions for adding supplements to complete the medium and for gas exchange are indicated.

Substantial advances have been made in formulation of a variety of hormonally defined, serum-free media. Such media offer the potential advantages of optimal tuning of the mixture of the medium for the particular organism and cultivation conditions, elimination of contamination problems, and more reproducibility. However, defined medium has the disadvantages of higher cost and of possible long-term effects on the organisms which are not easily anticipated or discovered during an initial short-term evaluation of the medium.

Animal cells do not possess cell walls to provide mechanical strength and are larger than microbial cells. Consequently, there are constraints on the forces which can be applied to a cell culture reactor in order to mix the cells, or cell-carrying or -containing particles, to maintain uniform environmental conditions and to accelerate transfer of oxygen into the culture. Animal cells require oxygen at a level of approximately 25-40 percent of air saturation, and design of oxygen

supply systems for large-scale animal cell cultivation is an ongoing engineering problem. The demands imposed on the reactor engineer are moderated here because of the relatively slow growth and metabolic rates of the cells.

Oxygen requirements for a culture of typical density  $10^6$  cells  $\text{mL}^{-1}$  is in the range of  $0.05 \text{ mmol O}_2 \text{ L}^{-1} \text{ h}^{-1}$  to  $0.6 \text{ mmol O}_2 \text{ L}^{-1} \text{ h}^{-1}$ . In small vessels characteristic of laboratory cultures, this oxygen requirement can be met simply by oxygen diffusion from the gas in the head space of the vessel into the bulk liquid. This gas overlay exchange is insufficient to meet oxygen needs of the culture in larger scale. Here direct sparging of gas into the fluid has been used successfully in some cases. In other instances, this direct sparging appears to damage the cells and may also cause excessive foaming, especially in media containing large quantities of serum. An alternative approach which has been proposed is immersion in the culture fluid of silicon tubing with oxygen diffusing from the flowing gas in the tubing into the medium without bubble formation. The overall mass-transfer coefficient for oxygen transfer through silicon tubing is around  $0.35 \text{ mmol O}_2 \text{ atm}^{-1} \text{ cm}^{-2} \text{ h}^{-1}$  from which the amount of tubing required can be calculated. As the scale of cultivation increases, the practical feasibility of providing the necessary tubing becomes increasingly problematic.

In relatively advanced technology for animal cell cultivation, the pH of the culture is monitored and controlled, typically at values near 7.0. Today, there is very little experience with highly instrumented cell culture reactors to which the fullest possible set of data analysis and control strategies have been applied. As we shall investigate in the following chapter, there are many available instruments and approaches from microbial bioreactors which can be applied in the future to improve performance of cell culture reactors.

pH control in cell culture systems has been provided by a number of different approaches. Use of buffers in the medium can moderate pH changes which often occur due to lactic acid production by the cells. pH can also be manipulated by adjustment of the CO<sub>2</sub> content of the gas in contact with the culture. Direct addition of base is another possible approach. In reactors with continuous or intermittent exchange of reactor medium with fresh medium, pH variations can also be moderated.

## 9.8.2 Reactors for Large-Scale Production Using Animal Cells

Different types of animal cells can be divided into two broad classes depending upon their need for attachment to a solid surface for growth. Cells from the blood stream, lymph tissue, tumors, and many transformed cells can be adapted for growth in suspension culture. Other types of animal cells must be anchored to a compatible solid surface in order to grow. Furthermore, in the latter case, a contact inhibition regulatory mechanism usually prohibits growth beyond single monolayer coverage of the surface. On a small scale, required agitation is provided by use of a magnetic stirrer and a small "spinner flask" for suspended cells and by use of a cylindrical "roller bottle" partly filled with medium which rolls on its side horizontally at about one revolution per minute.

Many reactor designs for larger scale cultivation of animal cells in suspension resemble microbial bioreactors. Often the flat-bladed turbine mixers common in microbial processes are replaced by propeller agitators. In another quite effective design at the 100-L scale, "sails" of monofilament fiber are used in place of impeller blades to provide mixing of the culture suspension. Not often encountered in microbial cultivation, the Vibromixer has been used in animal cell bioreactors. This mixer is a circular flat disk containing several holes, mounted horizontally on the bottom of the shaft in the fluid. Rapid vertical oscillation in shaft position vibrates the perforated disk vertically in the fluid, creating a circulation pattern in the vessel. Airlift designs similar to those discussed earlier have also been used for animal cell cultivation.

A different perspective is appropriate when using the term "large-scale" in connection with animal cell cultivation. Here, because of the high value of the product and the high operating expense, a reactor as small as 10 liters may qualify as large scale, and a reactor of 100 liters certainly does.

Another factor favoring the use of relatively small reactors for animal cell cultivation is the relatively slow growth rate of these cells. Shown in Fig. 9.41 is data on growth in batch cultivation of the human liver adenocarcinoma cell line SK-HEP-1. Table 9.14 summarizes observed specific growth rate and oxygen uptake rates for several cell lines. In the first two cases, the cells were grown in suspension in an airlift fermentor. The final two cell types mentioned are anchorage-dependence lines, cultivation of which will be considered shortly.

Two different types of encapsulation methods have been demonstrated for achieving very high local cell densities. Instead of growing suspended cells, the cells are immobilized by entrapment using ultrafiltration membranes or by microencapsulation. Although conceptually similar to cell immobilization methods discussed earlier for microbial cells, the opportunities and the requirements are somewhat different for animal cells which are relatively large. In one quite promising microencapsulation process [60], cells are first entrapped in alginate beads (see Fig. 9.27). A surface coating of polylysine is applied and cross-linked, after which the alginate gel can be dissolved and removed. In this formulation, the cells are suspended within an entrapping network of polylysine, and, after growth, can pack the interior to cell densities approaching that of tissue. These strategies offer promise of higher volumetric productivities in animal cell reactors.

Special requirements arise in scaling up bioreactors for anchorage-dependent cells. The surface-to-volume ratio for a roller bottle is low, making scale-up by use of larger bottles quite impractical. A number of different methods have been demonstrated for increasing surface-to-volume ( $S/V$ ) ratio in a bioreactor and thereby increasing the volumetric density of anchorage-dependent cells. Several of the possible designs and their  $S/V$  ratios are illustrated schematically in Fig. 9.42. Among these options, greatest attention recently has concentrated on application of microcarriers, small beads on which cells grow, which can be suspended in cultivation fluid. A major advantage of the microcarrier approach is the opportunity of using many of the same reactors and contacting designs for micro-

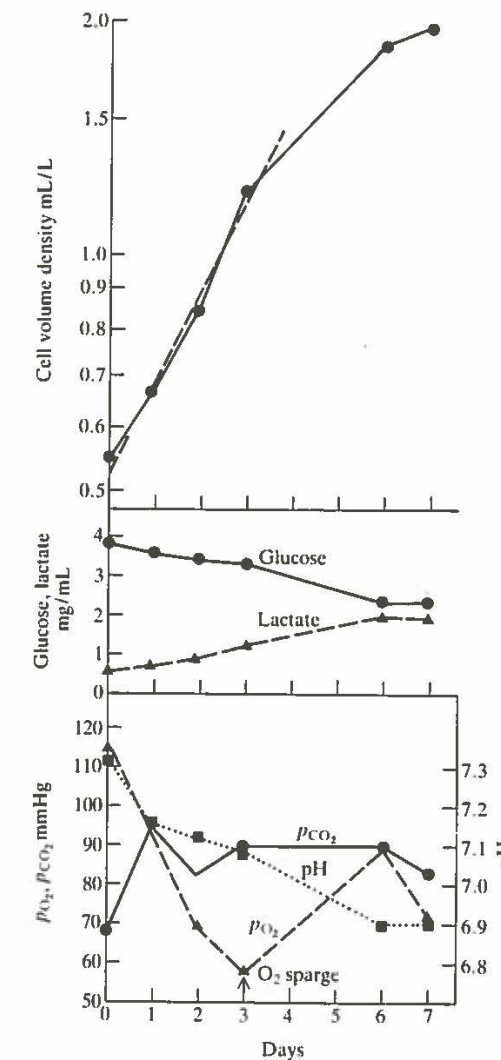


Figure 9.41 Time course of batch cultivation of SK-HEP-1 (human liver adenocarcinoma) cells in 100 L suspension culture. Dashed line in upper frame corresponds to exponential growth with 62 h doubling time. After three days, a sparge of 0.2 mL/min 100%  $O_2$  was initiated. (Reprinted by permission from W. R. Tolbert, R. A. Schoenfeld, C. Lewis, and J. Feder, "Large-Scale Mammalian Cell Culture: Design and Use of an Economical Batch Suspension System," *Biotech. Bioeng.*, vol. 24, p. 1671, 1982.)

carrier suspensions as are used for cultivation of animal cells which are not anchorage-dependent. The first demonstrated microcarriers were charged dextran beads. Inhibition observed with the early beads was subsequently eliminated by modifying bead composition and decreasing bead surface charge. For example, one commercially available microcarrier consists of a core matrix of cross-linked dextran to which is covalently bound a surface layer of denatured collagen. Reported bead densities in cell culture reactors range from 3 g/L to 25 g/L.

**Table 9.14 Summary of specific growth rates and specific oxygen uptake rates for different cell lines. Continuous culture was conducted in a bubble-column reactor.**  
 Reprinted by permission from H. W. D. Kutinger and W. Schirer, "Status and Developments of Animal Cell Technology using Suspension Culture Techniques," *Acta Biotechnologica* vol. 2, p. 3, 1982.

Cell type	Cultivation technique applied	Specific oxygen uptake ( $Q_{O_2}$ ), ( $\mu\text{mol O}_2/10^6$ cells $\times$ hour) $\times 10^{-3}$	Specific growth rate, ( $\mu/\text{h}^{-1}$ )	$P_{O_2}$ , mmHg
BIK 21c 13 Baby hamster kidney	Continuous culture	85	0.018	60
		110	0.033	60
Human lymphoblastoid cells (Namalwa)	Continuous culture	54	0.012	50
		75	0.020	50
Mouse L 929	Microcarrier	20	Stationary phase at monolayer coverage	60-80
		65		Exponential growth phase
Human foreskin FS-4	Microcarrier	50	0.010	ca. 60
		85	0.025	ca. 60

When propagating animal cells from an original stock culture to a high cell density in a large reactor, a number of sequential steps of increasing scale are used. Summarized in Fig. 9.43 is a schematic flow sheet showing the cultivation steps typically utilized for a free suspension culture and for an anchorage-dependent culture. Note that, compared to microbial systems, the inoculum size for the next largest reactor is quite large.

A number of different operating modes have been applied in animal cell cultivation. In addition to the simple batch process, repetitive batch operations have been conducted in which a fraction of the culture at the end of the batch is used as the inoculum for a refilled reactor which is then grown to maturity. Fed batch operation, which adds nutrient at some preprogrammed rate or based upon process measurements as the cultivation takes place, is another possibility. An additional option is a perfusion system in which cells are retained in the reactor while some of the reactor medium is removed and new medium is added. This is an example of the macroscale immobilization methods for cells discussed earlier. Finally, continuous culture with continuous removal of cells as well as medium has been conducted. Medium removal helps reduce cell inhibition caused by metabolic product accumulation. For example, ammonia inhibits cell growth at concentrations above 4 mM.

The rate at which products appear can be quite different depending upon the process and pathway by which the product is formed. In some cases, products appear as the cells grow. In other cases, particular precursors are added after

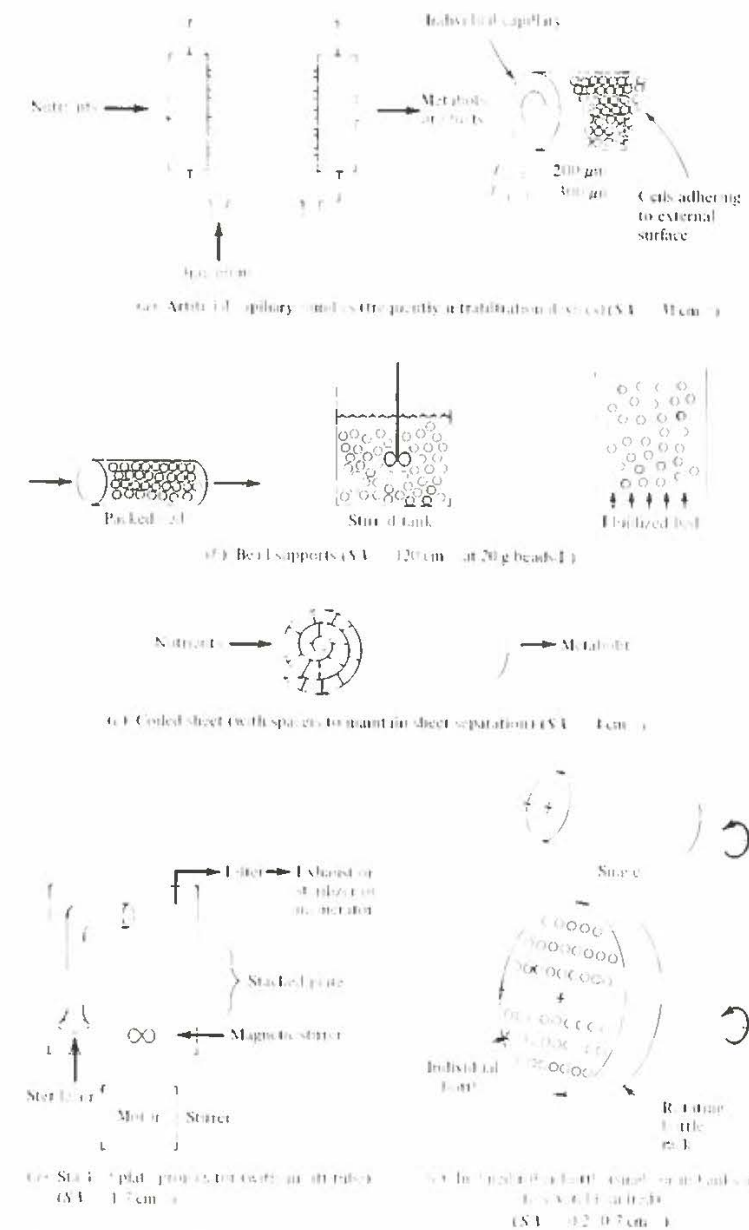


Figure 9.42 High surface area configurations for tissue culture.

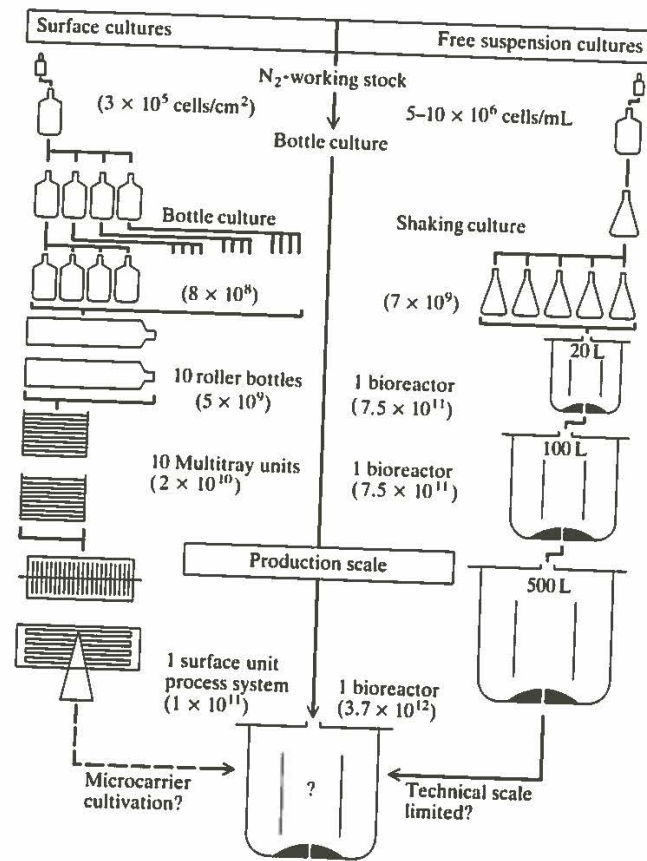


Figure 9.43 Scale-up of animal cell cultivation using BHK (baby hamster kidney) 21 cells as an example. Numbers in parentheses denote total amount of cells produced at the indicated stage. (Reprinted by permission from H. W. D. Katinger and W. Scheirer, "Status and Developments of Animal Cell Technology using Suspension Culture Techniques," *Acta Biotechnologica*, vol. 2, p. 3, 1982.)

some interval of growth giving rise to later product formation. Quite complicated kinetics can be observed in virus production in which the cells are serving essentially as a growth medium for the virus. In fact, it is common in the literature concerned with animal cell cultivation for virus manufacture to call the cell layer the "substrate." The infective virus is often added after the culture has grown to a high density. There then follows a subsequent life cycle of growth of the virus as was discussed in Sec. 6.2.1. This involves a lag for penetration of the virus, synthesis, and assembly of the virus components, followed by virus appearance in the cells or the medium.

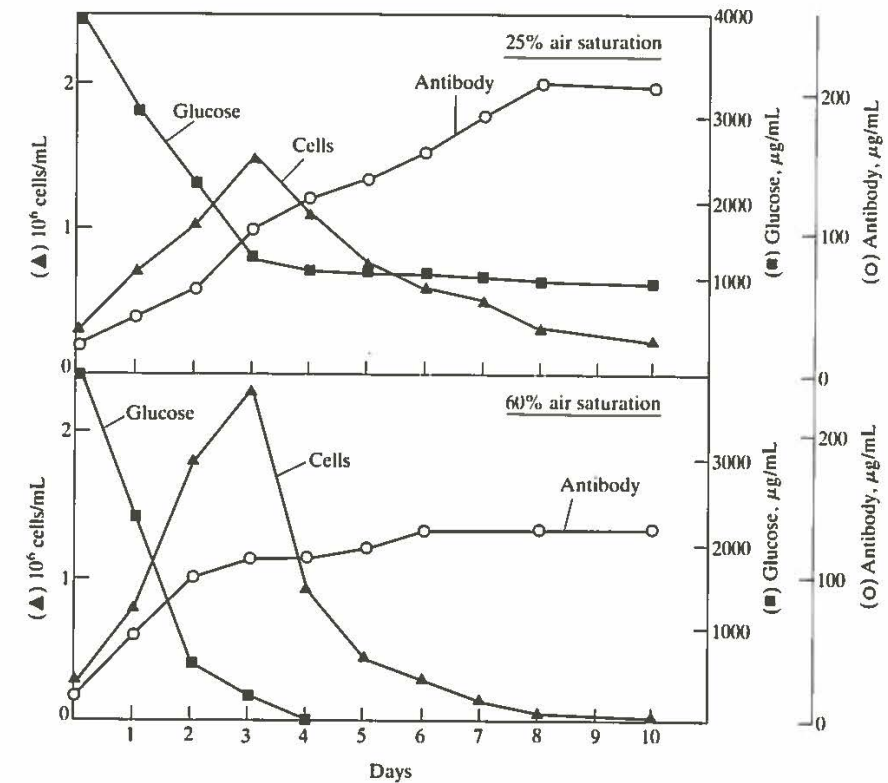


Figure 9.44 Time trajectories of hybridoma growth and monoclonal antibody production at different dissolved oxygen concentrations in a 3-liter fermentor. (Reprinted by permission from S. Reuveny, D. Velez, F. Riske, J. D. Macmillan, and L. Miller, "Production of Monoclonal Antibodies in Culture," *E.S.C.A.T. Mtg.*, Italy, May, 1984.)

An example of monoclonal antibody production strongly illustrates the potential for reactor optimization. A mouse-mouse hybridoma line has been propagated in batch, fed-batch and continuous culture to produce a MAb for a surface antigen of *Rhizobium japonica* NR-7 cells.<sup>†</sup> Medium studies showed that an inexpensive medium could be used, consisting of Dulbecco's Modified Eagle Medium, plus 0.25% Primatone RL, 0.01% Pluronic polyol F-68 and as little as 1% fetal bovine serum, achieving  $2 \times 10^6$  cells/mL in suspension culture with doubling times of 24 h. While a detailed kinetic model was not suggested, the results (Figs. 9.44 and 9.45) are intriguing. Maintenance of diminished oxygen

<sup>†</sup> S. Reuveny, D. Velez, F. Riske, J. D. Macmillan and L. Miller, "Production of Monoclonal Antibodies in Culture," *E.S.C.A.T. Mtg.*, Italy, May, 1984.

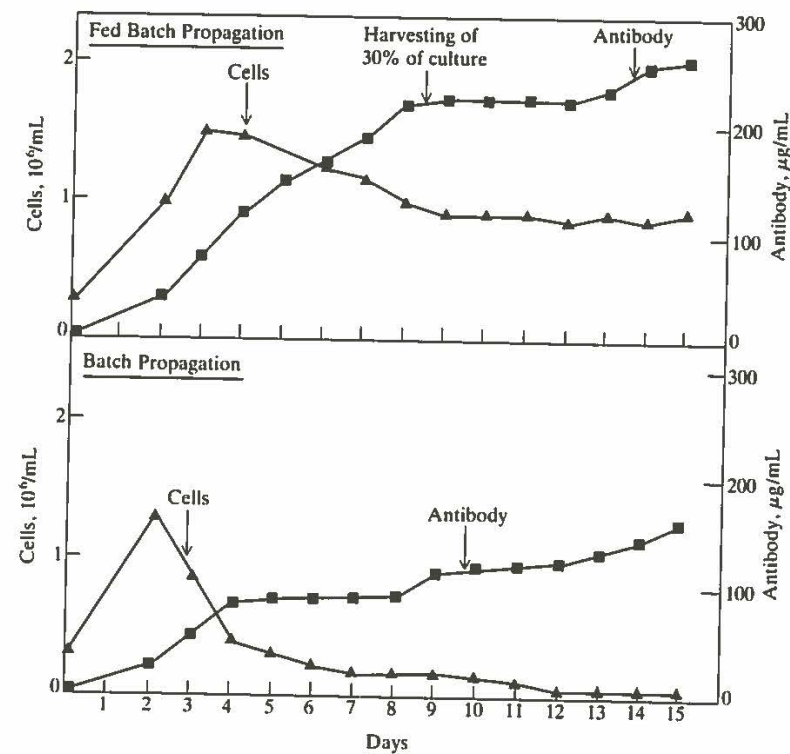


Figure 9.45 Comparison between batch and fed-batch production of monoclonal antibodies. Cells were grown in 100 mL spinner flasks. In fed-batch cultivation, 5-10 percent of growth medium was added for  $10^6$  cells every 24 h and 30 percent of the culture was harvested periodically. (Reprinted by permission from S. Reuveny, D. Valez, F. Riske, J. D. Macmillan, and L. Miller, "Production of Monoclonal Antibodies in Culture," E.S.C.A.T. Mtg., Italy, May, 1984.)

saturation (25 vs. 60 percent air saturation) provided a lower maximum cell density but a longer lived culture (Fig. 9.44) with a resultant higher final MAb titer.

In both conditions, production of a cell growth inhibitor was hypothesized in which case a fed-batch system should improve operation by stepwise dilution of inhibitor. The comparison of batch vs. fed-batch behavior (Fig. 9.45) is consistent with this notion; both cell viability and (consequent) antibody titer reached maximum values in the fed-batch operating mode. While MAb production for small quantities may be done most efficiently in the mouse peritoneal cavity, large-scale production points to bioreactor cultivation of hybridoma cells with emphasis on inexpensive nutrient medium, long cell viability, and optimization based on maximal antibody production. Hollow fiber propagation and perfusion culture are

among the promising modes of larger-scale operation for hybridoma growth and product (MAb) formation.

### 9.8.3 Plant Cell Cultivation

Plant tissue dissected from the interior of plant organs after washing and disinfection can be cultured on agar containing a suitable growth medium. Nutrient media for plant cells are usually comprised of a mixture of inorganic salts with sucrose or glucose as carbon and energy source. (Plant cells are usually propagated chemoheterotrophically rather than photoautotrophically.) This basic medium is typically augmented with particular plant growth regulators, phytohormones, vitamins, amino acids, and the sugar alcohol inositol. Plant cells so propagated require oxygen for division so that aeration is necessary either by diffusion from the top surface of the culture or by sparged gas. The increase of cell number during batch cultivation follows the traditional pattern discussed in Chap. 7, except it is possible to obtain only three to four doublings of the population, corresponding to an increase in mass by a factor of 10 to 15 times the initial inoculum mass.

Plant tissue culture can achieve several potentially useful functions. Proceeding from the chemically most simple to the most complicated, enzymes and metabolic pathways in plants can be used to achieve biotransformation. One example of this class is 12- $\beta$  hydroxylation of digitoxin to digoxin, an important heart stimulant drug, using cells of foxglove (*Digitalis*). Next, plant cells can be used for biosynthesis of complex compounds from simpler precursors. Plant tissue cultures can accomplish de novo synthesis of complex molecules, typically secondary metabolites, from simple media. Plant secondary metabolites of potential commercial interest include pharmaceuticals (currently plant-derived compounds account for about one-fourth of all U.S. prescriptions), dyes such as shikonin, gums, a group of natural insecticides called pyrethrins, and flavors and fragrances like vanilla and jasmine. Also, plant tissue culture provides a technology for rapid genetic engineering of plants for crop improvement and potentially for regeneration of crop plants. Compared with alternative technologies of growing plants in soil and harvesting their products, plant tissue culture may offer the advantage of more intensive production and more reliable and predictable supply.

When plant cells are grown in suspension culture, many different cell forms are present, including isolated cells and large aggregates. It has been noted that cells in plant cell aggregates are differentiated to some degree, with some cells in the interior of a clump being morphologically distinct from those on the outside. In some cases product formation does not occur from isolated single cells but results entirely from cells associated with the aggregates. This suggests that some degree of differentiation is necessary in certain circumstances to achieve the metabolic conditions necessary for product synthesis. In other situations, preservation of an undifferentiated state of the plant cells is the desired objective. Better understanding of the controls of differentiation, of the effects of differentiation, and

**Table 9.15 Doubling times and yield coefficients for cultured plant cells**

(Reprinted by permission from G. Wilson, "Continuous Culture of Plant Cells Using the Chemostat Principle," *Adv. in Biochem. Eng.*, (A. Fiechter, ed.) vol. 16, p. 1, 1980.)

Cell culture	Limiting nutrient	Yield coefficient (10 <sup>9</sup> cells/μmole)	Doubling time (h)
Galium	Phosphate (PO <sub>4</sub> )	3.95	40
Galium	Phosphate (PO <sub>4</sub> )	2.47	25
Acer	Phosphate (PO <sub>4</sub> )	3.47	182
Acer	Phosphate (PO <sub>4</sub> )	1.28	36
Acer	Nitrate (NO <sub>3</sub> )	0.263	109
Acer	Glucose	0.039	109

of ways to regulate differentiation in culture by adjustment of growth conditions are the primary technical unknowns in the field at present.

Relatively little information is available concerning kinetic parameters of plant cell growth in culture. An exception is the body of results developed by Wilson and coworkers based upon chemostat plant cell cultivation. Table 9.15 lists the yield coefficients and doubling times for two different plant cell types grown in media with different limiting components. Notice the extremely long doubling times, again a problem in experimental studies of plant cell culture and in economical exploitation of plant cells as biocatalysts. Estimates of the substrate saturation or Monod constant  $K_s$  for *acer* (sycamore) plant cells in culture on the limiting substrates NO<sub>3</sub>, glucose, and PO<sub>4</sub> are 0.13, 0.5, and 0.032 mM, respectively [66].

Suspended plant cell culture beyond the shake flask scale has been conducted in mechanically agitated tanks and also in bubble column reactors. In order to obtain greater volumetric density of cells, to allow reuse of cells, to permit containment and retention of cells in desired morphological and differentiation states, and to allow better control of contacting between medium and cells, several research groups have investigated immobilized plant cell reactors. Plant cells entrapped in hollow fiber membranes and in alginate and other types of matrices in beads have been investigated [67, 68]. Many products of plant metabolism accumulate intracellularly. This potential handicap for immobilized cell processes may be resolved by alternating permeabilization of cells and product recovery with exposure to growth and production medium [68].

As was noted in batch cultivation for secondary metabolite production using microorganisms, it is necessary for these products to separate in time or in space a growth phase from a phase of secondary metabolite production. This strategy is evident in the first large-scale, commercial plant cell culture process. In this process, developed by Mitsui Petrochemical Industries, the dye and pharmaceutical shikonin is obtained by culturing *Lithospermum erythrorhizon* over a period of longer than three weeks in three successive operations (Fig. 9.46). After growing

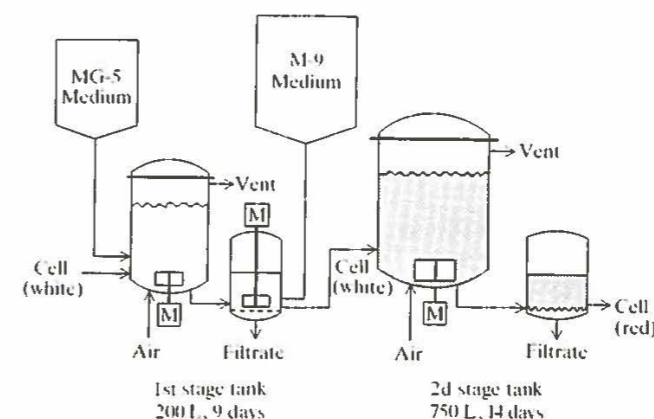


**Figure 9.46** Processing steps in manufacture of the secondary metabolite shikonin using plant tissue (*Lithospermum erythrorhizon*) culture. (Reprinted by permission from Mary Ellen Curtin, "Harvesting Profitable Products from Plant Tissue Culture," *BioTechnology*, October, 1983, p. 649.)

cells in an initial aerated tank, they are transferred to a smaller tank and a medium denoted M-9 is added which stimulates production of shikonin. Subsequent transfer to a third tank followed by reaction for 14 days results in accumulation of the desired product in the cells. Process yields have not been reported by the manufacturer, but independent estimates place the productivity of a single batch at 5 kg product. Obviously, the use of labor, capital, and expensive medium in the quantities involved in this process necessitate a high-priced product to justify commercialization. The selling price of shikonin as of October, 1983 was \$4000/kg!

## 9.9 CONCLUDING REMARKS

In this chapter we have examined the reactor design principles and reactor technologies which enjoy current application and which will likely be used in the future for product manufacture using microorganisms and higher cells. We have tried to indicate how knowledge of the kinetics of the biological reactions and flow and mixing processes in the reactor can be synthesized to achieve an overall mathematical description of the process useful for design and optimization. This is the traditional and very successful strategy for chemical reaction engineering that has emerged from the chemical and petroleum processing industries. Unfortunately, due to our inadequate knowledge of biological kinetics, use of complex growth media with undefined composition and effects, use of reactors with poorly defined flow and mixing characteristics, and the lack of concerted effort toward more systematic and predictive reactor design, one often does not find reactor operation or design specification accomplished using the systematic methodology



outlined in this chapter. Instead, process scale up proceeds through a succession of experimental investigations at increasing scales and costs, but with much smaller jumps in scale from one test to the next than can now be predictably accomplished in other types of chemical reactors. In designing a batch reactor for a biological application, for example, one is presently more likely to worry about providing a certain mass transfer capability than with calculating optimal operating strategies based upon knowledge of the kinetics.

Experience in those industries where chemical reaction engineering has been systematically applied shows that reductions in capital costs, lower operating expenses, fewer byproducts, and greater yields can be obtained. Also, it is not uncommon in the petroleum industry now to translate from bench to full scale, jumping in scale by factors of 10,000 based upon solid foundations in chemical reaction engineering. As opportunities for manufacture of many new products using new organisms and new processes increase in the future, we can expect a more central role for bioreactor engineering to increase the efficiency of scale-up, design, and operation of these reactors, to improve their reliability, and to accelerate commercialization.

Our theme in the next chapter is instrumentation and control, focusing mostly on bioreactors. Here too, our lack of knowledge about the fundamental transport and reaction processes in the reactor limit the types of control methods we bring to bear to obtain the best process performance. While the topics of the next chapter are considered primarily in the context of bioreactors, most apply equally well to upstream and downstream processing units. Following our consideration of instrumentation and control, we shall examine the essential separation processes which are used to convert the mixture emerging from the bioreactor to a stream of sufficiently pure useful product.

## PROBLEMS

- 9.1 CSTR analysis (a) Verify each CSTR design equation of Table 9.1.  
(b) For each CSTR case, indicate graphically how you would evaluate all terms in the reaction rate expression from an appropriate plot of CSTR performance.
- 9.2 PFTR design (a) Validate the results of Table 9.2 by direct integration.  
(b) What variables are most convenient to use for each PFTR design equation? Show by sketches how each kinetic parameter in the reaction-rate expression can be evaluated.  
(c) In general, do CSTRs lend themselves more easily to parameter evaluation than PFTRs? Why (not)?
- 9.3 Single-cell protein production *Methylomonas methanolica* grown on methanol at 30°C, pH 6.0 was observed to obey the following kinetic parameter values;  $\mu_{max} = 0.53 \text{ h}^{-1}$ ,  $Y_s$  (methanol yield coefficient) = 0.48 g/g,  $Y_{O_2} = 0.53 \text{ g/g}$ , carbon-conversion ( $c_{biomass}/c_{methanol}$ ) efficiency = 0.57 g/g, oxygen quotient = 0.90 mol  $O_2$  per mole  $CH_3OH$ , respiratory quotient (RQ) = 0.52 mol  $CO_2$  per mole  $O_2$ ,  $m$  = maintenance factor = 0.35 g  $CH_3OH/g$ ,  $K_s = 2.0 \text{ mg/L}$  [M. Dostolek and N. Molin, "Studies of Biomass Production of Methanol Oxidizing Bacteria" p.385 in *Single Cell Protein II*, S. R. Tannenbaum and D. I. C. Wang (eds.), MIT Press, Cambridge, Mass., 1975]. The specified yield factors correspond to a dilution rate of  $0.52 \text{ h}^{-1}$ .  
(a) Write down the equations for CSTR growth which describe the rates of cell-mass production, oxygen consumption, and  $CO_2$  production vs. dilution rate.

- (b) Plot  $x$ ,  $xD$ , and  $s$  vs.  $D$  ( $\text{h}^{-1}$ ) and locate the predicted maximum values of  $x$  and  $xD$  when  $s_{inlet} = 7.96 \text{ g/L}$ .  
(c) Display the variation in the oxygen consumption rate vs.  $D$  on the same graph. What stirrer power input per unit volume would be needed to operate the reactor at the maximum productivity  $(xD)_{max}$ ? State your assumptions.  
(d) On the same graph, plot the predicted heat-generation rate per volume vs.  $D$ .  
(e) The specific growth rate  $\mu$  is observed to be diminished by substrate in an approximately linear fashion from its maximum value of  $0.53 \text{ h}^{-1}$  at  $s = 3 \text{ g/L}$  to 0 at  $13 \text{ g/L}$  (extrapolated estimate). Repeat part (b) taking this design information into account.  
(f) Under what exit conditions would several equal tanks be better than a single tank of the same total volume?

9.4 Liquid sterilization Set up the equation to determine the probability of complete sterility ( $n < 1.0$ ) in a continuous sterilizer if plug flow is maintained and:

$$\text{Specific death rate} = 10 \text{ min}^{-1} \quad \text{sterilizer volume} = 10 \text{ L}$$

$$\text{Medium flow rate} = 10 \text{ L/min} \quad \text{temperature of medium} = 131^\circ\text{C}$$

$$\text{Collection time} = 5 \text{ min} \quad \text{original cell concentration } n_0 = 10^3 \text{ L}^{-1}$$

What would you expect to happen to this probability if all the variables given above were held constant but the sterilizer were shortened and widened? Explain your reasoning and show pertinent equations.

9.5 Growth with variable yield coefficient Derive equations for  $x(D)$  and  $s(D)$  analogous to Eqs. (7.14) and (7.15) for the case where  $Y$  is given by Eq. (7.26).

9.6 Homogeneous and film reactor A feed contains a suspension of inert particles as well as substrate for an anaerobic fermentation. The vessel agitation is sufficient to keep the particles suspended and well dispersed. The microbial (single) population partitions itself between the particles and the bulk solution by a linear isotherm:

$$x_p(\text{cells/cm}^2) = Kx_{bulk}(\text{cells/mL})$$

where  $K$  has units of  $\text{mL/cm}^2$ . The adsorption process does alter the maximum specific growth rate  $\mu_{max}$  but not  $K_s$  (assuming the Monod form is valid).

(a) Evaluate over all feasible dilution rates when  $d(\text{inert}) = 0.1 \text{ mm}$  and volume fraction = 1 percent (1) the ratio of substrate utilization in the presence of inert particles to that occurring in their absence and (2) the influence of the suspended particles on reactor washout.

(b) How would you design a cell-recovery scheme at the reactor exit to maximize biomass recovery?

9.7 Rapid  $K_s$  measurement Williamson and McCarty ("A Rapid Measurement of Monod Half Velocity Coefficients for Bacterial Kinetics", *Biotech. Bioeng.*, 17, 915, 1975) developed a relatively rapid means of determining  $K_s$  in microbial kinetics. A small, concentrated feed stream enters the microbial reactor, giving rise to a negligible volume increase over several hours. For values of  $s$  allowing less than the maximum possible substrate-utilization rate by the population,  $\mu_{max} \ll Y$ , steady state was achieved in less than 1 h.

(a) Show that a Lineweaver-Burk type of plot ( $\text{rate}^{-1}$  vs.  $1/s$  at "steady state") allows evaluation of  $K_s$ .

(b) Over what range of sampling times is the above analysis valid?

9.8 Fed batch reactor (a) Assuming exponential growth for cells at  $\mu = \mu_{max}$ , develop a general form for  $x(t)$  starting with Eq. (9.4).

(b) Under what conditions will  $x$  increase, decrease, or remain constant?

(c) If the feed function  $F(t)$  is alternated to be  $F = F_0$  ( $t_0 < t < t_1$ ),  $= 0$  ( $t_1 < t < t_2$ ),  $F_0$  ( $t_2 < t < t_3$ ), etc., derive expressions for  $x$  for  $t < t_1$ , for  $t_1 < t < t_2$ , and for any large  $t$ .

(d) Suppose a methanol utilizing strain has a specific growth rate given by Eq. (7.32) (Monod form plus substrate inhibition). Why could operation in fed batch mode be superior to operation as a simple batch reactor with full charge of methanol present at  $t = 0$ ?

**9.9 Serial substrate utilization** With multiple substrates, substrate consumption patterns in staged tanks or in towers may be complex as mentioned in the text. Consider a very simple model for diauxic growth on two substrates, glucose (G) and a second carbohydrate (S), such that

$$r_x = \mu(g, s)x$$

$$= \left[ \frac{\mu_G \cdot g}{K_G + g} + \frac{\mu_S \cdot s}{K_S + s} \cdot \frac{K_R}{K_R + g} \right] x$$

(a) For typical conditions involving glucose repression, we expect that  $\mu_S \gg \mu_G$  and  $K_S \sim K_G \gg K_R$ . Sketch the expected variation of  $g, s,$  and  $\ln x$  vs. time in a batch fermentation, showing clearly the relation between changes in the concentrations of biomass and the two substrates G and S. [Take  $(g_0, s_0) \gg (K_S, K_G)$ ].

(b) For diauxic fermentations aimed at complete utilization of cell substrates, could you usefully use a plug flow reactor?, Tanks (chemostats)-in-series? A single chemostat? Why (not)?

(c) Since  $K_R \ll K_G, K_S$ , the growth equation can be conveniently simplified depending on whether  $g > K_R$  or  $K_R > g \approx 0$ . Develop a simplified plug flow description and integrate it analytically to give  $x(z), g(z)$  and  $s(z)$ .

(d) For  $\mu_G = 1 \text{ h}^{-1} = 1.1 \mu_S, K_G = K_S = 10 \text{ mM}, K_R = 0.1 \text{ mM}, x_0 = 0.1 \text{ g/L}, Y_G = Y_S = 0.5 \text{ g/g}, g_0 = s_0 = 0.2 \text{ mM}$ , plot the results of part (c) for  $u_0$  (flow velocity)/L (reactor length) =  $1 \text{ h}^{-1}, 3 \text{ h}^{-1}$ , and  $5 \text{ h}^{-1}$ .

(e) Vertical tower fermentors may have microbial populations which agglomerate and slowly settle. How would you modify the simple equation of part (b) to account for cells which settle at an average velocity  $u_s (> u_0)$  (Net settling velocity =  $u_s - u_0$ ).

**9.10 Chemostat design from batch data** The mass balances for component C in batch (or plug flow reactor) and chemostat (CSTR) are:

Batch (or plug)  $\frac{dc}{dt} = f(c)$  (i)

steady-state chemostat  $D(c_0 - c) = -f(c)$  (ii)

Since  $f(c)$  is available from (i) by differentiation, a plot of  $f(c)$  vs.  $c$  can be constructed from batch data. Similarly, equation (ii) indicates that a plot of  $D(c - c_0)$  vs.  $c$  will intersect  $f(c)$  vs.  $c$  at  $c^*$  corresponding to the solution of equation (ii). (This technique, which provides the solution  $c^*$  for any given  $D$ , is applicable *only* if the fermentation can be described by a single variable; e.g.,  $c$ .) (This solution technique was used by R. Luedeking and E. L. Piret "Transient and Steady States in Continuous Fermentation; Theory and Experiment," *J. Biochem. Microbiol. Technol. Eng.*, 1, 431, 1959). Its usefulness is seen in the following comparison of bacterial concentration (UOD/mL) from their paper

Measurement	Graphical solution from batch data
5.37	5.35
2.4	2.3
8.0	7.15

(a) Consider the logistic equation,  $dx/dt = \mu x(1 - x/x_{max})$ . With  $\mu = 1 \text{ h}^{-1}, x_{max} = 10 \text{ g/L}$  and  $x_0$  (in feed) = 0. Solve for  $x^*$  graphically for the cases  $D = 1.5 \text{ h}^{-1}, 0.75 \text{ h}^{-1}$ , and  $0.25 \text{ h}^{-1}$  using the method discussed above. Verify your results by direct solution analytically.

(b) For fermentors in series, the outlet from one chemostat is the inlet condition to the next. Show graphically how you would evaluate  $x_3^*$ , the biomass concentration in the third CSTR in a three-reactor cascade with an overall dilution rate of  $D = 0.75 \text{ h}^{-1}$ .

(c) Inspect the data for diauxic growth (Fig. 7.14) carefully. Differentiate it graphically and plot  $dx/dt$  vs.  $x$ . How does this plot differ from the shape for the simple logistic form? Sketch, using the graphical design procedure above, a solution for 5 tanks in series which will consume all of the glucose and most of the second carbohydrate as well.

**9.11 Fluidized beds of immobilized enzymes** (a) Chinloy (PhD thesis, Princeton University, 1976) examined the conversion vs. reciprocal space velocity  $\theta^{-1}$  (milliliter per gram of catalyst particles per second) obtained in packed and fluidized beds of protease immobilized on nonporous stainless-steel particles. In both cases, the data fell on the same straight line passing through the origin. Assuming  $s_0 \gg K_m$ , show that the data are not mass-transfer-influenced and that the specific rate constant can be evaluated directly from the data if the enzyme loading per catalyst particle (milligrams E per gram of catalyst) is known.

(b) Gelf and Boudrant ("Preliminary Study of a Fluidized Bed Enzyme Reactor" *Biochim. Biophys. Acta*, 334, 467, 1974), studied hydrolysis of benzoylarginine ethyl ester (BAEE) by papain immobilized in porous 170 to 250  $\mu\text{m}$  particles. The following parameter values were reported:

Soluble papain:  $K_m = 5 \times 10^{-3} \text{ M}$

$$v_{max} = 19 \text{ IU } [\mu\text{mol BAEE}/(\text{min} \cdot \text{mg}) \text{ at pH 6.0 and } 20^\circ\text{C}]$$

Immobilized papain:  $K_m$  (apparent) =  $1.2 \times 10^{-2} \text{ M}$

$$v_{max} = 0.05 \text{ IU } [\mu\text{mol}/(\text{min} \cdot \text{mg of support})]$$

The porous support was largely iron oxide particles. From the data in Fig. 9.P11.1 determine whether these studies were influenced by external or internal mass transfer. State your assumptions. The catalyst charge in the fluidized bed was 10 g of particles; it was fabricated from a mixture including 100 mg crystalline papain per 30 g oxide.

(c) Discuss how you would design a fluidized-bed reactor of immobilized proteases for hydrolysis of (1) BAEE, (2) casein, (3) 1- $\mu\text{m}$ -diameter gelatin particles.

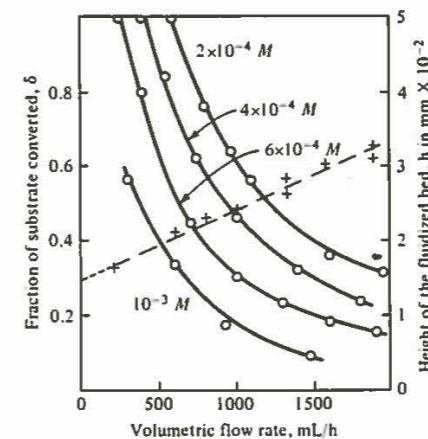


**Figure 9P11.1** Fraction of substrate converted (O-O) and height of fluidized bed (+ + +) vs. volumetric flow rate. Molarities of inlet substrate concentrations are indicated on the curves. [From G. Gelf and J. Boudrant, *Enzymes Immobilized on a Magnetic Support*, *Biochim. Biophys. Acta*, vol. 334, p. 468, 1974.]